

## **General Disclaimer**

### **One or more of the Following Statements may affect this Document**

- This document has been reproduced from the best copy furnished by the organizational source. It is being released in the interest of making available as much information as possible.
- This document may contain data, which exceeds the sheet parameters. It was furnished in this condition by the organizational source and is the best copy available.
- This document may contain tone-on-tone or color graphs, charts and/or pictures, which have been reproduced in black and white.
- This document is paginated as submitted by the original source.
- Portions of this document are not fully legible due to the historical nature of some of the material. However, it is the best reproduction available from the original submission.

NASA CONTRACTOR REPORT 166612

POINTING AND CONTROL SYSTEM DESIGN STUDY FOR  
THE SPACE INFRARED TELESCOPE FACILITY (SIRTF)

K. R. LORELL  
J-N. AUBRUN  
B. SRIDHAR  
R. W. COCHRAN

(NASA-CR-166612) POINTING AND CONTROL  
SYSTEM DESIGN STUDY FOR THE SPACE INFRARED  
TELESCOPE FACILITY (SIRTF) (Lockheed  
Missiles and Space Co.) 210 p HC A10/MF A01

N85-15795

CSCCL 03A G3/18

Unclas  
13247

CONTRACT NAS2- 11550  
November 1984



POINTING AND CONTROL SYSTEM DESIGN STUDY FOR  
THE SPACE INFRARED TELESCOPE FACILITY (SIRTF)

K. R. LORELL  
J-N. AUBRUN  
B. SRIDHAR  
R. W. COCHRAN

LOCKHEED PALO ALTO RESEARCH LABORATORY  
RESEARCH AND DEVELOPMENT DIVISION  
LOCKHEED MISSILES AND SPACE COMPANY, INC.  
3251 HANOVER STREET  
PALO ALTO, CALIFORNIA 94304

PREPARED FOR  
AMES RESEARCH CENTER  
UNDER CONTRACT NAS2-11550

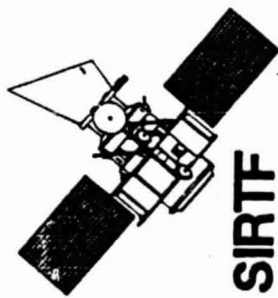


National Aeronautics and  
Space Administration

**Ames Research Center**  
Moffett Field, California 94035

## TABLE OF CONTENTS

EXECUTIVE SUMMARY . . . . .	1
STUDY OBJECTIVES . . . . .	9
STUDY OVERVIEW . . . . .	12
SYSTEM REQUIREMENTS . . . . .	16
SUMMARY OF RESULTS . . . . .	24
SIRTF FREE FLYER DYNAMIC MODELS . . . . .	27
DISTURBANCE MODELS . . . . .	53
POINTING AND CONTROL SYSTEM CONFIGURATION . . . . .	67
POINTING AND CONTROL SYSTEM PERFORMANCE EVALUATION . . . . .	101
SIMULATION RESULTS . . . . .	131
REPRESENTATIVE TIME HISTORIES . . . . .	161
CONCLUSIONS . . . . .	183
APPENDIX A - IRAS SLOSH MEMO . . . . .	193
APPENDIX B - SYSTEM MATRICES . . . . .	213



**SIRTF**

---

## EXECUTIVE SUMMARY

---

## EXECUTIVE SUMMARY FOR THE SIRTf TISS MODIFICATION STUDY

The Space Infrared Telescope Facility (SIRTf) is being designed as a one meter class, cryogenically-cooled, free-flying observatory to be launched from the Space Shuttle sometime in the early 1990's. SIRTf will contain between 500 and 600 kilograms of liquid cryogen to keep its optical system and infrared focal plane instrumentation at temperatures near absolute zero for up to two years. In order to take full advantage of its extremely sensitive instruments, SIRTf will be equipped with a fully automatic precision pointing and control system capable of orienting the telescope towards any spot on the celestial sphere with an absolute accuracy of one arcsecond. In addition, the pointing and control system will be able to make small, rapid changes in the telescope line of sight to facilitate the exploration and mapping of regions of the sky containing diffuse infrared sources.

Two possible orbits have been selected for SIRTf; a polar sun-synchronous orbit with an inclination of 98 degrees, and an equatorial orbit with an inclination of 28 degrees. The 98 degree orbit will be at an altitude of 700 km and the 28 degree orbit at 600 km. Although the basic SIRTf concept and instrumentation will be identical for each of these orbit selections, there will be several fundamental differences between spacecraft designed for the two orbits. As an example, a sun-synchronous orbit does not require as large a solar array as does an equatorial orbit, but may require more cryogen to keep the period between service visits to an acceptable interval.

The purpose of this study is to examine, in a substantial amount of detail, the design and performance of pointing and control systems for the two SIRTf vehicles, each system tailored to meet whatever special requirements are imposed by the selected orbit. In particular, this study defines a baseline system concept and configuration along with the primary operational modes in which the pointing and control system will be operated. Simplified models of the spacecraft structural dynamics, and disturbance sources both on-board and environmental, were also developed.

Once system concepts were in hand, combined with knowledge of the spacecraft and orbit environment, it was possible to design a control system to meet the pointing requirements. The performance of the designs was evaluated by simulating the operation of the system in its various operating modes and with the disturbance sources defined earlier.

The study consisted of three main tasks which are listed and described briefly below.

- (1) System Definition: Develop simplified dynamic models of the 98 deg and 28 deg spacecraft along with the primary disturbance sources expected for each system. Develop a baseline pointing and control system configuration.
- (2) Pointing and Control System Design: Develop the appropriate mathematical model for the pointing and control system including the proper sizing of actuators, selection of control laws, and selection of gains to account for and minimize effects due to on-board and environmental disturbances.
- (3) Performance Evaluation: Determine how well the systems designed in the preceeding two tasks perform relative to the baseline specifications. Primary modes of operation are large and small angle slews, and system response to previously specified disturbance sources. Evaluation criteria include time for pointing error to settle below 0.1 arcsec, total time required for a given maneuver, total required control effort, and whether or not active image stabilization is required.

These tasks describe a standard methodology for the initial phases of control system configuration and design. They were executed chronologically in the order listed above, and the remainder of this Executive Summary gives a condensed description of that process.

The basic requirements for the SIRTf pointing and control system are relatively general and straightforward. The system must be able to provide three axis inertial attitude control and point with an accuracy of one arcsecond. Reorienting the telescope between observations, a process called slewing, is specified in terms of the largest angular motion that will be required to avoid viewing the earth's limb, i.e., slewing 120 degrees in eight minutes. The other basic requirement which has a major impact on the design is for jitter, or image stability, to be better than 0.1 arcseconds in the presence of the typical kinds of disturbances found both onboard the spacecraft and in the orbital environment.

Constraints on the design of the pointing and control system must also be considered early in the design process in order to arrive at a configuration which will not only meet the performance requirements, but not violate important considerations related to the mission. For example, use of mass expulsion (thrusters) is a common means of providing backup attitude control and momentum dumping for reaction wheels. However, on SIRTf, the effluent from any kind of thruster control system (hot or cold gasses) will generate so much contamination that the use of any type of mass expulsion device is essentially eliminated. Other constraints include minimizing power consumption by the control system, and minimizing (or at least controlling) the effects of vehicle flexibility. A major subtask in the selection of a system configuration is the tradeoff of various types of actuators. Even though mass expulsion systems are not viable candidates, there are numerous other techniques for attitude and pointing control that have a wide array of advantages and disadvantages. The selection of single gimbal control moment gyroscopes (CMG's) was based on past experience combined with a review of available technology.

The heart of the study is contained in the second task in which models are developed for the two vehicles and for the set of disturbance phenomena to be used in the performance evaluation. The vehicle models are simplified in that the structural dynamics has been reduced to a set of rigid bodies connected by gimbals, springs, and dampers. While this approach does not come close to the level of detail available with conventional finite element modelling techniques, it does provide an excellent physical understanding of the main dynamical effects and is relatively easy to develop.

The disturbance sources considered in the study represent the primary types of forces acting on a spacecraft of this type which will affect the accuracy and image stability of the control system. After the baseline system configuration and spacecraft overall mass/geometric properties have been determined, then aerodynamic torques, gravity gradient torques, momentum unload torques, etc., can be calculated.

One of the more unusual, and potentially most severe, disturbance forces is the reaction inside the spacecraft of sloshing liquid helium. The problem of fuel slosh in rocket boosters has been studied over a period of nearly 35 years (Jack Lorell, "Forces Produced by Fuel Oscillations", Jet Propulsion Laboratory, October, 1951) and, in 1978, a study was made of cryogen slosh for the IRAS spacecraft which utilized a number of the results of previous efforts. The model for cryogen slosh developed for SIRTf was taken directly from the IRAS study (the IRAS study memo is reproduced in full in the appendix) and represents a simple, but physically accurate description of helium motion in the SIRTf dewar.

Once the basic performance requirements, modes of operation, vehicle dynamical properties, and primary disturbance sources are known and analysed, the actual design of the control system can take place. This iterative process consists of utilizing specialized, semi-automated design software to generate the set of feedback gains which control how much of each error signal is sent to the CMG's to torque the vehicle. The designer can request the software to configure a system which responds very quickly (but may

excite vibrations in the flexible appendages) or one which has longer time constants and therefore may take an excessive amount of time to execute a critical maneuver. The part of the process which cannot be automated is the judgment needed to select the control system characteristics that are the best compromise between these types of conflicting requirements.

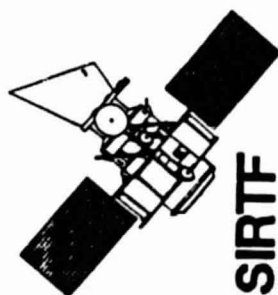
The final task consists of making a large number of computer runs of the combined vehicle/control system models with all of the various combinations of operating modes and disturbance inputs. Because there are two different spacecraft, all the simulations must be run in duplicate with the correct changes made to the inputs peculiar to the particular vehicle/orbit combination in order to generate the appropriate comparisons. The results of these simulations have been displayed in the body of report in three different forms: (1) as tabular data, (2) as parametric graphs, and (3) as representative time histories. It is therefore possible to see not only how the two spacecraft compare in performance, but comparisons can also be made among different control strategies, and levels of system capability.

The results of this study can be summarized in a few main points

- (1) The 98 degree orbit spacecraft is substantially more rigid than the 28 degree orbit spacecraft because the single fixed solar panel in the 98 degree design can be much more firmly attached to the vehicle than the two cantilevered panels in the 28 degree design.
- (2) The flexibility in the 28 degree orbit spacecraft is a driver in the selection of control strategies and poses a limitation on the pointing system performance if active image stabilization is not used.
- (3) Disturbance sources considered in this study did not cause degradation of pointing performance. Cryogen slosh, even during maneuvers with the largest acceleration profiles, did not interfere with control accuracy or stability.

- (4) The major driver for sizing the CMG's is related to requirements on small angle slews. The 120 degree slew in 8 minutes requirement is very mild and a system designed with this maneuver as its maximum capability would take in excess of 15 seconds to move seven arcminutes.
- (5) Active image stabilization will substantially improve performance for both spacecraft, especially for settling times of small angle slews in the 28 degree orbit case. However, AIS is not required to meet baseline performance requirements.

This report also includes, in appendices, specific numerical data related to the dynamical models used in the performance evaluations so that these models may be implemented and tested as required for future design studies. In addition, the complete graphical output of the computer simulations have been provided to personnel at the Ames Research Center as an archival record.



---

STUDY OVERVIEW  
DESIGN REQUIREMENTS  
SUMMARY OF RESULTS

---

## STUDY OBJECTIVES

The TISS Modification Study has four primary objectives as listed in the chart opposite. Basically they are: (1) to develop a concept for the SIRTf pointing and control system that meets the baseline requirements, (2) evaluate the performance of the system against a preselected set of onboard and environmental disturbance sources and a standard set of maneuvers to see if the design actually does what it's supposed to do, (3) determine what the performance limitations of the system are with respect to the kinds of maneuvers that may be required (or desired), the capability of the actuators, and the dynamics induced in the flexible structure of the spacecraft, and (4) evaluate whether or not some form of active compensation is required in the optical system to provide a suitably stable image in the presence of the various disturbing torques acting on the spacecraft.

An additional objective of the study, although not explicitly stated in the chart, is to gain an understanding of the differences in performance of pointing and control systems tailored for spacecraft designed for a 98 degree inclination sun synchronous orbit and a 28 degree inclination equatorial orbit.



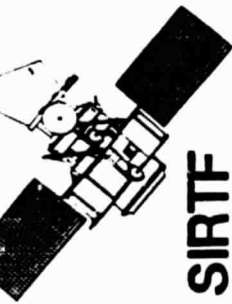
## STUDY OBJECTIVES

---

- DEVELOP DESIGN CONCEPT FOR THE SIRTF POINTING AND CONTROL SYSTEM
- EVALUATE SYSTEM PERFORMANCE BASED ON SELECTED OPERATING MODES AND DISTURBANCE SOURCES
- DETERMINE PERFORMANCE LIMITATIONS BASED ON SYSTEM SIZING, MANEUVER REQUIREMENTS, AND STRUCTURAL DYNAMICS
- EVALUATE NEED FOR ACTIVE IMAGE STABILIZATION

## STUDY OVERVIEW (1)

This chart describes the tasks related to defining which type of spacecraft model will be used and in which environment. The two orbit inclinations, 98 degrees and 28 degrees, define the general spacecraft configuration. The configuration, in turn, impacts the disturbance models, such as gravity gradient and aerodynamic torques, as well as the dynamics of the vehicle related to its size, flexibility, and shape.



# SIRTF

## SIRTF TISS MODIFICATION STUDY OVERVIEW (1)

---

### SIRTF FREE FLYER POINTING AND CONTROL SYSTEM

- SYSTEM DEFINITION
  - DEVELOP SIMPLIFIED DYNAMICAL MODELS OF 98<sup>0</sup> ORBIT AND 28<sup>0</sup> ORBIT SIRTF SPACECRAFT
  - DEVELOP MODELS OF PRIMARY DISTURBANCE AND ERROR SOURCES
  - DEFINE OPERATING MODES SENSITIVE TO POINTING AND CONTROL SYSTEM PERFORMANCE
  - SELECT A POINTING AND CONTROL SYSTEM CONFIGURATION CAPABLE OF MEETING BASELINE PERFORMANCE REQUIREMENTS

## STUDY OVERVIEW (2)

The design of the pointing and control system is, of course, directly dependent on the tasks listed in the previous chart. Once the system has been defined, then a control strategy, control laws, control gains, and actuator sizing can all take place. In particular, flexibility effects are a very important consideration in the selection of the torque profiles used to command the vehicle and also in the selection of control gains. The operating modes have direct impact on the sizing of the actuators. High performance maneuvers, such as fast slews, require larger torque and/or angular momentum capability than do maneuvers with low angular accelerations and rates. Closed loop performance evaluation consists of developing a simulation of the operating control system and exercising it in various modes to determine how well it performs. Objectives include comparing the performance of the 98 deg orbit vehicle and the 28 deg orbit vehicle, and evaluating the necessity for Active Image Stabilization.



## STUDY OVERVIEW (2)

---

- POINTING AND CONTROL SYSTEM DESIGN
  - GAIN SELECTION TO MINIMIZE FLEXIBILITY EFFECTS
  - TORQUE PROFILE SELECTION
  - ACTUATOR SIZING
  - ACTIVE IMAGE STABILIZATION SYSTEM DESIGN
- CLOSED LOOP PERFORMANCE EVALUATION
  - LARGE ANGLE SLEWS
  - SMALL ANGLE SLEWS
  - DISTURBANCE RESPONSE

#### BASIC REQUIREMENTS FOR POINTING AND CONTROL SYSTEM

This chart summarizes the basic requirements for a pointing and control system for use with an orbiting infrared observatory. Full three axis attitude control with inertial pointing capability in all attitudes are basic requirements. The low rate slew of 120 deg in 8 min is based on the need to perform three observations per orbit. The small slew angle capability requires very small attitude changes be made in a short time in order to scan a small section of sky. The goal is to move the vehicle and have the pointing error settle out in the minimum amount of time. The last requirement is by far the most demanding from the attitude control system. It is thus a potential driver for Active Image Stabilization (AIS) utilizing the telescope secondary mirror to correct for small pointing errors. A goal of the study is to determine whether or not some form of AIS is necessary to meet this requirement.



BASIC REQUIREMENTS FOR  
FREE FLYER POINTING AND CONTROL SYSTEM

---

- FULL 3-AXIS ATTITUDE CONTROL WITH BACKUP
- INERTIAL POINTING IN ANY ATTITUDE
- 120° SLEW IN 8 MIN (0.25°/SEC AVERAGE)
- SMALL ANGLE SLEW CAPABILITY - UP TO 7 ARCMIN
- 0.1 ARCSEC RMS IMAGE STABILITY IN PRESENCE OF ORBITAL AND ONBOARD DISTURBANCE SOURCES

## DESIGN CONSTRAINTS FOR POINTING AND CONTROL SYSTEM

This chart summarizes some of the considerations to be taken into account in designing the pointing and control system. Mass expulsion systems, which are a common way to provide attitude control and/or momentum unloading on many spacecraft (including the Shuttle Orbiter), are not acceptable for the reasons shown. In addition, any actuator(s) selected for the vehicle will have to operate with a relatively modest power budget of about 1 kW. While this is not a major constraint, it does have to be considered during the actuator sizing process. The third bullet enumerates the types of disturbances the pointing and control system is most likely to encounter and have to overcome. This list, which includes environmental, on board, and structural flexibility disturbances, defines the inputs to the simulation of the control system for the purpose of performance evaluation.



**SIRTF**

DESIGN CONSTRAINTS FOR  
FREE FLYER POINTING AND CONTROL SYSTEM

- MASS EXPULSION SYSTEM (OTHER THAN HE BOILOFF) NOT ACCEPTABLE
  - OPTICS CONTAMINATION FROM EFFLUENT
  - LIFETIME CONSIDERATIONS
  - IMPULSIVE EXCITATION OF STRUCTURAL DYNAMICS
- MINIMIZE POWER UTILIZATION BY CONTROL SYSTEM
- DISTURBANCE SOURCES
  - ENVIRONMENTAL (GRAVITY GRADIENT, AERO DRAG)
  - ONBOARD (ANTENNAS, SOLAR PANELS)
  - CRYOGEN SLOSH, STRUCTURAL DYNAMICS
  - MOMENTUM UNLOAD DISTURBANCE
  - CMG BEARING STICKION

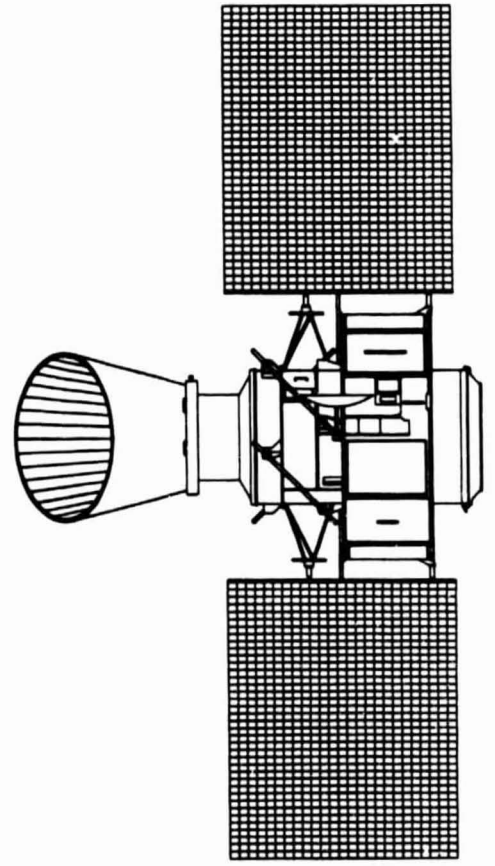
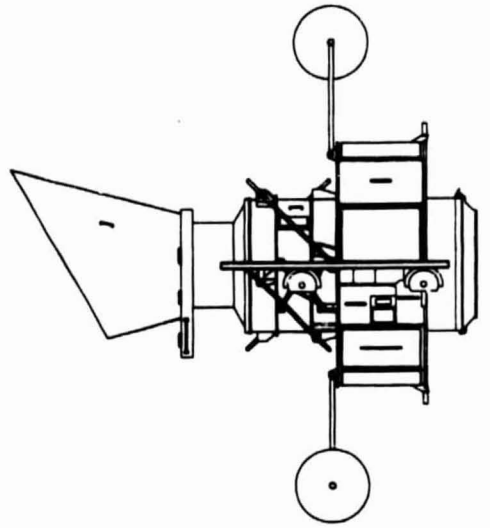
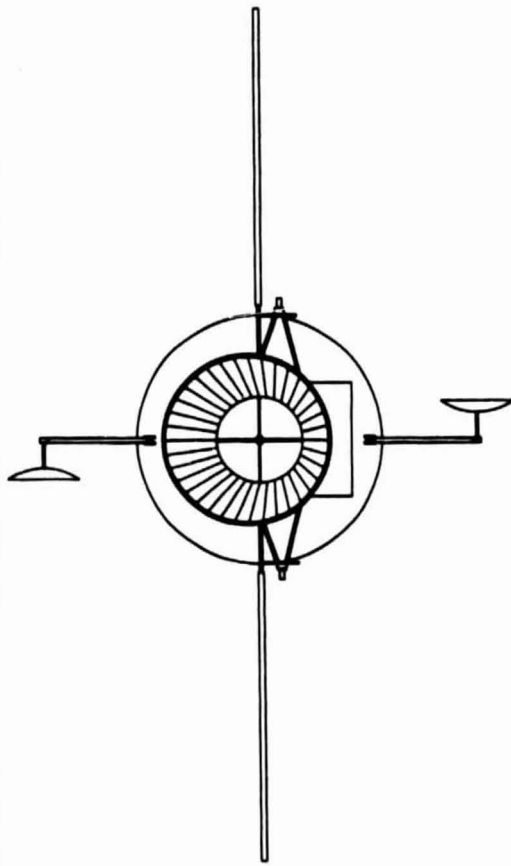
## 28 DEGREE ORBIT SPACECRAFT

This is a visual representation of the 28 degree orbit spacecraft which illustrates the major components dealt with in the development of the dynamic model used in this study. Features include the large (40 sq m) solar panels, sun shade, TDRSS antennae, dewar, and spacecraft support module.



**SIRTf**

28° ORBIT SIRTf SPACECRAFT



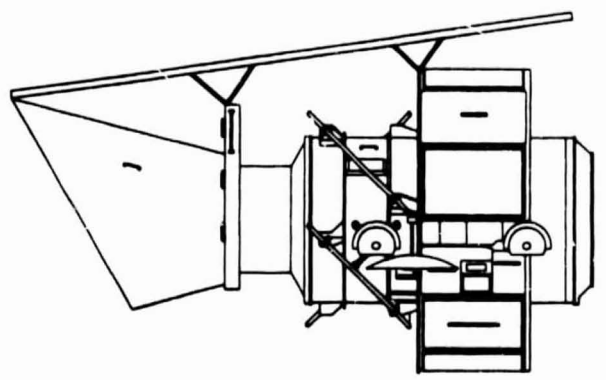
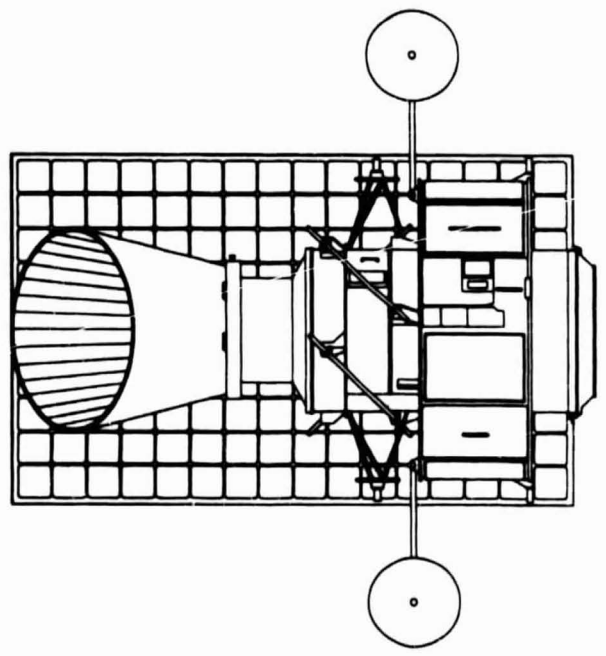
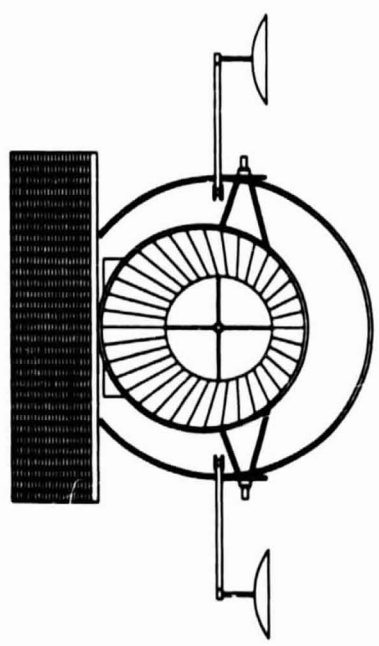
#### 98 DEGREE ORBIT SPACECRAFT

This chart shows the design, for the purposes of this study of the 98 degree orbit spacecraft. Virtually all of the components related to the telescope and spacecraft system are identical to the 28 degree design. The primary difference is the use of a single, relatively rigid solar panel which is firmly anchored to the vehicle proper in three locations. An additional difference is the increased mass of liquid helium in the cryogenic system.



**SIRTf**

98° ORBIT    SIRTf SPACECRAFT



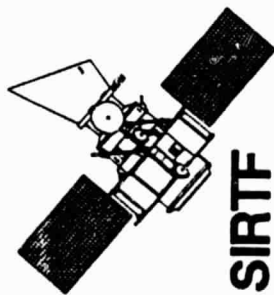
## SUMMARY OF RESULTS

This chart is a condensed summary of the results of the study. It is intended to provide highlights of the major conclusions reached through the analysis of the simulation results. The first two points indicate that the baseline models for the spacecraft and the pointing and control systems designed for them are capable of meeting the performance goals set out in the requirements section. That is, it was possible to perform the desired maneuvers, such as the rapid 90 deg in 90 sec slew or the various small angle slews, without causing undue structural excitation or requiring excessively large amounts of control torque. In addition, none of the on-board or environmental disturbance sources posed a problem for the pointing and control system. The most difficult results to interpret are the potential benefits to the operation of SIRT of using Active Image Stabilization. For the case of the 28 degree orbit vehicle, it is clear that use of AIS will substantially improve the response times during the small angle slew maneuvers. If the additional waiting period required for the pointing angle to settle out is a critical factor in the utilization of the telescope, then including some form of AIS would be justified. The use of AIS for the 98 degree orbit vehicle is less clear. While AIS definitely improves response to small angle slews, the spacecraft is so much more rigid that the incremental improvement in performance is not as large as for the 28 degree orbit case.



## SUMMARY OF RESULTS

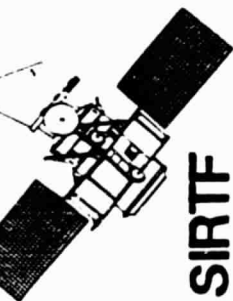
- BOTH SPACECRAFT CAN MEET PERFORMANCE GOALS EVEN IN WORST CASE MANEUVER/DISTURBANCE CONDITIONS
- FLEXIBILITY AND SLOSH DO NOT POSE SERIOUS PROBLEMS
- ACTIVE IMAGE STABILIZATION (AIS) IMPROVES SETTLING TIME RESPONSE FOR SMALL ANGLE SLEWS
- AIS PROVIDES MUCH GREATER BENEFITS TO 28<sup>0</sup> ORBIT SPACECRAFT THAN 98<sup>0</sup> ORBIT SPACECRAFT



---

## SIRTF FREE FLYER DYNAMIC MODELS

---



## 28° ORBIT SPACECRAFT

### DYNAMIC MODEL CONFIGURATION

- 7 RIGID BODIES
- TELESCOPE ASSEMBLY (WITH CRYO-TANKS AND INSTRUMENT CHAMBER) MODELLED AS ONE RIGID BODY
- CRYOGEN SLOSH MODELLED AS CONSTRAINED PENDULUM
- FLEXIBILITY MODELLED LOCALLY AT:
  - PODS
  - TDRSS ANTENNA MAST ATTACH POINTS
  - SOLAR PANEL ATTACH POINTS

#### 7-BODY DYNAMICS MODEL DEFINITION

This chart defines the body by its identification number (for location on drawings which follow), the number of degrees of freedom permitted in the model for the body, and a description of the physical meaning of the degrees of freedom.



## SIRTF 7-BODY DYNAMICS MODEL DEFINITION

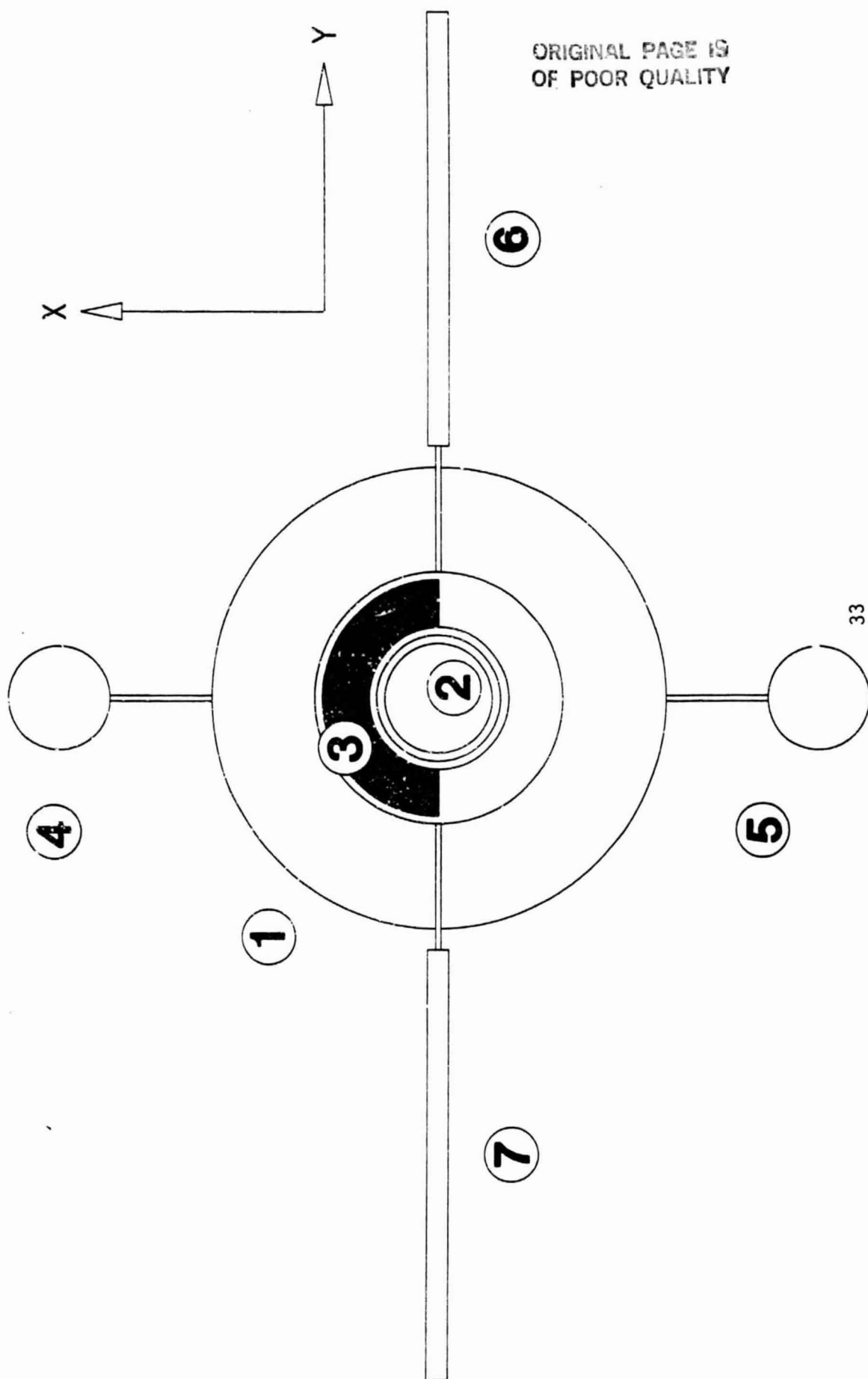
BODY #	DESCRIPTION	No of DOFs and Types
1	Spacecraft	6 X,Y,Z Translation, X,Y,Z Rotation
2	Telescope	2 X and Y Rotation (Flexibility)
3	Liquid He	1 Z Rotation (Slosh Model)
4	TDRSS Antenna #1	2 Y and Z Rotation (Flexibility)
5	TDRSS Antenna #2	2 " " " "
6	Solar Array #1	3 X,Y and Z Rotation "
7	Solar Array #2	3 " " " "

#### 28 DEGREE SPACECRAFT MODEL X-Y PLANE

This view of the 28 degree spacecraft model looking down the telescope optical axis (model z-axis) and illustrates all seven bodies in the model.



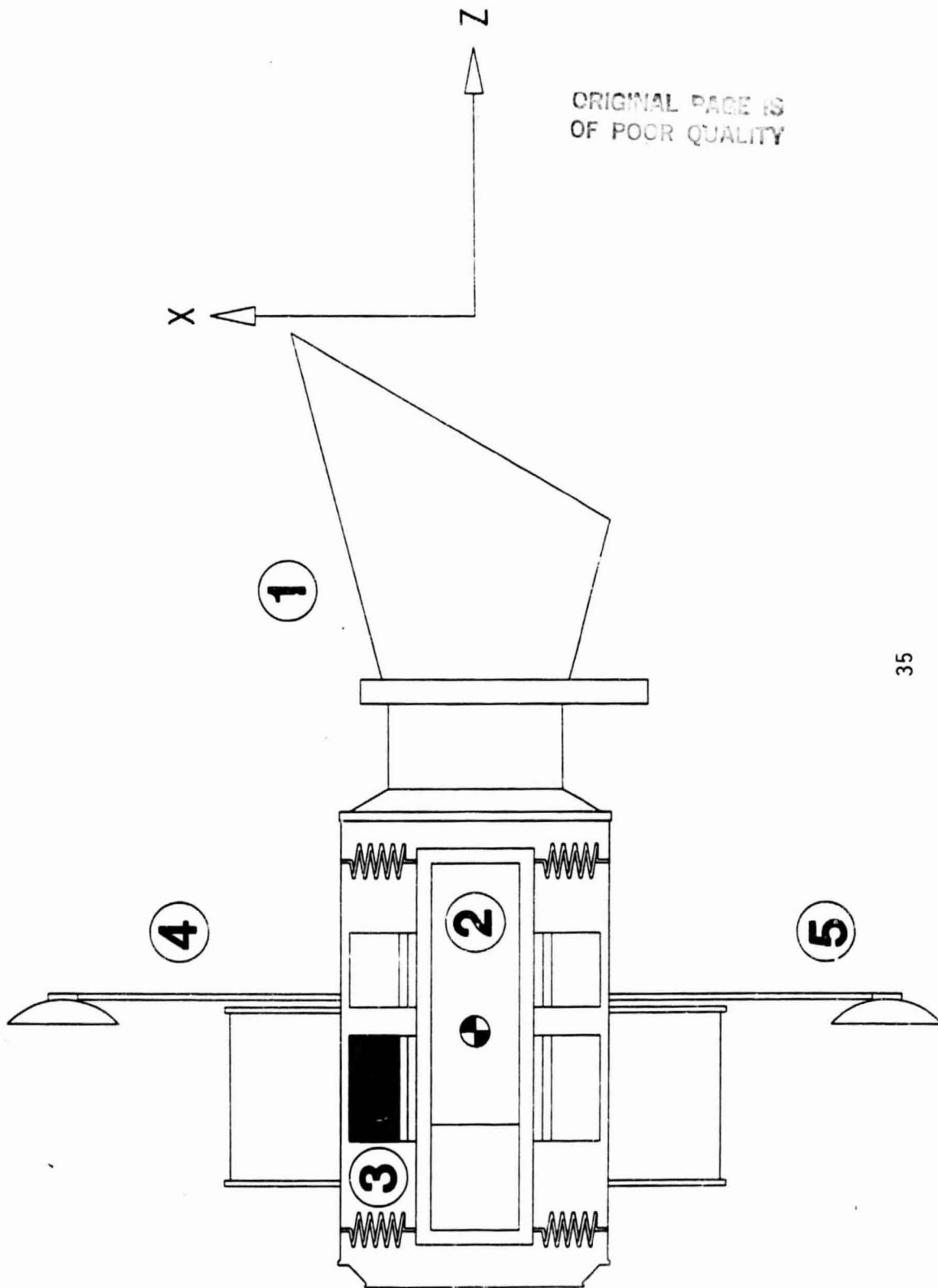
# 28° ORBIT MODEL - VIEW OF X-Y PLANE



## 28 DEGREE SPACECRAFT MODEL X-Z PLANE

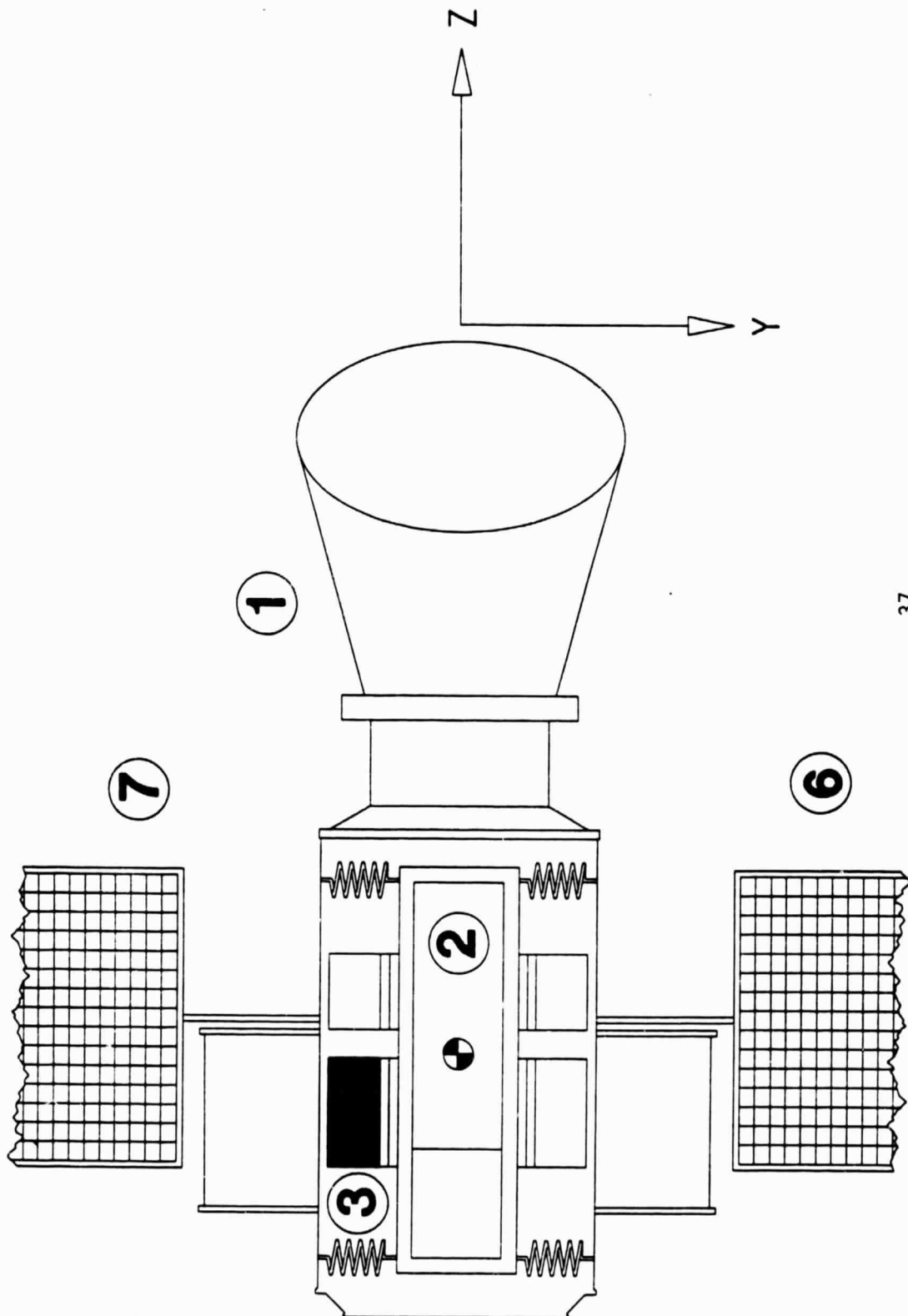
This view of the 28 degree spacecraft model shows how the telescope, dewar and solid cryogen comprise body #2 with spring attachments (PODS) connecting body #2 to the spacecraft (body #1). The liquid cryogen is shown as body #3.

28° ORBIT MODEL - VIEW OF X-Z PLANE



#### 28 DEGREE SPACECRAFT MODEL Y-Z PLANE

This chart is similar to the preceeding chart except that the solar panels are shown in this view instead of the TDRSS antennae.



## 28 DEGREE ORBIT DYNAMICS MODEL MASS/INERTIA PROPERTIES

The table in this chart lists the mass and inertia properties of the 28 degree orbit spacecraft. There are two important points to note. The first is the product of inertia Iyz which is a result of the axial asymmetry of the sunshade and vacuum closure. The second is the fact that the individual moments of inertia for the each body have been calculated with respect to the hinge or pivot point for that body. This was done because the NBODY computer program requires input with this format. However, the total moments of inertia are calculated with respect to the vehicle center of mass so that the values listed under the heading "TOTAL SYSTEM" represent total moments with respect to the center of mass.



# SIRTF

## SIRTF 28 DEG ORBIT

### DYNAMICS MODEL DEFINITION - MASS/INERTIA PROPERTIES

SIRTF 28 Deg ORBIT		DYNAMICS MODEL DEFINITION		MASS/INERTIA PROPERTIES		
DESCRIPTION	Mass (Kg)	Ixx *	Iyy	Izz	Iyz	
1 Spacecraft	5766.	13241.	12661.	12748.	-1560.	
2 Telescope	1086.	1865.	1865.	472.		
3 Liquid He	208.	102.	102.	130.		
4,5 TDRSS Antennas	@ 21.	93.7	93.7	17.		
6,7 Solar Arrays	@ 85.	532.	44.	488.		
TOTAL SYSTEM	7282.	18608.	15583.	17259.	-1764	

\* INERTIAS are in  $\text{Kg-m}^2$ . They are referred to each body own pivot point. However, inertias of the total system are with respect to the composite center of mass.

## 98 DEGREE ORBIT SPACECRAFT

The the 98 degree orbit spacecraft model is very similar to the 28 degree one. The main differences are in the solar panels and the disposition of the cryogen tanks. In this study, the sunshade was made identical to the 28 deg design for simplicity, although in a real system it would be smaller, like IRAS. The dynamic model configuration for the 98 degree orbit spacecraft consists of five rigid bodies which are interconnected with springs and/or three-axis gimbals. The telescope, the dewar, and the instrument chamber have been modelled as a single rigid body connected by the PODS to the Support Systems Module with a system natural frequency of approximately 20 Hz. The liquid cryogen has been modelled as a rotating mass which behaves like a constrained pendulum. The details of this model are described in a later section. The flexibility in the spacecraft system has been simplified to consider only the major components which will exhibit noticeable dynamical effects. These are listed in the fourth bullet.



## 98° ORBIT SPACECRAFT

### DYNAMIC MODEL CONFIGURATION

- 5 RIGID BODIES
- TELESCOPE ASSEMBLY (WITH CRYO-TANKS AND INSTRUMENT CHAMBER MODELLED AS ONE RIGID BODY)
- SUPPORT MODULE INERTIAS INCLUDE SOLAR PANEL
- FLEXIBILITY MODELLED LOCALLY AT
  - PGDS
  - TDRSS ANTENNA ATTACH POINTS

## 5-BODY DYNAMICS MODEL DEFINITION

This chart defines the body by its identification number (for location on drawings which follow), the number of degrees of freedom permitted in the model for the body, and a description of the physical meaning of the degrees of freedom.



SIRTF 98 DEG ORBIT  
5-BODY DYNAMICS MODEL DEFINITION

BODY #	DESCRIPTION	Number and Type of Degrees Of Freedom
1	Spacecraft *	6 X,Y,Z Translations X,Y,Z Rotations
2	Telescope	2 X and Y Rotations (PODS Flexibility)
3	Liquid He	1 Z Rotation (Slosh model)
4	TDRSS Antenna #1	2 X and Z Rotations (Flexibility)
5	TDRSS Antenna #2	2 " " " "

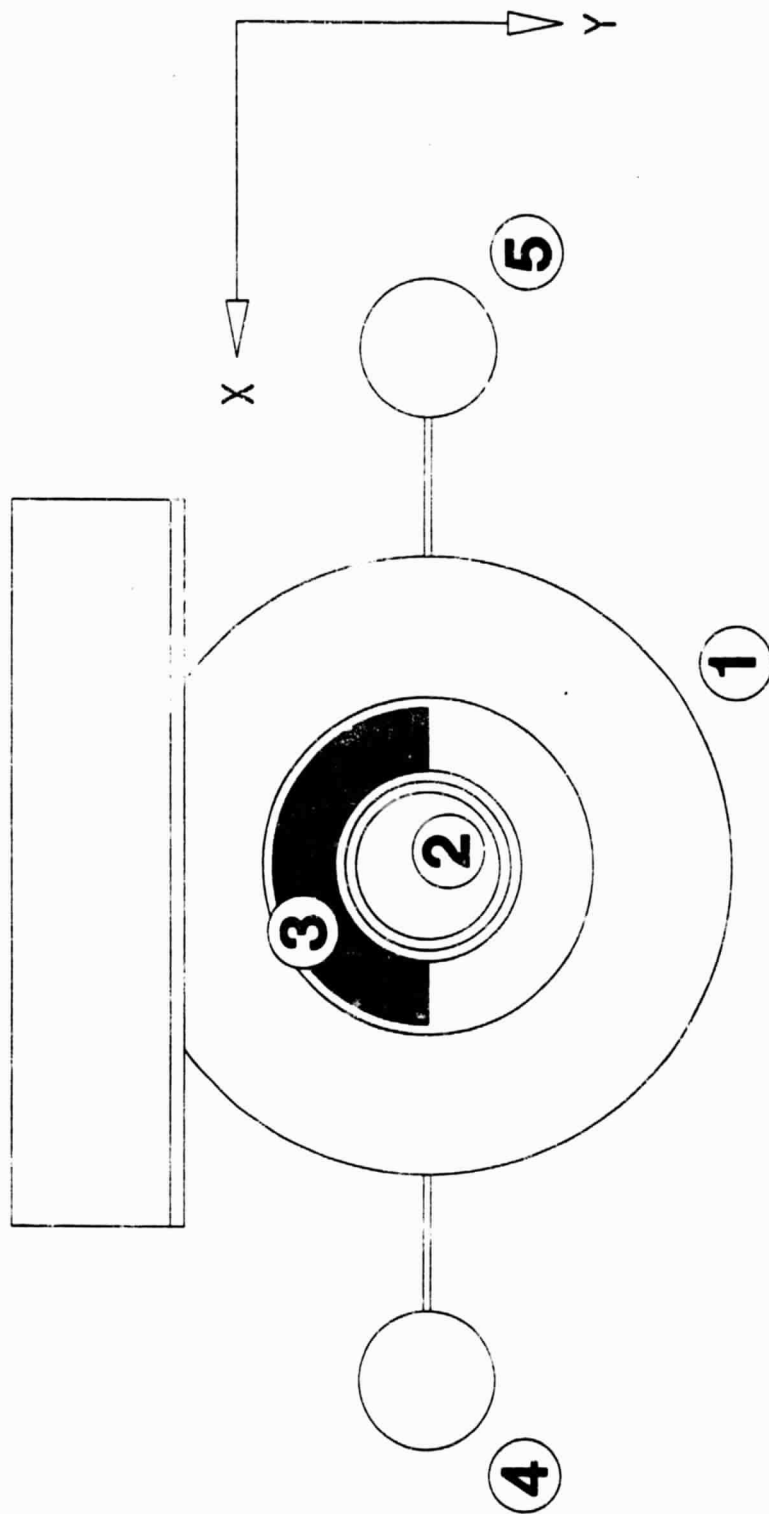
\* Includes the Solar Array attached to it.

98 DEGREE SPACECRAFT MODEL X-Y PLANE

This view of the 98 degree spacecraft model looking down the telescope optical axis (model z-axis) illustrates all five bodies in the model.



# 98° ORBIT MODEL - VIEW OF X-Y PLANE

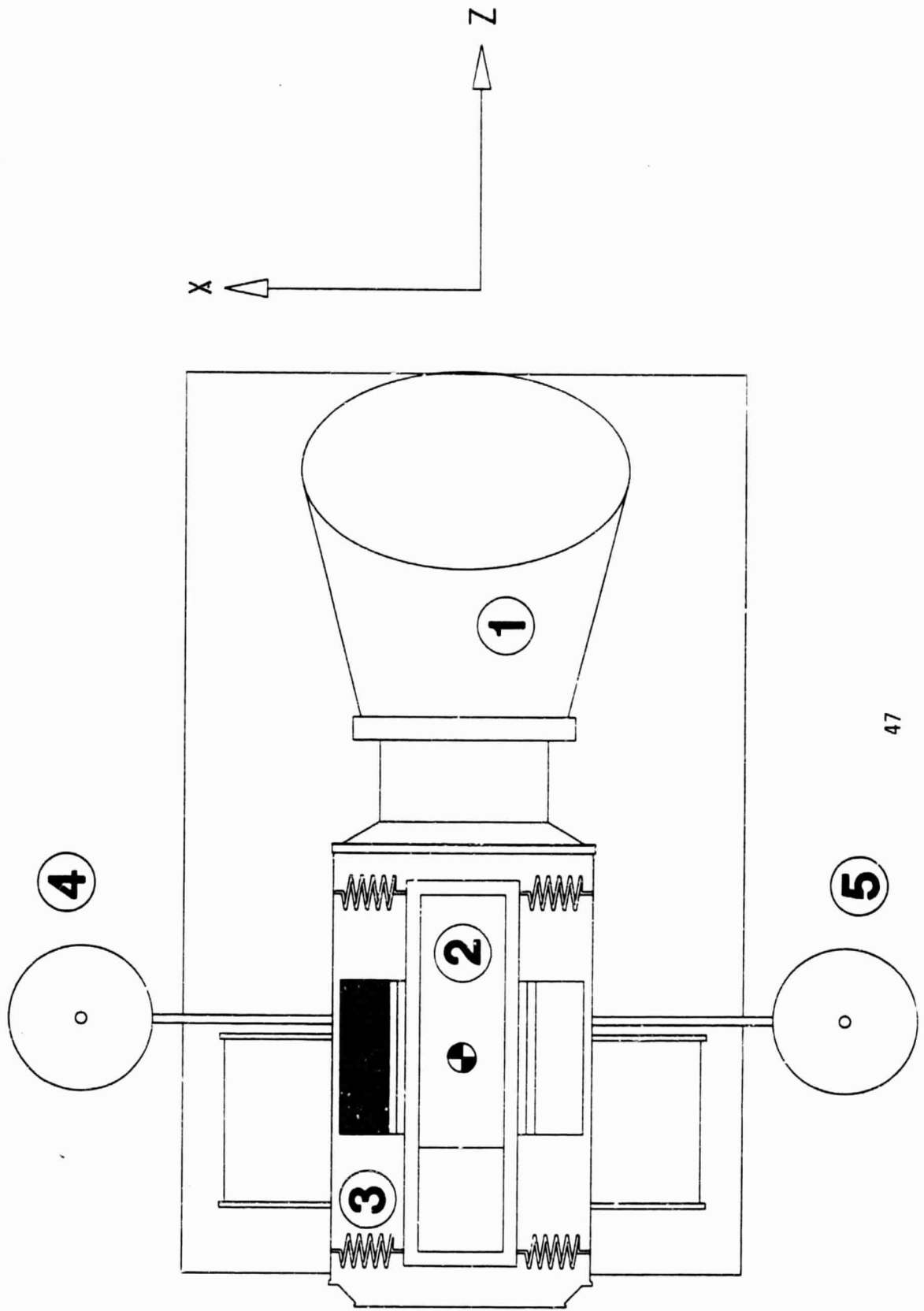


#### 98 DEGREE SPACECRAFT MODEL X-2 PLANE

This view of the 98 degree spacecraft model shows how the telescope and dewar comprise body #2 with spring attachments (PODS) connecting body #2 to the spacecraft (body #1). The liquid cryogen is shown as body #3, TDRSS antennae as bodies #3 and #4.



98° ORBIT MODEL - VIEW OF X-Z PLANE

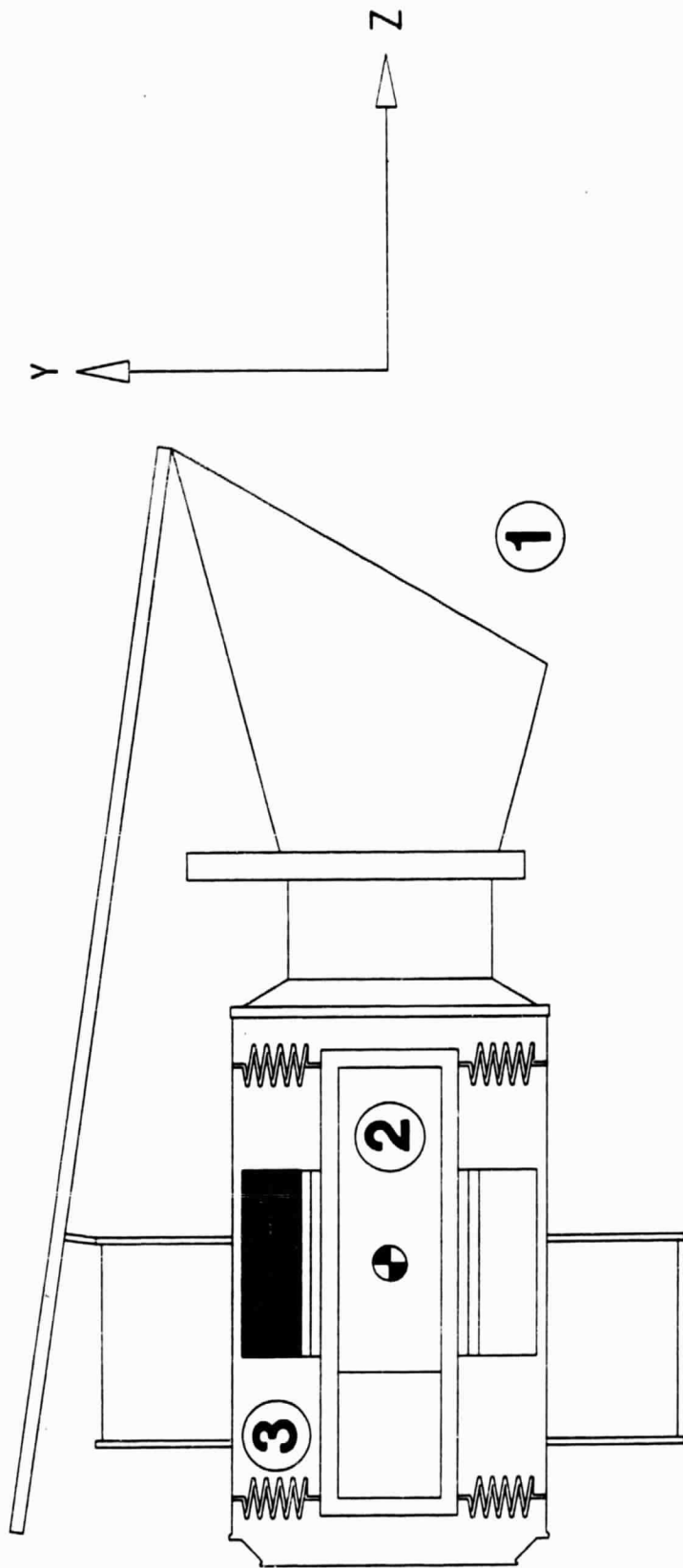


#### 98 DEGREE SPACECRAFT MODEL Y-Z PLANE

This chart is similar to the preceeding chart except that the TDRSS antennae are not shown (vehicle rotated 90 deg). Note how the solar panel is rigidly attached to and considered a part of body #1. Note also the different location of the helium tank (as compared to the 28 degree model) and the identical sunshade.



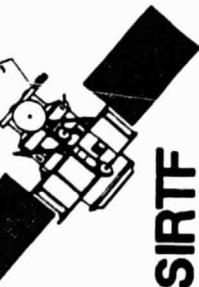
98° ORBIT MODEL - VIEW OF Y-Z PLANE



## 98 DEGREE ORBIT DYNAMICS MODEL MASS/INERTIA PROPERTIES

The table in this chart lists the mass and inertia properties of the 98 degree orbit spacecraft. There are two important points to note. The first is the product of inertia Iyz which is a result of the axial asymmetry of the sunshade, vacuum closure and solar panel. The second is the fact that the individual moments of inertia for each body have been calculated with respect to the hinge or pivot point for that body. This was done because the NBODY computer program requires input with this format. However, the total moments of inertia are calculated with respect to the vehicle center of mass so that the values listed under the heading "TOTAL SYSTEM" represent total moments with respect to the center of mass.

Note that the sunshade used in this model is conservative for a polar orbit and thus the moments of inertia would probably be smaller with a lighter sunshade of the IRAS type. The increase in cryogen mass is compatible with the current sunshade geometry. Note also that the value for the cryogen mass which appears in the table is half of the total initial mass. This was deliberate so that the effect of cryogen slosh would be maximized.

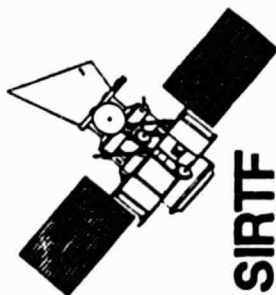


# SIRTF

## SIRTF 98 DEGREE ORBIT DYNAMICS MODEL DEFINITION - MASS/INERTIA PROPERTIES

DESCRIPTION	MASS (Kg)	Ixx *	Iyy	Izz	Iyz
1 Spacecraft (Includes S.A)	5831.	14940.	12650.	13309.	-2608.
2 Telescope	936.	1366.	1366.	327.	
3 Liquid He	320.	285.	285.	200.	
4,5 TDRSS Antennas @ 21.		85.	85.	17.	
TOTAL SYSTEM	7129.	16520.	15017.	14626.	-2608.

\* Inertias are in Kg.m<sup>2</sup> with respect to each body own pivot point. However, inertias of the Total System are with respect to the composite mass center.



---

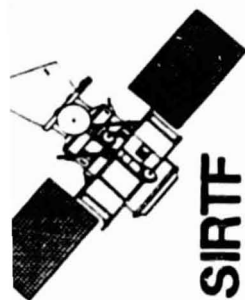
## DISTURBANCE MODELS

---

PRECEDING PAGE PLANK NOT FILLED

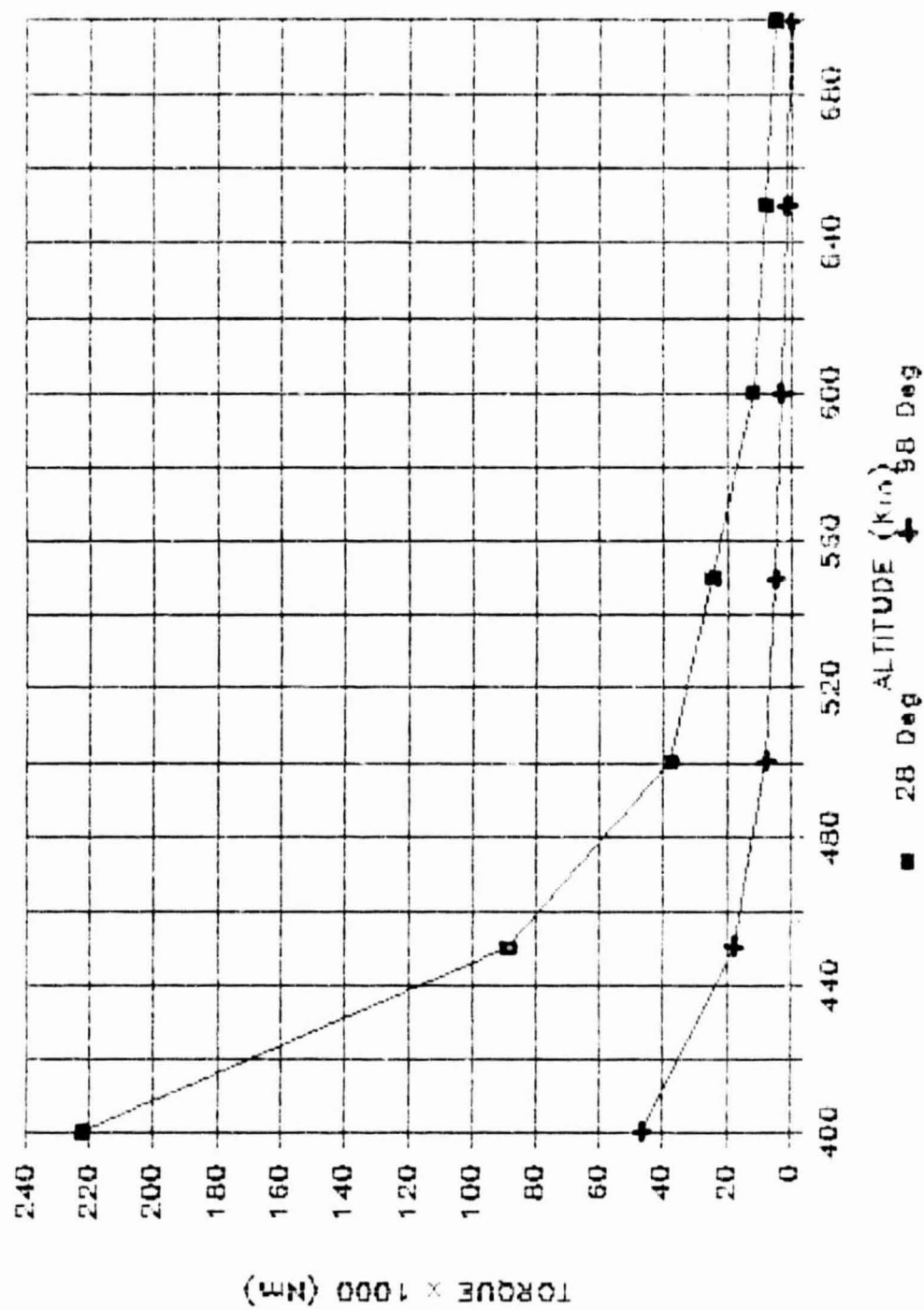
#### AERODYNAMIC TORQUES

This chart is a plot of the aerodynamic torque experienced by each spacecraft model as a function of altitude. The calculation requires knowledge of the density as a function of altitude, an approximation of the drag coefficient for the spacecraft configuration, and the incident surface area. In addition, the center of pressure relative to the center of mass must be calculated. It is important to note that this is not a measure of the aerodynamic drag responsible for the rate of decay of the orbit. Also note the rather steep slope of the curve for the 28 degree orbit case, indicating that orbits in the 600 km to 700 Km range are preferable.



**SIRT**

# AERODYNAMIC TORQUES

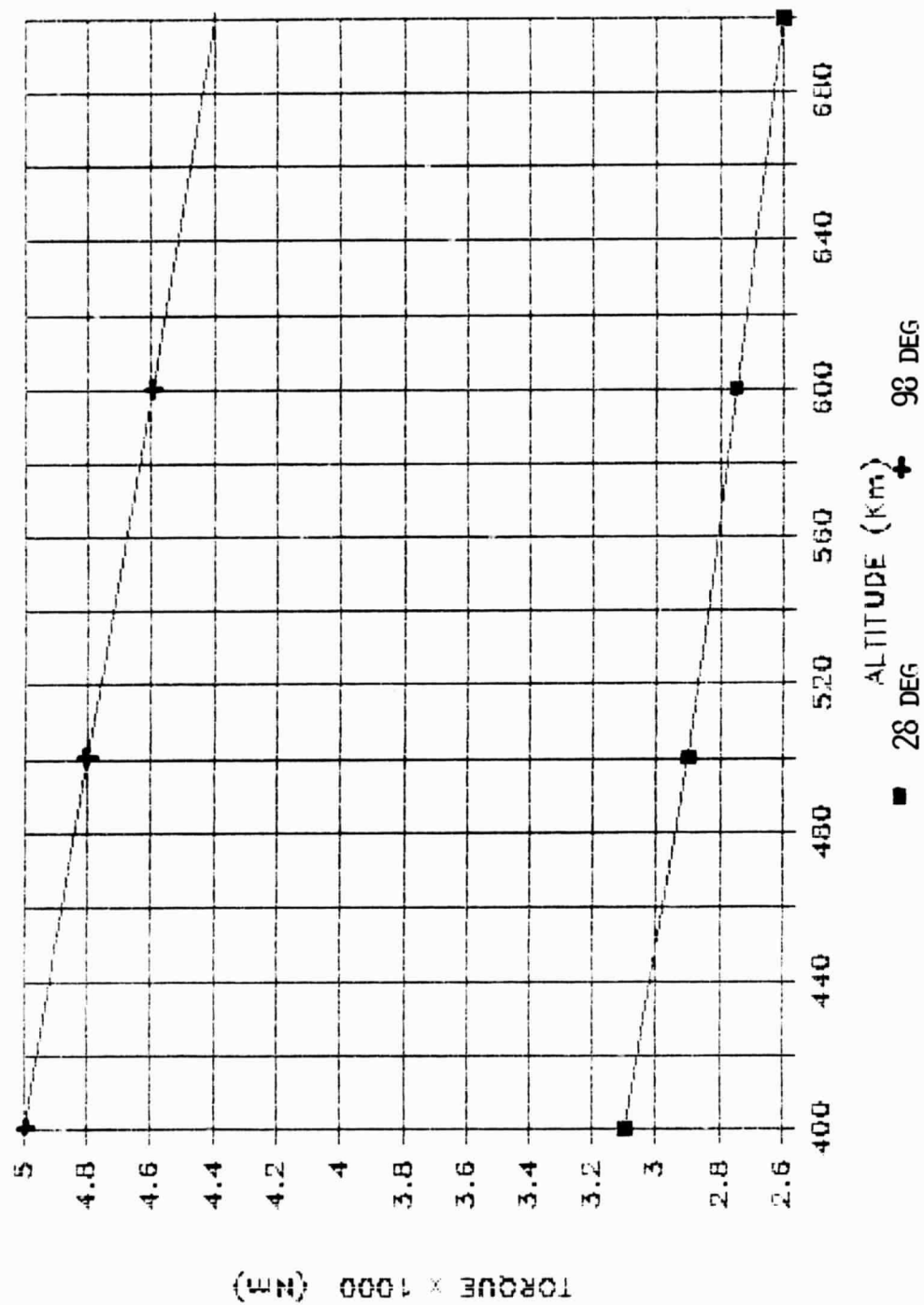


#### GRAVITY GRADIENT TORQUES

This chart plots the worst case gravity gradient torque on each of the two spacecraft as a function of orbital altitude. The primary term that drives the magnitude of gravity gradient forces is the difference between principal moments of inertia. Especially in the case of the 28 degree orbit spacecraft, the moments of inertia are nearly equal due to the contribution to  $I_{zz}$  of the large solar panels.



# GRAVITY-GRADIENT TORQUES



#### ONBOARD DISTURBANCES    CRYOGEN SLOSH

The cryogen slosh model used in this study is a highly simplified model derived from work done for the Space Tug Proposal at Lockheed and for the IRAS project by individuals at ARC, JPL, Fokker, and Stanford. The documentation for the model is available as an ARC memo. The memo develops three possible configurations for a sloshing fluid in a toroidal tank and cites experimental data with liquid helium in zero g to justify some of the assumptions and choices of values for parameters.



## CRYOGEN SLOSH

- MODEL DEVELOPED FROM IRAS ACS SIMULATION MODEL (NASA-ARC MEMO SPI-8-93:244-13, SEPT. 1978)
- PHYSICAL DATA DOCUMENTED BY MASON AND COLLINS ON NASA KC 135 ZERO G EXPERIMENTS
- PENDULUM CONCEPT ORIGINALLY DEVELOPED BY MARGULIES FOR LMSC SPACE TUG PROPOSAL (APRIL 1975)

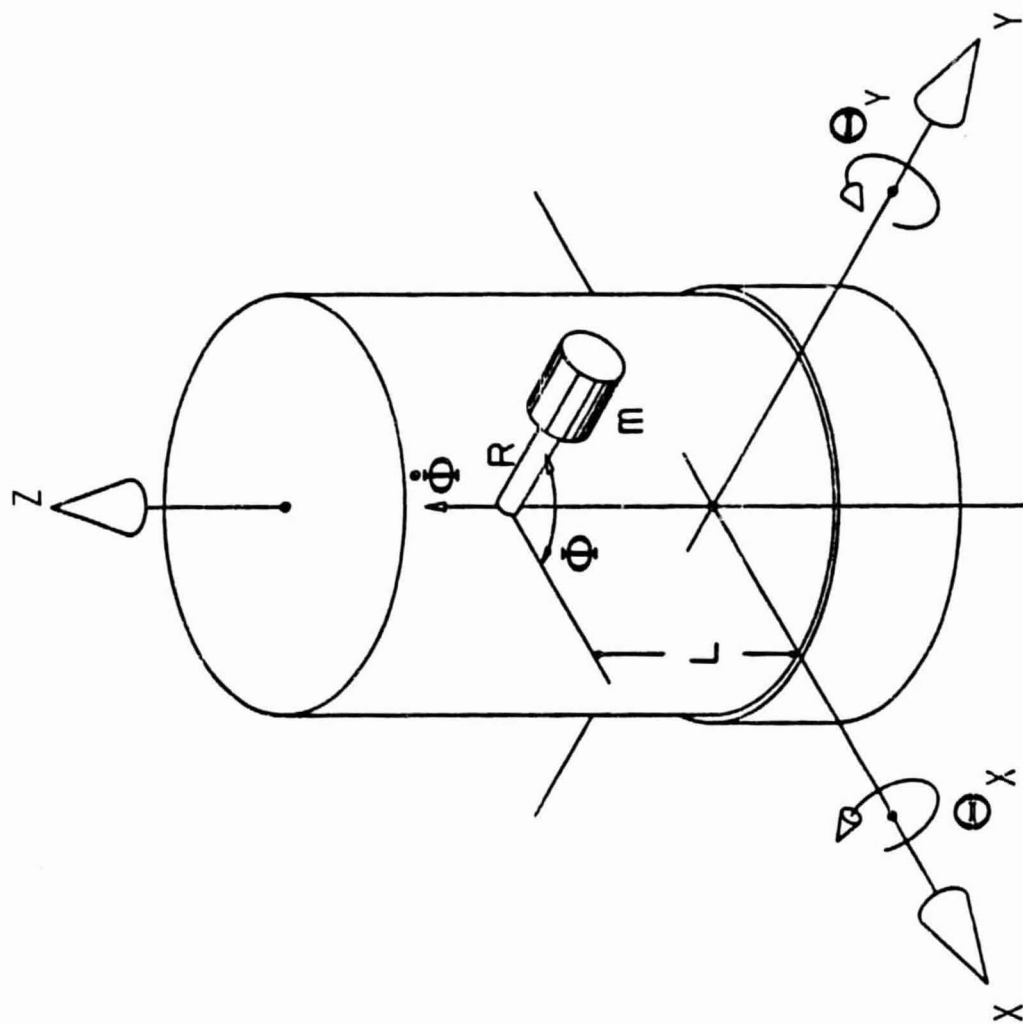
#### CRYOGEN SLOSH MODEL GEOMETRY

This chart illustrates the general configuration of a rotating pendulous mass inside a cylindrical body. The mass  $m$  represents a large volume of liquid which is rotating about the longitudinal axis of the spacecraft. Spacecraft attitude motions about the X and Y axes will excite the motion of the pendulum which in turn will apply reaction forces on the spacecraft proper as it (the pendulous mass) rotates.



**SRTF**

# CRYOGEN SLOSH MODEL GEOMETRY



## SOURCES AND DISTURBANCE MAXIMUM VALUES

This chart is a brief summary of the types of disturbance sources considered in this study and the maximum values these sources attain. The onboard disturbances are of much greater significance and, in particular, the reaction forces from the solar panel dynamics can become quite large. It should be noted that these values are the maximum that could be expected and that these maxima occur primarily during transients in the more extreme maneuvers (e.g., a bang-cruise-bang 90 deg/ 90 sec slew).

The disturbance levels shown for antenna and solar panel actuation are representative of the performance during an observation if an one of these devices were activated. The torque level of 0.1 Nm is the maximum reaction step torque that the antennas or solar panels should apply to the vehicle .



**SIRTF**

SOURCES AND DISTURBANCE MAXIMUM VALUES

	98° ORBIT (700 KM)	28° ORBIT (600 KM)
• ENVIRONMENTAL		
- GRAVITY GRADIENT	$2.6 \times 10^{-3}$ N-M	$4.4 \times 10^{-3}$ N-M
- AERODYNAMIC (ARDC MODEL)	$1 \times 10^{-3}$ N-M	$12 \times 10^{-3}$ N-M
• ONBOARD		
- STRUCTURAL DYNAMICS	-	-
- FLEXIBLE APPENDAGES	.15 N-M	30 N-M
- CRYOGEN SLOSH (IRAS MODEL)	$2 \times 10^{-3}$ N-M	.1 N-M
- ACTUATOR STICKION	.3 N-M	.3 N-M
- MOMENTUM DUMP	.1 N-M	.1 N-M
- ANTENNA AND SP ACTUATION	.1 N-M	.1 N-M

#### COMPARISON OF 28 DEG AND 98 DEG MISSION DYNAMICAL MODELS

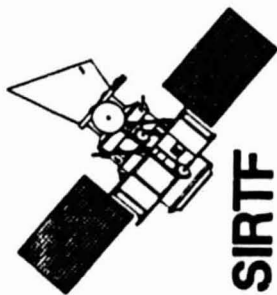
This chart summarizes the salient characteristics of the two dynamical models and points out where differences exist and for what reasons.



COMPARISON OF 28° AND 98° MISSION  
DYNAMICAL MODELS

SIRTF

	28° ORBIT VEHICLE	98° ORBIT VEHICLE
OVERALL CONFIGURATION	SIMILAR TO SPACE TELESCOPE	SIMILAR TO IRAS
SOLAR PANELS	TWO - EXTENDED FROM VEHICLE	ONE MOUNTED DIRECTLY ON VEHICLE
CRYOGEN	SOLID HYDROGEN AND SUPERFLUID H <sub>E</sub>	SUPERFLUID H <sub>E</sub>
VEHICLE INERTIAS	AFFECTED BY LARGE SOLAR ARRAYS	LESS DUE TO MORE COM- PACT CONFIG.
VEHICLE FLEXIBILITY	AFFECTED BY LARGE SOLAR ARRAYS	STIFFER VEHICLE MORE CRYOGEN TO SLOSH
ALTITUDE	600 KM	700 KM
DISTURBANCES	GRAVITY GRADIENT LESS DUE TO SMALLER $\Delta I$	HIGHER ORBIT REDUCES GRAV. GRAD. TORQUE
	AERO TORQUE LARGER DUE TO SOLAR PANELS AND LOWER ORBIT	HIGHER ORBIT AND COMPACT CONFIG. REDUCES AERO TORQUE



---

POINTING AND CONTROL SYSTEM CONFIGURATION

---

67

PRECEDING PAGE BLANK NOT FILMED

PAGE 67 INTENTIONALLY BLANK

## POINTING AND CONTROL SYSTEM BASIC TRADEOFFS (1)

This chart describes in tabular form the advantages and disadvantages of a number of candidate actuation mechanisms for attitude and pointing control. In particular, the basic reasons for selecting devices such as reaction wheels and single- or double-gimbal control moment gyroscopes are enumerated. The data on this chart and the continuation chart on the next page form the rationale for the system configuration discussed in detail later in this section.



# POINTING AND CONTROL SYSTEM SYSTEM CONFIGURATION

## BASIC TRADEOFFS (1)

<u>CANDIDATE SYSTEM</u>	<u>ADVANTAGES</u>	<u>DISADVANTAGES</u>	<u>COMMENT</u>
He BOILOFF	CONVENIENT FUEL SUPPLY - PRECISE DIFFERENTIAL TORQUE CAPABILITY	CONTROL AUTHORITY AT NOMINAL MASS FLOW RATE IS TOO LOW	GP-B MAY HAVE TO INCREASE MASS FLOW TO GET CONTROL AUTHORITY
MASS EXPULSION			NOT CONSIDERED
GEOMAGNETIC TORQUERS	ACCURACY, RELIABILITY, LOW COST	LOW CONTROL AUTHORITY	GOOD MOMENTUM DUMP AND BACKUP STABILIZATION SYSTEM (IRAS)
REACTION WHEELS	FULL 3-AXIS CONTROL LARGE MOMENTUM STORAGE CAPABILITY	RELATIVELY LOW TORQUE AVAILABLE, BEARING STICITION, AND VARIABLE NOISE PSD	POWER REQUIRE- MENTS ARE HIGH
MOMENTUM WHEELS	ACCURACY, ONLY MODERATE MECHANICAL NOISE	RELATIVELY LOW TORQUE AND MOMENTUM STORAGE CAPABILITY, LARGE MOMENTUM BIAS	REQUIRES 4 WHEELS TO OBTAIN A ZERO- MOMENTUM CONFIGUR- ATION

## POINTING AND CONTROL SYSTEM BASIC TRADEOFFS (2)

This chart compares double- and single-gimbal CMG's in the same format as the preceding chart. Based on the discussion in the "Advantages" and "Disadvantages" columns, single gimbal CMG's were selected as the best available candidate for the SIRTf pointing and control system. The overall mechanical simplicity, the redundancy provided by a cluster of six units (six pack configuration, to be described later in this section), and the wide range of available capability were the three factors motivating the selection. It is important to note that double-gimbal CMG's would easily meet SIRTf's requirements and the selection of different technology was a matter of engineering judgment.



**SIRTF**

POINTING AND CONTROL SYSTEM  
SYSTEM CONFIGURATION

BASIC TRADEOFFS (2)

<u>CANDIDATE SYSTEM</u>	<u>ADVANTAGES</u>	<u>DISADVANTAGES</u>	<u>COMMENT</u>
DOUBLE-GIMBAL CMG's	LARGE MOMENTUM 2-AXES OF CONTROL PER UNIT, CONSTANT NOISE PSD	LOW TORQUE CAPABILITY MECHANICAL COMPLEXITY LOWER RELIABILITY	3 UNITS REQUIRED FOR REDUNDANCY
SINGLE-GIMBAL CMG's	LARGE MOMENTUM AND TORQUE CAPABILITY CONSTANT NOISE PSD GOOD RELIABILITY OFF-THE-SHELF FLIGHT HARDWARE AVAILABLE	BEARING COMPLIANCE AND STICKION, COMPLEX STEERING LAWS REQUIRE DEDICATED CONTROL PROCESSOR	MODEST POWER, CLUSTER OF 6 SUPERIOR TO CLUSTER OF 4

# CMG SIZING AS A FUNCTION OF DESIRED SLEW PERFORMANCE

This chart shows graphically the relationships between the desired slew performance, i.e. slew time and slew angle, and the momentum and torque required from the CMG to achieve this performance. The slew time/slew angle plane can be parametrized by lines corresponding to a given torque capability, or by lines corresponding to a given momentum capability. This is because, for a given slew profile, the torque  $T$  is proportional to slew angle and to the reciprocal of the square of the slew time, while the momentum  $H$  is proportional to the slew angle, but to the reciprocal of the slew time only. In other words :

$$T \sim \theta / t^2 \quad \text{and} \quad H \sim \theta / t$$

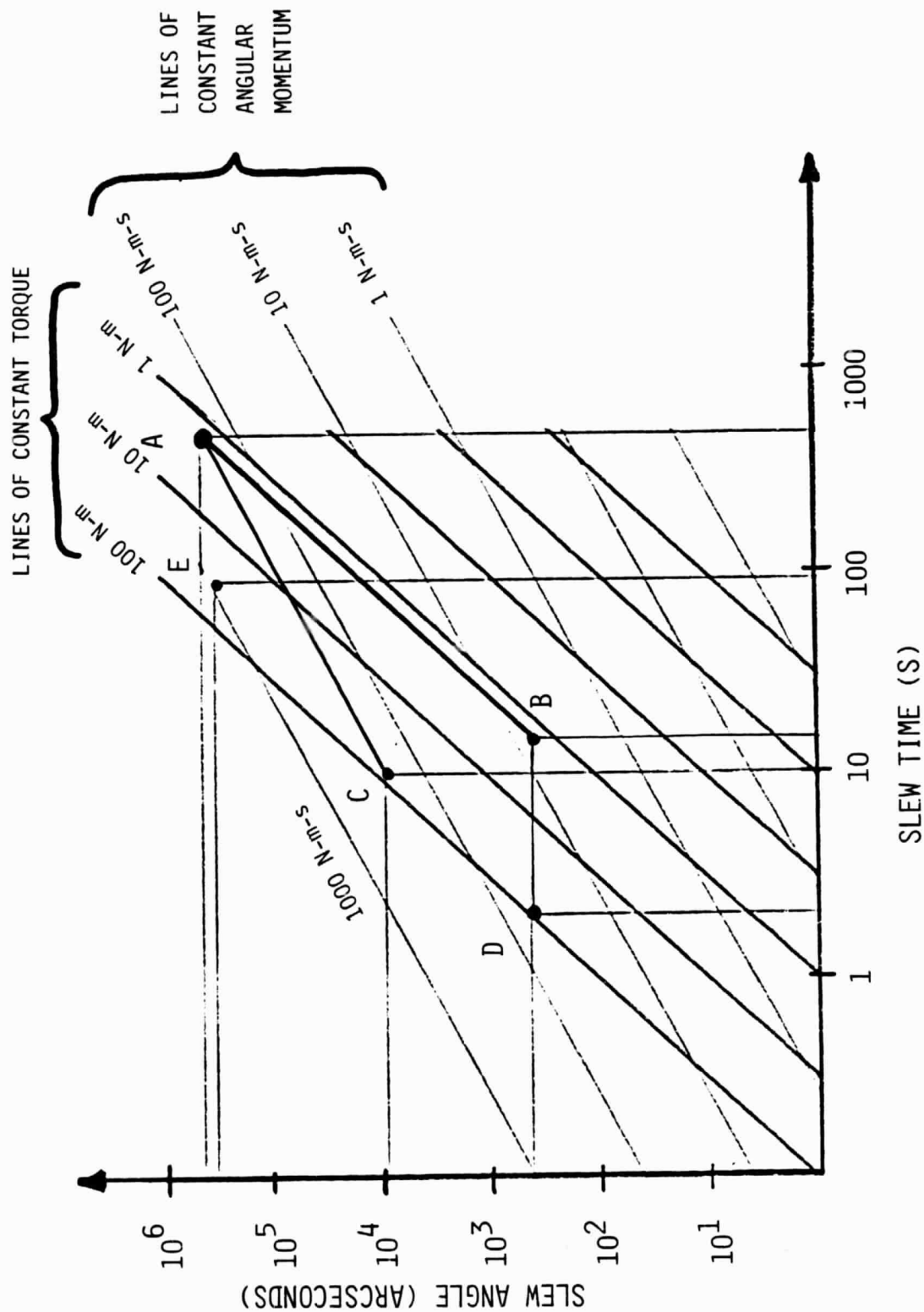
The curves shown on the chart correspond to Sine-Versine slews and to the 28 deg orbit vehicle. Curves corresponding to the 98 degree case would be only slightly different, since  $T$  and  $H$  are directly proportional to the inertias.

Various slew conditions are shown on the chart and labeled as A, B, C, D, and E. Point A corresponds to the nominal requirement of 120 degrees in 8 minutes slew. If the CMG system is sized to meet this requirement and no more, then the system cannot operate on the left of either lines AC or AB which define the maximum torque and maximum momentum respectively. Point B corresponds to a 7 arcmin slew, and it can therefore be seen that the minimum achievable slew time is about 15 seconds. If one decides to relax the torque limitation, but maintain the momentum limitation, then points C or D can be achieved. Point D corresponds to a 7 arcmin slew in 2 seconds, while point C is a 2.5 degree slew in 10 seconds, requiring the same momentum storage capacity as A. Finally, if high performance is desired, such as a 90 degree slew in 90 seconds (point E), larger values for torque and momentum are needed.



**SIRTF**

# CMG SIZING AS A FUNCTION OF DESIRED SLEW PERFORMANCE



## MINIMUM MOMENTUM AND TORQUE REQUIREMENTS

This chart shows the magnitude of momentum and torque that must be achieved by the spacecraft momentum exchange device system (wheel or CMG packages) in order to perform the different maneuvers required by the SIRTf mission. Two main types of maneuver are examined: 1) large angle slews, in which the spacecraft orientation may undergo changes ranging from a few degrees up to 120 degrees, in a relatively long time (up to 8 minutes), and, 2) small angle slews in which the slew angle may reach a maximum of 7 arcmin, but the slew time may be as short as 2 seconds.

In addition, a high performance earth-sun avoidance maneuver (90 deg in 90 sec) was examined for the 28 deg orbit case. Although not a hard requirement for SIRTf at the present time, it was felt to be important to determine whether or not the vehicle could execute this maneuver.

The maximum angular rate of the spacecraft determines the maximum amount of stored momentum needed, while its angular acceleration determines the torque. These two parameters, angular rate and angular acceleration, depend upon the slew time and the slew angle, and also on the torque profile chosen to achieve these end conditions. These profiles are of three types and are denoted by B-B (for Bang-Bang), S-V (for Sine-Versine) and B-C-B (for Bang-Cruise-Bang). The S-V profile is used to minimize the structural excitation and thus to improve the settling time. The B-B profile is more favorable in terms of torque and momentum. The B-C-B profile is the most favorable in terms of momentum, but requires higher torques. The characteristics of these torque profiles are described in detail in the SIMULATION RESULTS section.

The requirements for torque and momentum obviously depend directly upon the inertias of the vehicle. Thus, the 98 deg configuration, which has smaller inertias, requires less torque and momentum in comparable conditions.



**SIRTF**

MINIMUM MOMENTUM AND TORQUE REQUIREMENTS

Maneuver Type	Maneuver Parameters		Requirements				Torque Profile
			28 Deg Orbit		98 Deg Orbit		
			Momentum (N.m.s)	Torque (N.m)	Momentum (N.m.s)	Torque (N.m)	
Large Angle *	120 deg	8 min	162.4	0.7	144.2	0.6	B-B
	120 deg	8 min	216.5	1.8	192.2	1.6	S-V
	2.5 deg	10 s	216.5	84.4	192.2	74.9	S-V
	90 deg	90 s	649.5	14.4			B-B
	90 deg	90 s	866.0	37.5			S-V
	90 deg	90 s	324.8	300.0			B-C-B
Small Angle Slews	7 arcmin	2 s	37.9	37.9	33.6	33.6	B-B
	7 arcmin	2 s	50.5	98.5	44.8	87.4	S-V
	7 arcmin	5 s	20.2	15.7	17.9	13.9	S-V

\*This set of slews is included as an example of a high performance earth-sun avoidance maneuver which may be required when the 28 degree orbit spacecraft passes through the plane of the ecliptic.

## CONTROL TORQUE AND MOMENTUM STORAGE REQUIREMENTS

This chart is a graphical representation of the previous chart. Each maneuver is represented by a point in the torque-momentum space so that an envelope may be defined to help size the actuator system. Requirements arising from environmental or on-board disturbances have been plotted on the same chart.

Three classes of systems can be derived from this chart. First, a "minimum capability" system is derived from the 120 degrees in 8 minutes slew requirement (Point SV in the 120 deg slews). This system is defined by a 2 Nm/200 Nms envelope and will achieve the 7 arcmin slew in a minimum of 15 seconds (SV 15s).

The second system, a "medium capability" system, could achieve a Sine-Versine small angle slew in 2 seconds (SV 2s). It is thus defined by a 100 Nm/200 Nms envelope. This envelope has as its upper corner the capability for a 2.5 degrees in 10 seconds slew. Both 120 and 2.5 degree slews correspond to the same average rate of 0.25 degree/s.

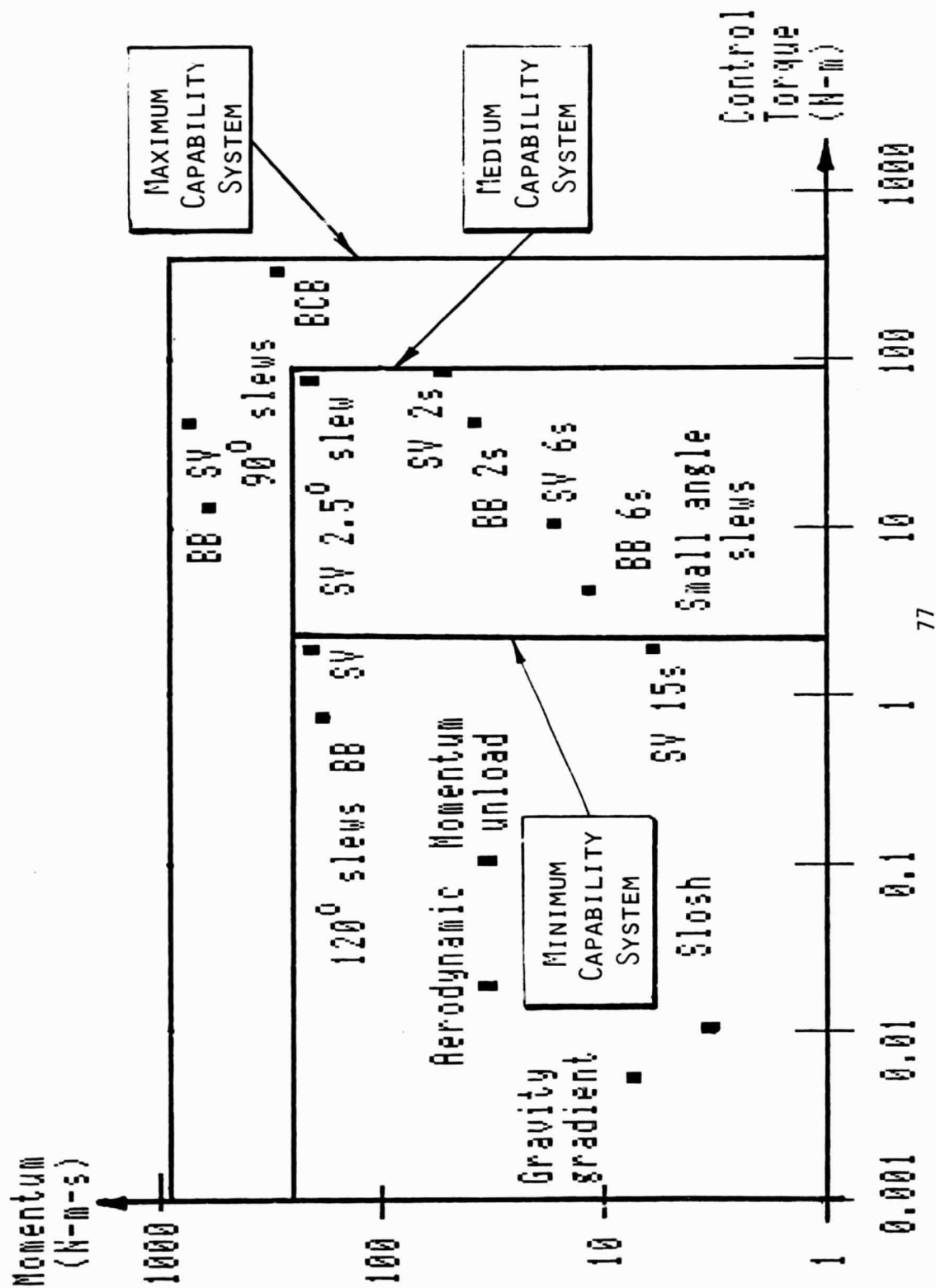
The most severe requirements arise from the 90 degrees in 90 seconds slews. This "high capability" system will require a 300 Nm/900 Nms envelope.

In all cases, this chart shows that slew requirements, rather than environmental or disturbance torques, are driving actuator selection and sizing.



**SIRTF**

# CONTROL TORQUE AND MOMENTUM STORAGE REQUIREMENTS



## MOMENTUM STORAGE DEVICE OPERATING RANGE

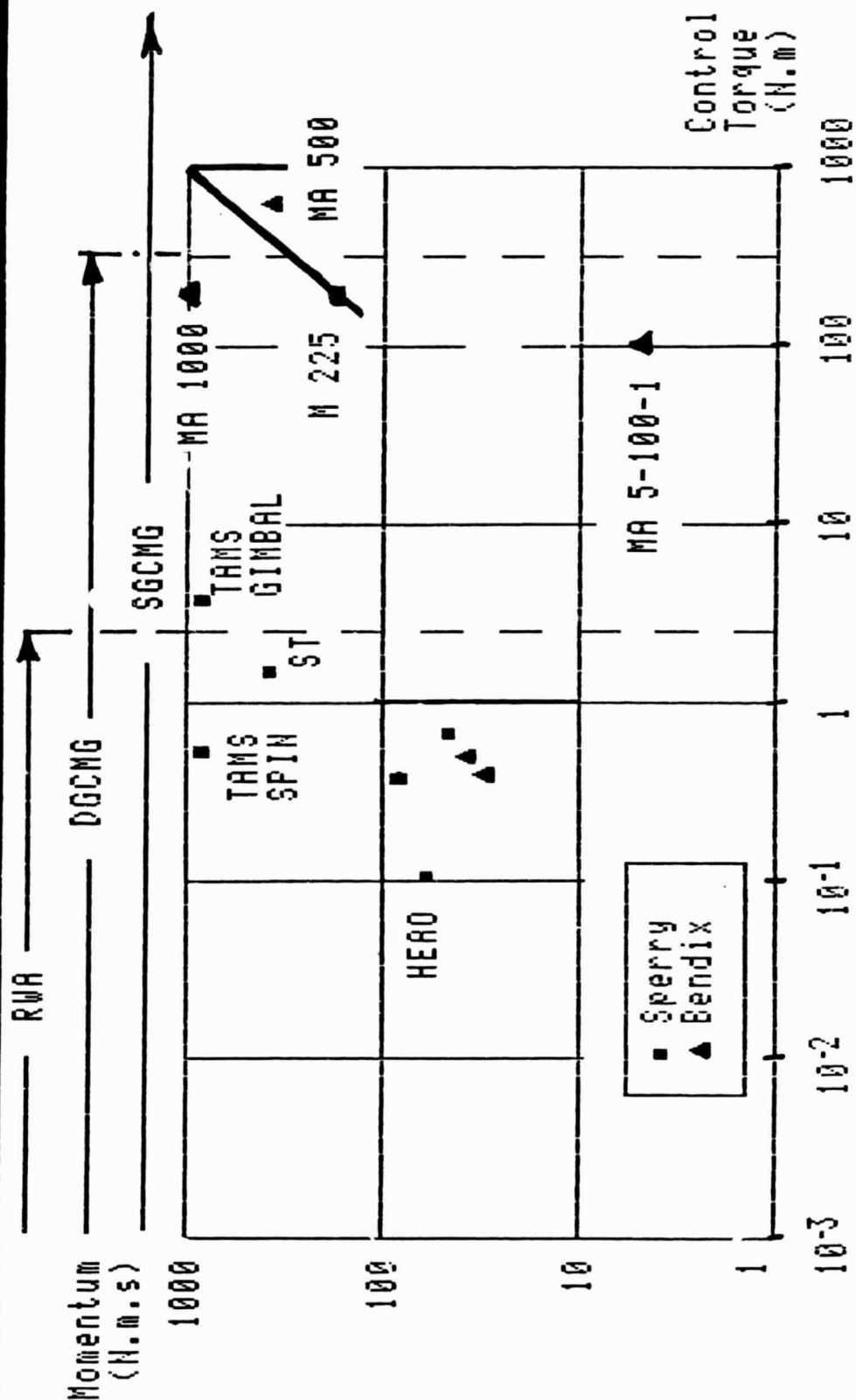
This chart utilizes the same torque/momentum coordinate system as the previous chart to display representative existing momentum exchange device characteristics. The data were provided by SPERRY and BENDIX corporations. The domain is roughly divided into three regions pertaining each to a different class of momentum exchange devices. Reaction wheels are found in the low torque/momentum region. Double-Gimbal CMGs can usually produce more torque than reaction wheel assemblies, but the highest torque/momentum capabilities are usually associated with Single-Gimbal CMGs, although these systems can be used as well in low momentum/torque conditions. In fact some manufacturers like SPERRY use the same basic design (M225 series) to cover a wide range of conditions. This design could be a valid candidate for the SIRTf system.

Among the typical systems shown on the chart are the Space Telescope (ST) and HEAO satellite wheels. A good representative of a Double-Gimbal CMG is the BENDIX MA 1000 built for NASA LRC. In the Single-Gimbal CMG category, the MA 5-100-1 built for LMSC fast tracking mirror applications and later used in several structural control experiments, and the MA-500 series built for the Air Force. The SPERRY M225 SGCMG design covers a range of conditions which are represented by a straight line on the chart. Other labelled and unlabelled data points correspond to existing flight hardware and only appear on this chart to give some idea of the kind of systems that have been built and of their performance.



# SIRTf

## MOMENTUM STORAGE DEVICE OPERATING RANGE



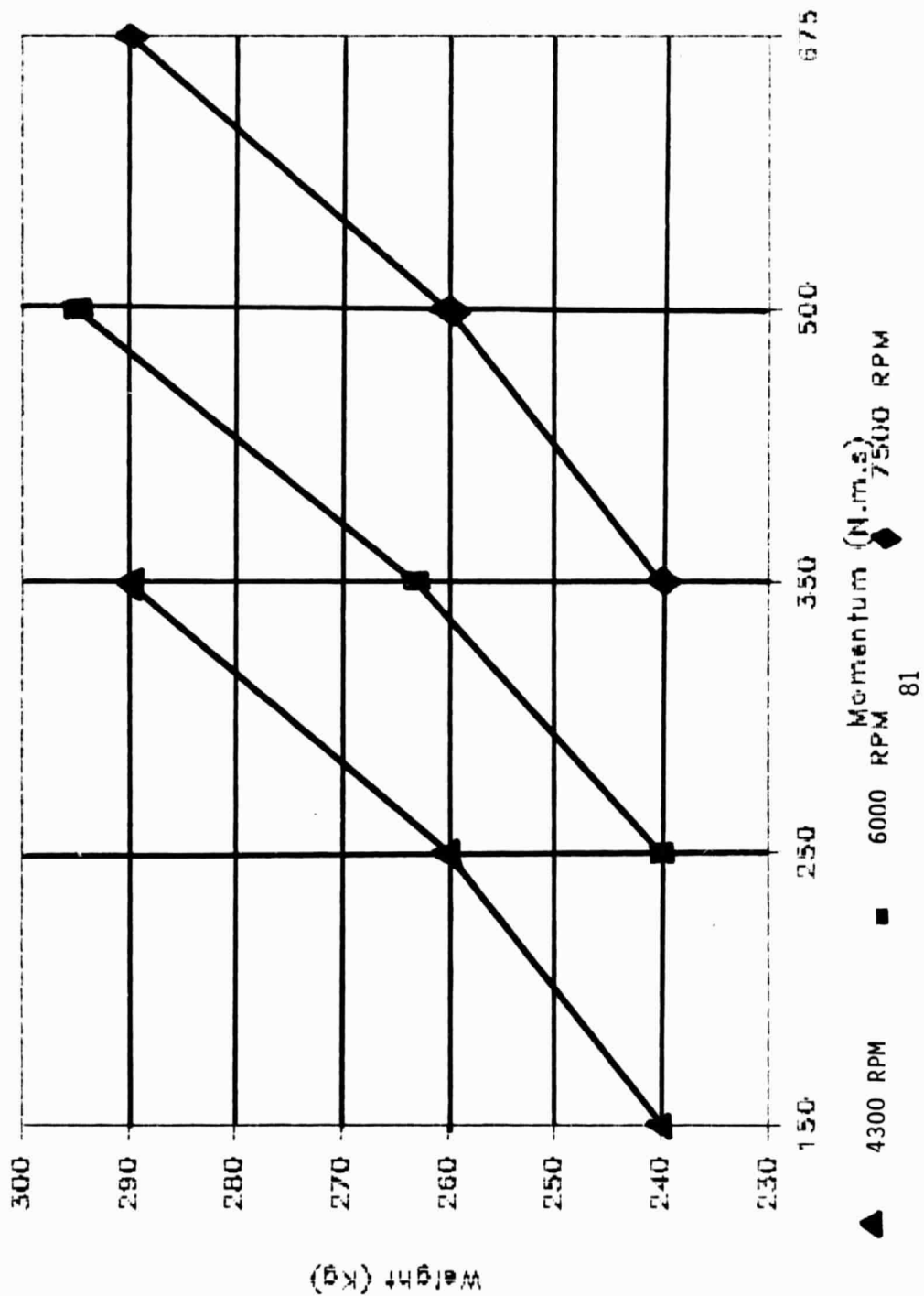
#### SPERRY M225 CMG OPERATING RANGE

This chart shows the range of application of the SPERRY CMG M225. The same basic hardware can be tuned for various applications by either making the wheel lighter, or by reducing the spin rate. The RPM reduction presents obvious advantages with respect to life-time and reliability. On the chart, the 4300 RPM case, with a weight of about 240 Kg, can produce a momentum of about 180 N-m-s. A cluster of 6 CMGs could produce around 600 N-m-s, which will meet all the SIRTf requirements. The torque capability of a single unit running with a 1 rad/s max gimbal rate will be around 180 N-m, which also will enable the 6-CMG system to easily meet the SIRTf requirements.



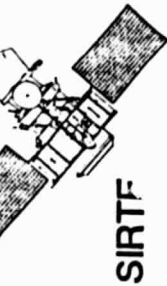
**SIRTf**

# SPERRY M 225 CMG OPERATING RANGE



#### BASELINE SYSTEM CONFIGURATION (1)

The baseline system utilizes single gimbal CMGs in a 6-pack cluster to provide control torque. Momentum dumping is accomplished with magnetic coils acting against the earth's magnetic field. The design for the coils and their sizing was taken directly from the Space Telescope. The primary attitude sensors for the spacecraft are rate integrating gyros combined with periodic stellar-inertial updates from star tracker(s) and/or the Fine Guidance Sensor. The baseline design also assumes the use of an active secondary mirror for image stabilization, but it is a goal of this study to evaluate under what conditions this capability is required.



## BASELINE SYSTEM CONFIGURATION (1)

---

- ATTITUDE CONTROL TORQUE PROVIDED BY 6-UNIT CLUSTER OF SINGLE GIMBAL CMG's
- MOMENTUM DUMPING AND BACKUP SYSTEM USING ELECTRO-MAGNETIC TORQUING
- RATE INTEGRATING GYROS WITH STELLAR-INERTIAL UPDATES FOR ATTITUDE REFERENCE
- ACTIVE SECONDARY MIRROR FOR SPATIAL CHOPPING AND 2-AXIS IMAGE STABILIZATION (AIS)

## BASELINE SYSTEM CONFIGURATION (2)

This chart gives some of the engineering details of the Sperry Model 225 single gimbal control moment gyroscope and the electro-magnets used on the Space Telescope spacecraft for momentum unloading. It should be noted that the Sperry unit was selected because it is a virtually off-the-shelf item whose space qualifications are well documented. This does not mean that CMGs designed by other manufacturers (notably Bendix) are not acceptable. The model 225 is given here only as a representative example of available hardware.



## BASELINE SYSTEM CONFIGURATION (2)

- CONTROL MOMENT GYROS

SPERRY MODEL M225	- 4500 RPM	
MAX TORQUE	25 N-M	
MOMENTUM STORAGE	50 N-M-SEC	
PEAK POWER	75 W	PER UNIT
QUIESCENT POWER	35 W	
STANDBY POWER	15 W	

- ELECTROMAGNETS

### SPACE TELESCOPE DESIGN

MAX TORQUE	0.04 N-M	
MAX MAGNETIC MOMENT	2000 A-M <sup>2</sup>	PER AXIS

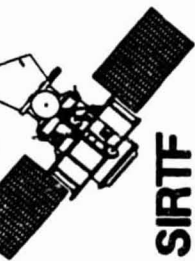
## 6-CMGs ON A CONE (GAMS CONFIGURATION)

This chart represents the geometric orientation of six single gimbal CMGs in a configuration called the Gyro Attitude Maneuvering System (GAMS) configuration. This configuration was originally analysed by W. Hooker and G. Margulies in the mid-sixties and a number of in-depth studies have been conducted since then at LMSC on GAMS (see for instance "Geometric Theory of Single-Gimbal Control Moment Gyro Systems", G. Margulies and J-N. Aubrun, J. of Astronaut. Sci., Vol. 26, No. 2, Apr 1978).

The chart shows a typical arrangement in which the gimbal axes are equidistributed on a cone. By changing the cone angle, it is possible to shape the momentum envelope to approximately match the vehicle inertias. A 30 degree cone for instance, will result in an envelope 42% smaller in the direction of the cone axis than in any perpendicular direction.

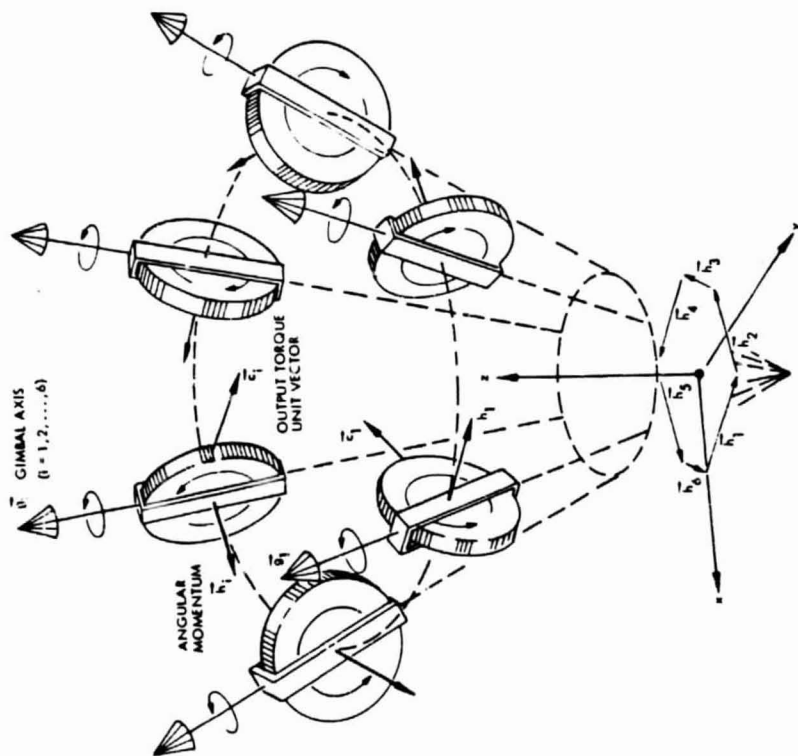
The advantages of the GAM system are its high capability in torque and momentum, its very high reliability because of the mechanical simplicity of a SGCMG unit (compared to a DGCWG) and, most of all, because of its high level of redundancy. As shown in the next chart, such a system can tolerate up to three failures and still be operational (with reduced performance).

By commanding gimbal angle rates with appropriate control laws, the system can produce the desired torques while utilizing the extra degrees of freedom to optimize its capability. It has been shown possible to make use of up to 70% of the absolute maximum (i.e. 6 times the momentum or torque of one unit). Thus, a system using 25 Nm/50 Nms units could produce about 100 Nm and 200 Nms, which will satisfy the requirements for a "medium capability" SIRT system.



**SIRTF**

# 6 CMGs ON A CONE (GAMS CONFIGURATION)



#### 6-CMG MOMENTUM ENVELOPES (GAMS Configuration)

This chart represents momentum envelopes corresponding to a 6-CMG system with a 30 degree cone angle. The momentum envelop is the geometric locus of the maximum total momentum vector that can be obtained from the system for all possible combinations of the gimbal angles. Any momentum vector whose origin is at the center and whose extremity is within the envelope can be generated by the system. In other words, there are no holes or unattainable regions inside this envelope. The twelve circular patterns seen on the surface are very shallow dimples and correspond to the directions of the six gimbal axes.

This chart shows a general 3-D view of the envelope and a planar view for the nominal case, and cases corresponding to successive failures. It is remarkable that even after two failures, the envelope is still reasonably spherical, although of smaller dimensions. In fact, a third failure will not cripple the system, since with three CMGs it is still possible to produce torque along three independent axes. But of course, the performance of the system will be degraded and saturation effects more severe.



6-CMG MOMENTUM ENVELOPES (GAMS CONFIGURATION)

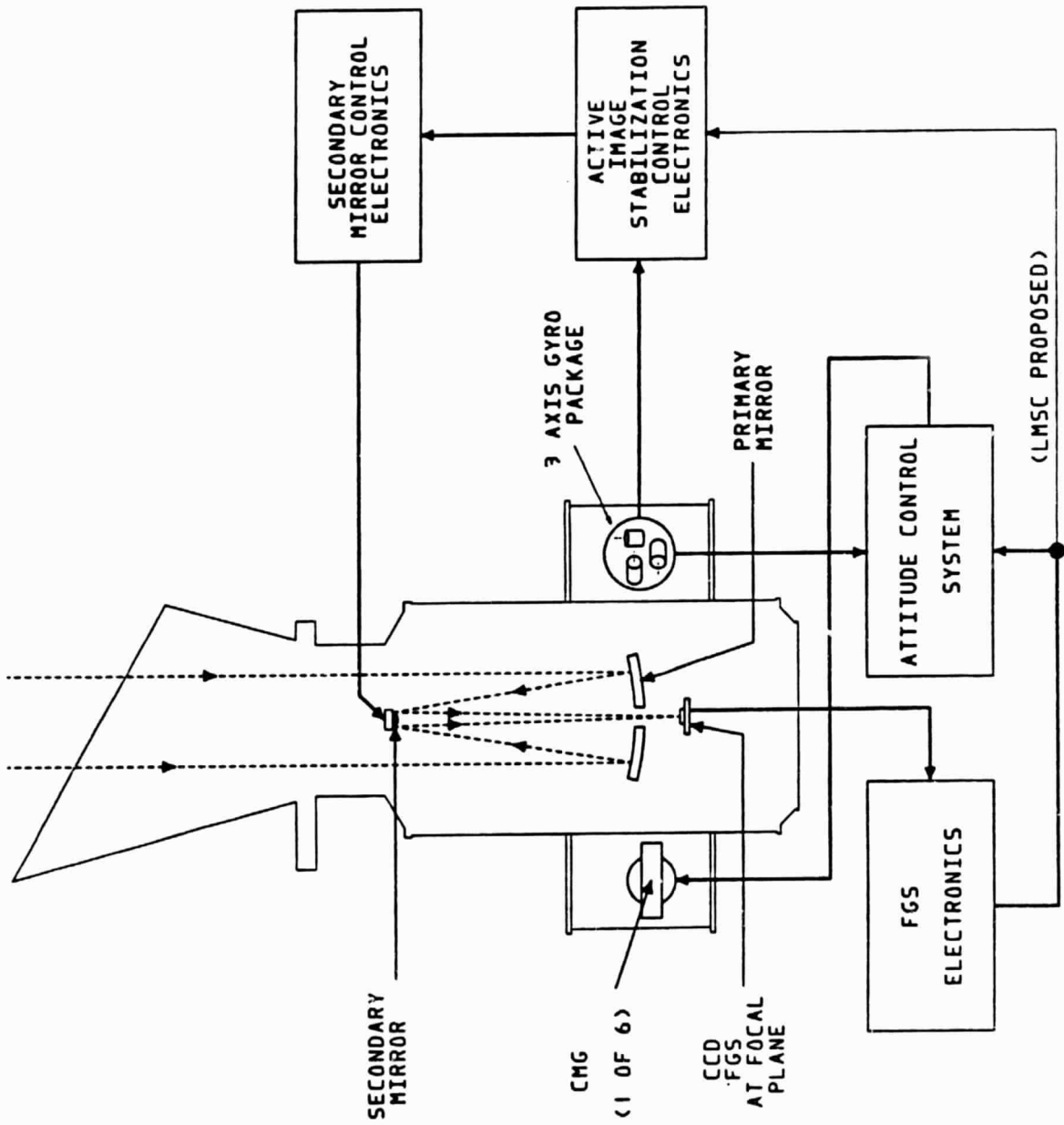
	GENERAL VIEW	PLAN VIEW (x, y PLANE)
NO FAILURES		
ONE CMG FAILURE		
TWO CMG FAILURES		

#### PICTORIAL DIAGRAM OF POINTING AND CONTROL SYSTEM

This chart is a simplified diagram of the SIRTf pointing and control system. It illustrates the relationship between the primary components of the system. Note that the attitude control system uses inputs from both the Fine Guidance Sensor (FGS) and the 3-axis gyro package. In addition, the FGS and the secondary mirror both require special subsystems for their operation. This figure also provides an illustration of the relative physical locations of the main electro-mechanical components of the control system.

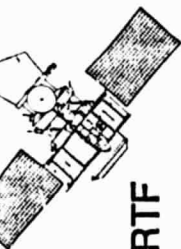


# PICTORIAL DIAGRAM OF POINTING AND CONTROL SYSTEM



## POINTING AND CONTROL SYSTEM COMPONENTS

This chart summarizes in matrix form the principal components for the individual subsystems which comprise the pointing and control system. The three primary categories are SENSORS, ACTUATORS, and PROCESSORS. Components are listed in each of these categories for the Attitude Control System, the Backup System, the Fine Pointing System, and the Secondary Mirror Control System. Probably the most important aspect of this table is the use of distributed control processors in the control system. The complex logic associated with, for example, the CMG control laws or the FGS pattern recognition algorithms are most easily developed and implemented with separate, semi-autonomous processors. Given the current state of the art for flight computers and the probable advances by the time the flight hardware is designed, this approach is a logical one and does not represent a significant technical risk.



SIRTf

## POINTING AND CONTROL SYSTEM

### OVERALL SYSTEM CONFIGURATION

#### COMPONENTS

	ATTITUDE CONTROL	BACK-UP SYSTEM	FINE POINTING	CHOPPING AND AIS
SENSORS	INTEGRATING GYROS	MAGNETOMETERS	FGS	SECONDARY MIRROR
	STAR TRACKER	RATE GYROS		
	SUN/EARTH SENSOR			
ACTUATORS	6 CMG's	4 ELECTROMAGNETS	SECONDARY MIRROR ELECTRODYNAMIC ACTUATORS	SECONDARY MIRROR ELECTRODYNAMIC ACTUATORS
PROCESSORS	CONTROL COMPUTER FOR ATTITUDE/ POINTING  DEDICATED μPROCESSOR FOR CMG STEERING LAWS	DEDICATED μPROCESSOR	CONTROL COMPUTER FOR FGS PATTERN RECOGNITION	DEDICATED μPROCESSOR

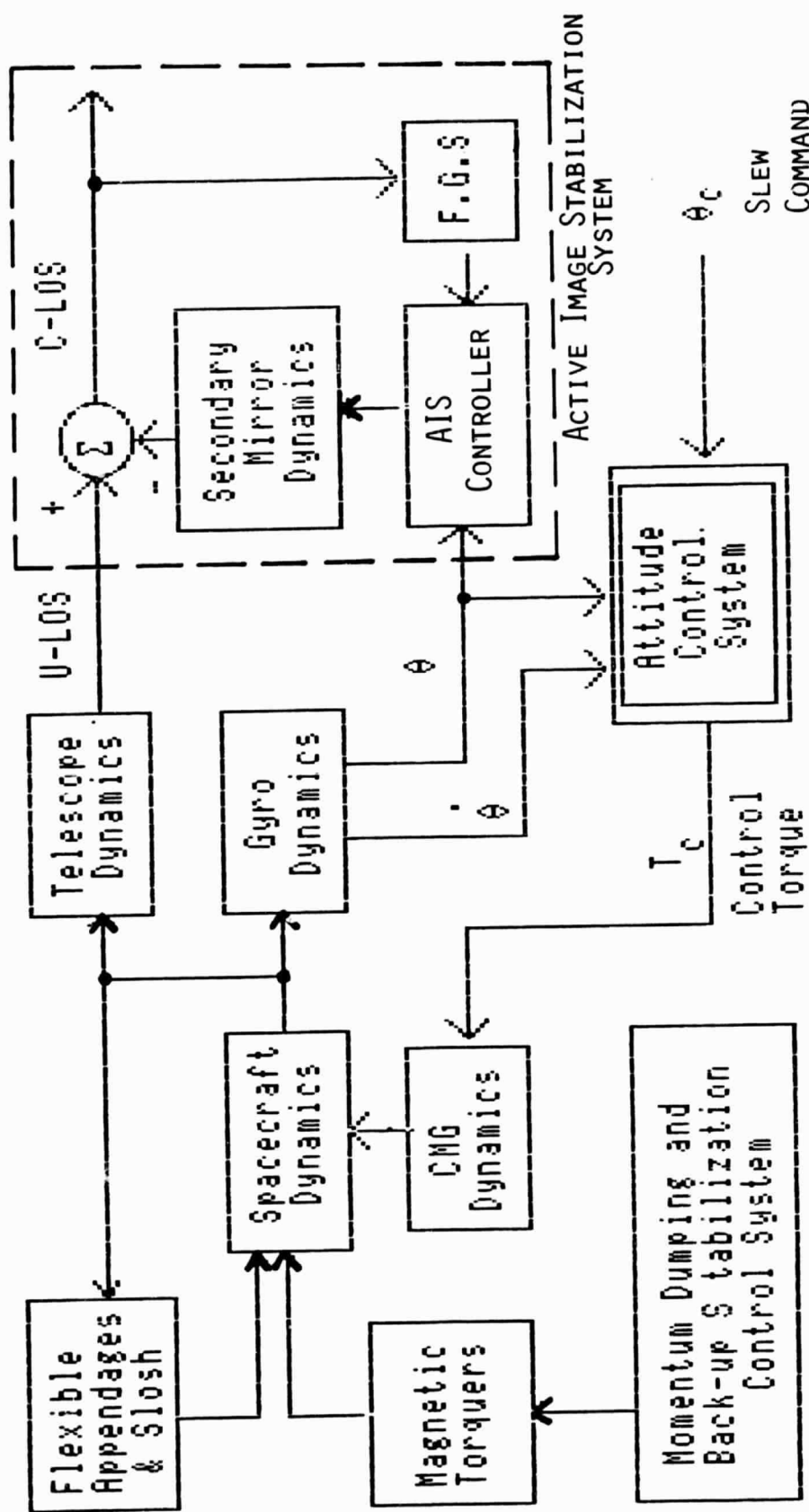
#### SYSTEM BLOCK DIAGRAM

This block diagram illustrates how the major components of the control system and the spacecraft dynamics interact. The relationship of the Active Image Stabilization System to the rest of the pointing and control system and the input of the AIS to correct the telescope line of sight is clearly shown. The interaction between Spacecraft dynamics, Telescope dynamics, and Flexible Appendages/Slosh is also illustrated. The possibility for an unstable interaction between the attitude control system and the flexible appendages can also be seen in the two loops intersecting in the Spacecraft Dynamics block.



**SIRTf**

# SYSTEM BLOCK DIAGRAM



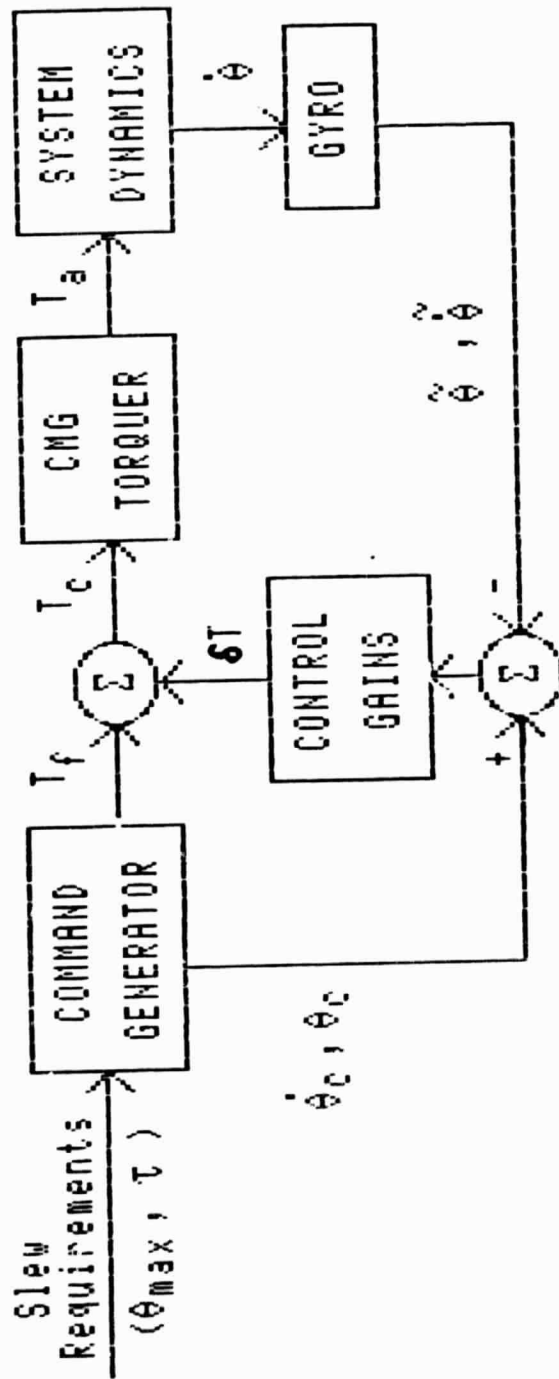
#### ATTITUDE CONTROL SYSTEM BLOCK DIAGRAM

This chart shows the details of the attitude control system. Probably the most important concept in this diagram is the Command Generator which produces both a feedforward torque  $T_f$  as well as position and rate commands  $O_c$  and  $\dot{O}_c$ . The use of the command generator is what allows the attitude control system to perform slews, especially small angle slews, in a relatively short time frame. Given that the spacecraft has potential problems with flexible appendages, the command generator is the component that produces the commanded time histories for attitude angle and rate along with the corresponding varying torque profile (e.g. sine-versine) tailored to substantially reduce structural excitation.



**SIRTF**

# ATTITUDE CONTROL SYSTEM BLOCK DIAGRAM



## ACTIVE IMAGE STABILIZATION CONTROL LOOP

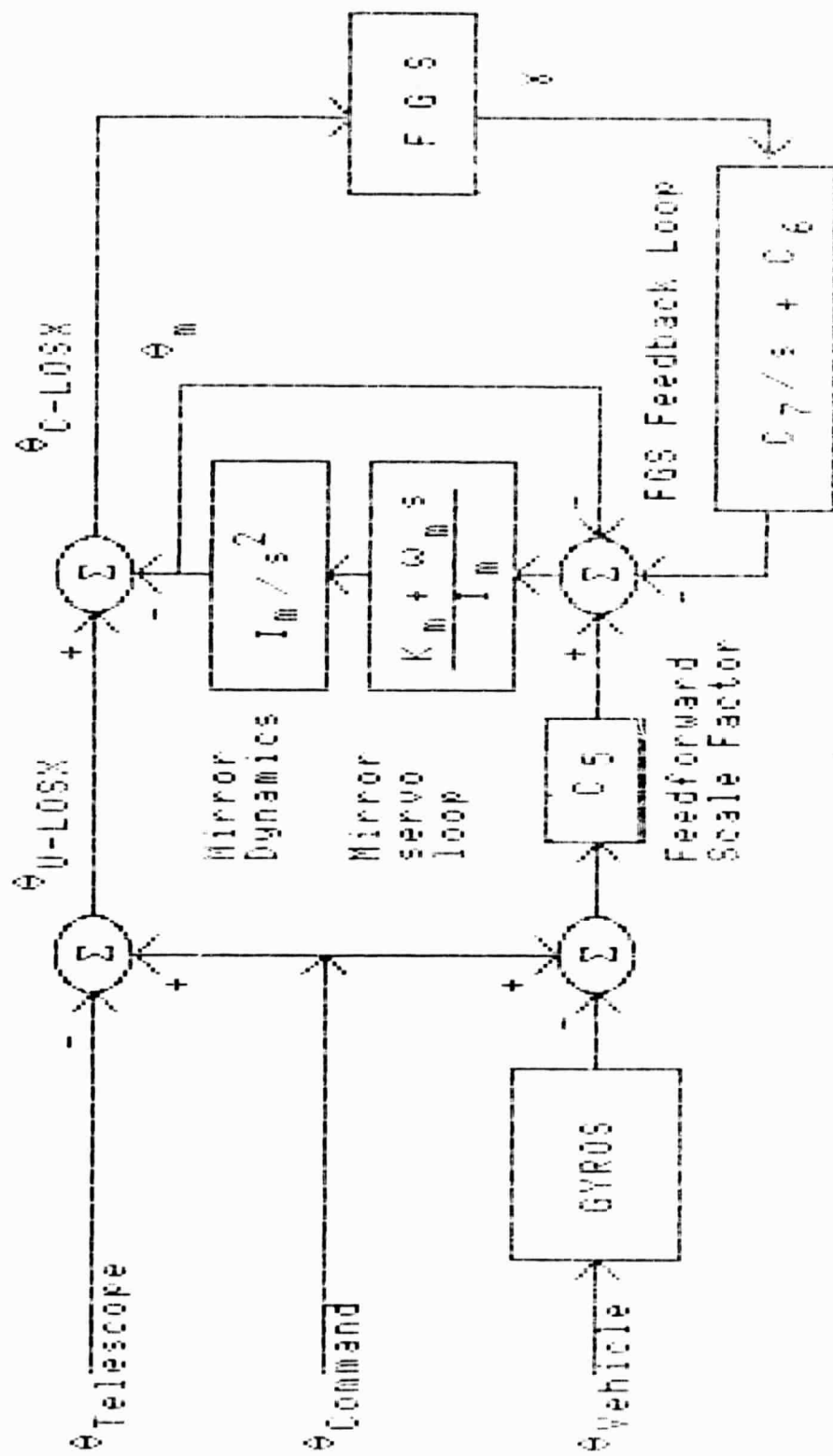
This block diagram illustrates the details of the Active Image Stabilization control loop. In particular, it shows how output from the Fine Guidance Sensor is combined with gyro signals (which are corrupted by a scale factor error represented in the gain C5 being different from 1 by two percent) to drive the telescope secondary mirror. Note that the secondary mirror has its own control system which attempts to keep the mirror at sensor null except when requested to move by the combined gyro/FGS commands. The use of FGS inputs in the outer loop wrapped around the mirror control system is a concept developed at Lockheed to overcome some of the errors inherent in the baseline design, which drives the mirror with gyro outputs only. Thus, to get a picture of the baseline concept, the lines connecting the FGS to the summing junction for the mirror control system would have to be removed.

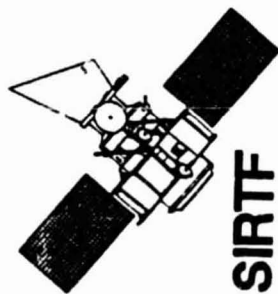


**SIRTF**

# ACTIVE IMAGE STABILIZATION (AIS) CONTROL LOOP

## CONTROL LOOP





C-2

POINTING AND CONTROL SYSTEM  
PERFORMANCE EVALUATION

---

PRECEDING PAGE BLANK NOT FILMED

101

PAGE 100 INTENTIONALLY BLANK

## MODEL LIMITATIONS

This chart delineates the major characteristics and limitations of the spacecraft dynamic model and of the AIS model that are used in the simulation. The primary purpose of the SIRTf dynamic model is to represent the major components of the dynamic behavior of the spacecraft. The use of rigid bodies interconnected by gimbals, springs and dampers is adequate to model the principal structural flexibility effects. Only the lowest modal frequencies can be attained in this way, but they are the ones usually responsible for the major degradation in pointing and stability performance. Flexible appendages such as TDRSS antennae and solar panels were modelled using data pertinent to the Space Telescope, with proper scaling for SIRTf use. The telescope (including instrument chamber and cryogen tanks) is connected to the Support System Module (SSM) by the PODS. The characteristic frequencies of this assembly were derived from ground experimental data.

Effects connected with the structural dynamics of the telescope structure itself, of higher modes of the appendages, or of the SSM, are not modelled. Such modelling requires a precise definition of the spacecraft, which is beyond the scope of the present study. The model for cryogen slosh is likely to represent a worst case, in which the whole fluid behaves as a lump mass. There is no claim to represent the actual complexity of the fluid dynamics. Finally, the FGS model is based on the best present estimates of the capability of this system.

**MODEL LIMITATIONS**

---

- MODELS ARE ESSENTIALLY RIGID BODIES CONNECTED BY SPRINGS
- FLEXIBILITY IS SIMULATED BY SETTING SPRING CONSTANT SO RESONANCE IS AT FIRST BENDING MODE
- FLEXIBILITY WAS SIMULATED FOR MAJOR COMPONENTS ONLY (USING ST DATA)
- CRYOGEN SLOSH MODEL IS SIMPLE CONSTRAINED PENDULUM (BASED ON ANALYSIS DONE FOR IRAS)
- FGS OUTPUT IS CONTINUOUS WITH BANDWIDTH LIMITED AT 0.5 HZ (500 - 1000 MSEC SAMPLE RATE)

## DESIGN AND SIMULATION METHODOLOGY

This chart enumerates the various steps involved in modelling, control design, and simulation of the SIRTf system. The first step is to obtain a model for the dynamics of the spacecraft. To that effect, the N-BODY/TERFLEX program is used. This program assembles the various bodies, given their mass properties, relative geometry, and degrees of freedom, and can either solve the corresponding non-linear equations of motions (if large interbody angles or inertial rates are present), or generate the constant coefficient matrices corresponding to linearized equations of motion. These matrices must then be used, along with those defining the control equations, to generate a first order, state-space, control synthesis model. Computer Aided Control Synthesis and Analysis software is used with advantage to perform the various tasks required. Finally, the closed-loop model, along with the definition of the time histories of the various disturbances and feedforward torques to be applied to the spacecraft, is used in specialized simulation software to generate system response time histories.



**SIRTF**

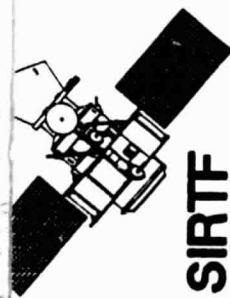
## DESIGN AND SIMULATION METHODOLOGY

---

- N-BODY DYNAMIC SIMULATION PROGRAM
  - 1) GENERATE LINEARIZED MATRIX EQUATIONS
  - 2) OBTAIN TIME-DOMAIN NON-LINEAR SIMULATIONS
- CONTROL DESIGN AND ANALYSIS SOFTWARE
  - 1) GENERATE CONTROL SYNTHESIS MODEL
  - 2) EVALUATE OPEN AND CLOSED LOOP STABILITY
- LINEAR SIMULATION AND ANALYSIS SOFTWARE
  - 1) DETERMINE PRINCIPAL MODES OF THE SYSTEM
  - 2) EVALUATE TIME DOMAIN CLOSED-LOOP PERFORMANCE

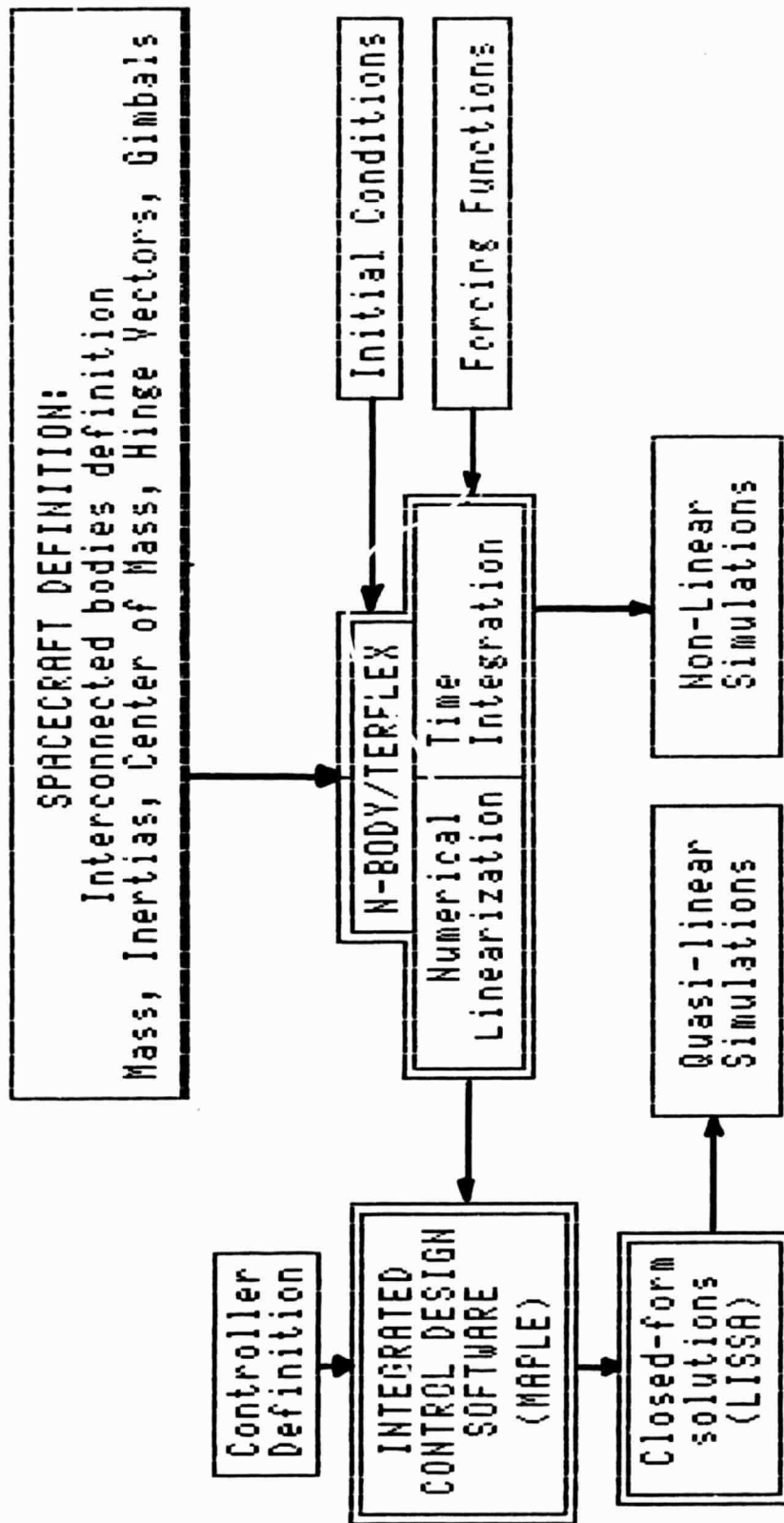
## CONTROL DESIGN AND SIMULATION METHODOLOGY

This chart depicts the logical interconnection of the various pieces of software used to perform modelling, control design and performance evaluation. The N-BODY/TERFLEX program handles the non-linear dynamics of a system of interconnected rigid bodies with flexible appendages (TERminal FLEXible bodies). It also generates linearized equations, using a numerical differentiation algorithm. The MAPLE program is Lockheed proprietary interactive software for matrix operations, model building, control synthesis and analysis; its data base is shared with various other large scale software packages such as TERFLEX and LISSA. The LISSA program performs linear simulations using closed-form solutions, which makes it extremely efficient for large system simulations. In addition, it has the capability for simulating actuator non-linearities and discrete control systems.



# SIRTF

## CONTROL DESIGN AND SIMULATION METHODOLOGY



## SIMULATION MODEL EQUATIONS

This chart describes the equations which are used to simulate the response of the SIRT system to various commands and disturbances. The vehicle dynamics are represented by the matrices  $F_v$  and  $G_v$  which are computed by the N-BODY/TERFLEX program. The definition of these matrices and the associated state vector  $X_v$  is different for the 28 and 98 degree orbit cases and is given in the next two charts. The second set of equations represents the secondary mirror dynamics/servo system combination used in the AIS system model. The two mirror tilt angles are denoted by  $\theta_{mx}$  and  $\theta_{my}$ , while the corresponding command angles are  $\theta_{dx}$  and  $\theta_{dy}$ . The third group of equations represents the FGS pointing error output,  $\delta x$  and  $\delta y$ . The actual pointing error is represented by the combination of angles in parentheses, commanded pointing angles  $\theta_{cx}$  and  $\theta_{cy}$ , actual pointing angles  $\theta_x$  and  $\theta_y$ , and pointing corrections from the secondary mirror  $\theta_{mx}$  and  $\theta_{my}$ . The FGS is modelled as a second order continuous filter, with a bandwidth equal to  $\omega_c$  (3 rad/s). This model for the FGS is a crude but simple way of describing the truly discrete output delivered by the focal plane FGS at a sampling rate of about 1 Hz.



- **VEHICLE DYNAMICS**

$$\dot{X}_v = F_v X_v + G_v U_v$$

- **MIRROR DYNAMICS**

$$\dot{\theta}_{mx} = -\omega_m (\theta_{mx} - \theta_{dx}) - K_m \int (\theta_{mx} - \theta_{dx}) dt$$

$$\dot{\theta}_{my} = -\omega_m (\theta_{my} - \theta_{dy}) - K_m \int (\theta_{my} - \theta_{dy}) dt$$

- **AIS**

$$\ddot{r}_x = -2\zeta\omega_c \dot{r}_x - \omega_c^2 r_x + \omega_c^2 (\theta_{mx} - \theta_x + \theta_{cx})$$

$$\ddot{r}_y = -2\zeta\omega_c \dot{r}_y - \omega_c^2 r_y + \omega_c^2 (\theta_{my} - \theta_y + \theta_{cy})$$

#### SYSTEM STATE DEFINITIONS (1)

This chart defines the notation for different quantities which make up the complete State, Control and Command vectors defined in the Definitions (2) chart which follows.



# SYSTEM STATE DEFINITIONS (1)

$\theta$	$=$	$[\theta_x, \theta_y, \theta_z]^T$	ATTITUDE ANGLES
$\theta_c$	$=$	$[\theta_{cx}, \theta_{cy}, \theta_{cz}]^T$	POSITION COMMANDS
$\theta_m$	$=$	$[\theta_{mx}, \theta_{my}]^T$	MIRROR ANGLES
$\gamma$	$=$	$[\gamma_x, \gamma_y]^T$	F.G.S. MEASURED POINTING ERRORS
$\theta_d$	$=$	$[\theta_{dx}, \theta_{dy}]^T$	MIRROR ANGLE CONTROL INPUTS
$u_v$	$=$	$[u_{vx}, u_{vy}, u_{vz}]^T$	CMG CONTROL TORQUE COMMAND INPUTS

## SYSTEM STATE DEFINITIONS (2)

$\beta_{28}$  represents the inter-body angles used in the 28 deg orbit case and  $\beta_{98}$  represents the inter-body angles for the 98 deg orbit. The state vector  $X$ , and the control vector  $U$  consisting of control inputs, commands and disturbances, are defined in this chart. The presence of integral terms in the state vector arises from the attitude control system integral loop which requires extra states. The command vector depends on the desired maneuver angles and angular rates, and on the feed-forward torque  $T_f$ . The actual time functions defining these quantities depend upon the torque profile chosen. The disturbance vector  $T_d$  depends on the specific performance being evaluated.

## SYSTEM STATE DEFINITIONS (2)

113

## SYSTEM STATE EQUATIONS

This chart defines the state equations which are used in the Linear Systems Simulation and Analysis (LISSA) program to perform the various simulations. It is worth noting that the vector  $U$  consists of the control vector  $U_c$ , and of the command vector and the disturbance vector globally denoted as  $U_d$ . The matrix  $B$  is used to implement feedforward loops. The matrices  $H$  and  $K$  are needed in order to construct the output vector  $Y$  which thus can be any linear combination of  $X$  and  $U$ . These two matrices  $H$  and  $K$  are used to output different variables from the simulation and do not affect the control design or performance.



# SYSTEM STATE EQUATIONS

$$\begin{aligned} \dot{X} &= FX + G_1 U_c + G_2 U_e && \text{STATE EQUATION} \\ U &= \begin{bmatrix} U_c^T & U_e^T \end{bmatrix}^T && \text{CONTROL, COMMAND, AND DISTURBANCE VECTOR} \\ G &= \begin{bmatrix} G_1 & G_2 \end{bmatrix} && \text{CONTROL DISTRIBUTION MATRIX} \\ U &= CX + B U_e && \text{CONTROL TORQUE INPUT TO CMG'S AND AIS} \\ Y &= HX + KU && \text{OUTPUT VECTOR} \end{aligned}$$

#### STATE VARIABLE VECTOR AND MATRIX DIMENSIONS FOR 28 DEG AND 98 DEG MODELS

The dimensions of the matrices F, G, and C in the System State Equations vary with the spacecraft model and are shown in this chart. The 28 deg orbit model has 16 degrees-of-freedom, thus the vector  $X_v$  has 32 states, while the 98 deg model has only 10 degrees-of-freedom, corresponding to a 20-state vector  $X_v$ . The total state vector,  $X$ , includes  $X_v$  and 13 other states corresponding to the ACS integral error states, and additional states corresponding to the secondary mirror, FGS, and servo loop dynamics. Thus the 28 deg orbit closed-loop system is represented by 45 states, while the 98 deg model requires only 33 states.



# STATE VARIABLE VECTOR AND MATRIX DIMENSIONS FOR 28° AND 98° MODELS

VARIABLE	DIMENSION	
	28° ORBIT	98° ORBIT
B	13X1	7X1
x <sub>v</sub>	32X1	20X1
x	45X1	33X1
U <sub>c</sub>	5X1	5X1
U <sub>e</sub>	12X1	12X1
U	17X1	17X1
F <sub>v</sub>	32X32	20X20
F	45X45	33X33
G <sub>v</sub>	32X3	20X3
G <sub>1</sub>	45X5	33X5
G <sub>2</sub>	45X12	33X12
G	45X17	33X17
C	5X45	5X33
B	5X17	5X17

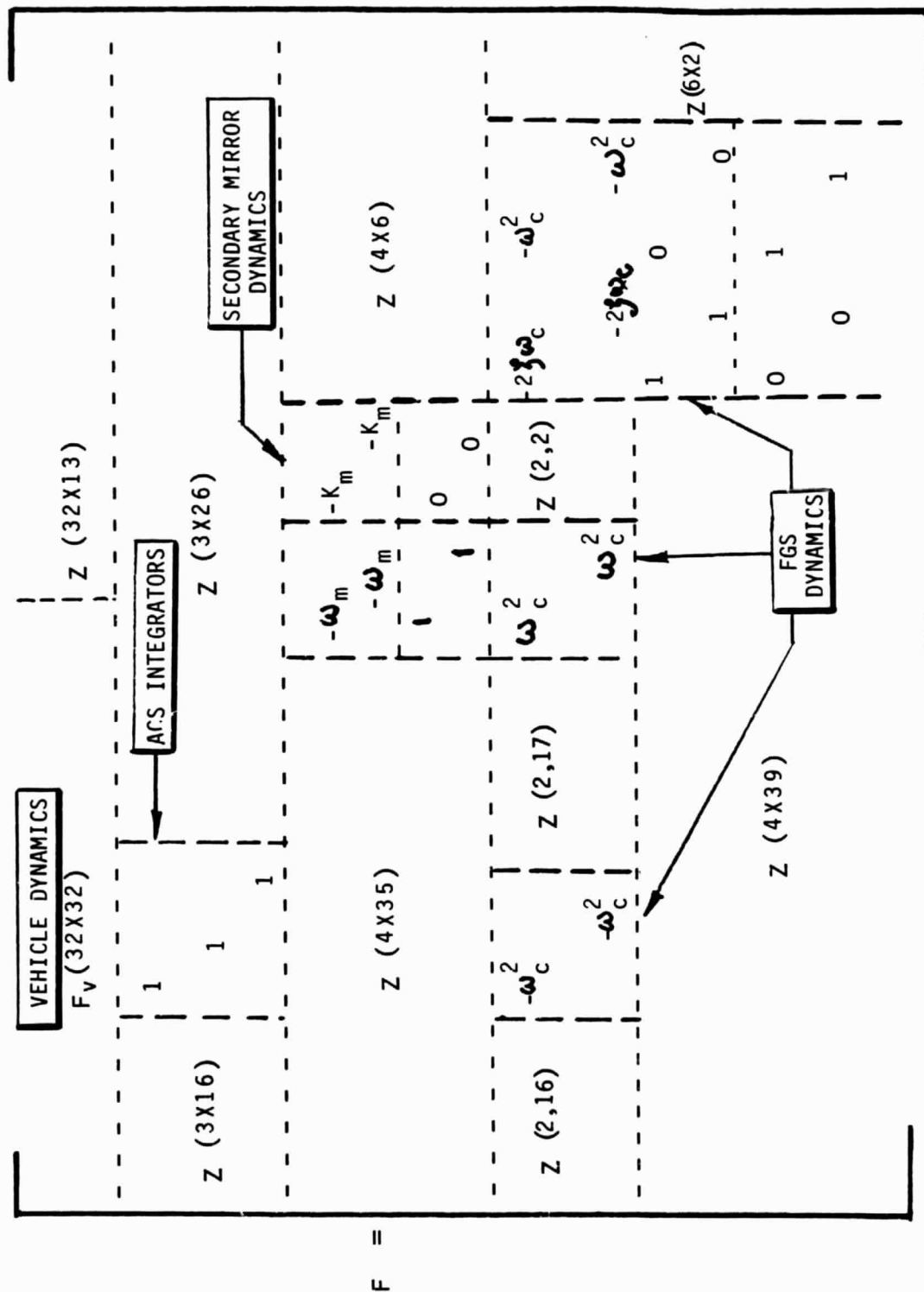
## SYSTEM MATRICES (1)

This chart shows the F matrix (describing the total system dynamics) for the 28 deg model. The notation  $Z(I \times J)$  is used to denote a zero matrix consisting of I rows and J columns. These zeros result from states which are normally uncoupled, e.g., telescope pointing and mirror angles.

Non-zero blocks can be identified as representing the vehicle dynamics (Fv), mirror dynamics (~~am~~ and Km block), and so on. Other blocks related to the FGS, AIS system, and various integrators can also be identified in the chart.



# SYSTEM MATRICES (1)

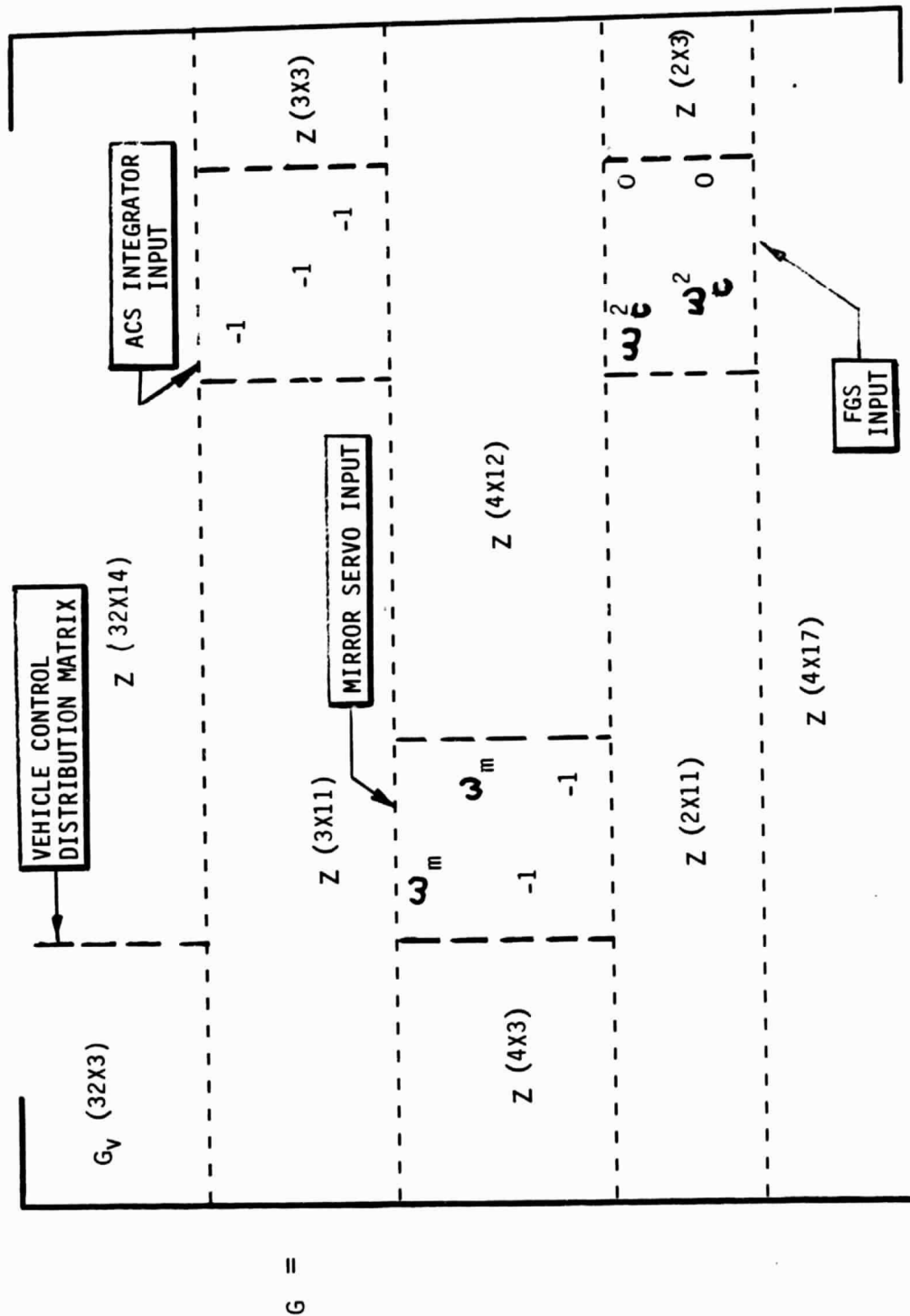


SYSTEM  
DYNAMICS  
MATRIX

## SYSTEM MATRICES (2)

This chart shows the control distribution matrix  $G$  for the 28 deg model. This matrix connects the system states to the control inputs. The left upper corner expresses the response of the vehicle (32 states) to the 3 control torques applied by the CMGs. The  $3 \times 3$  diagonal matrix with elements equal to -1 is required to construct the integral of the attitude error angle vector  $\theta - \theta_c$ . The other non-zero terms describe the effects of control inputs to the FGS and AIS systems.

**SYSTEM MATRICES (2)**



## ATTITUDE CONTROL LAWS

This chart describes the attitude control law. The total CMG torque command consists of a feed-forward torque  $T_f(t)$  and a feedback torque  $T_c$ . The feed-forward torque is computed based on the nominal values of the spacecraft inertias, and depends upon the chosen torque profile, and the desired value of the final slew angle  $\theta_c$ . The time dependent quantities  $T_f$ ,  $\theta_c$ , and  $\dot{\theta}_c$ , are computed by the command generator. The error vector is the difference between the commanded and actual attitude angles. The feedback torque is a linear combination of the error vector, its rate, and the integral of the error vector. The  $3 \times 3$  gain matrices  $C_1$ ,  $C_2$  and  $C_3$  in this proportional-integral-derivative (PID) controller were computed by a pole-placement algorithm. These matrices have non-diagonal elements which compensate for the product of inertia of the vehicle. This feature is particularly important for the 98 deg orbit vehicle which has relatively large products of inertia.

# ATTITUDE CONTROL LAWS

$$\begin{aligned}
 \text{TOTAL CMG TORQUE COMMAND} \quad u_v &= \text{FEEDFORWARD TORQUE COMMAND} \quad T_f(t) - \underbrace{c_1 (\dot{\theta} - \dot{\theta}_c) - c_2 (\theta - \theta_c) - c_3 \int (\theta - \theta_c) dt}_{\text{TORQUE COMMAND}}
 \end{aligned}$$

$$u_v = \begin{bmatrix} u_{vx} \\ u_{vy} \\ u_{vz} \end{bmatrix}^T \quad \theta = \begin{bmatrix} \theta_x \\ \theta_y \\ \theta_z \end{bmatrix}^T \quad \text{ATTITUDE VECTOR}$$

$T_f(t)$  SELECTED TORQUE PROFILE VECTOR

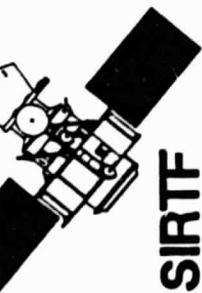
$$\dot{\theta}_c \quad \text{COMMANDED SLEW RATE VECTOR} = \int I^{-1} T_f(t) dt, \quad I \quad \text{SPACECRAFT INERTIA TENSOR}$$

$$\theta_c \quad \text{COMMANDED SLEW ANGLE VECTOR} = \int \dot{\theta}_c dt$$

$c_1, c_2, c_3$  3 X 3 MATRICES OF CONTROL GAINS

## AIS CONTROL LAW

This chart describes the AIS control law. The commanded mirror angle vector  $\theta_d$  is a combination of a feedforward term (difference between the actual line-of-sight angle and the estimated line-of-sight angle measured by the gyros) and a feedback term from the FGS pointing error vector output. The scale factor error in the feedforward loop is embedded in the matrix C5. This matrix is identity if no scale factor error is present. In the simulations, a 2% scale factor error was assumed, thus C5 was equal to 1.02 times the identity matrix.



# AIS CONTROL LAW

$\theta_d = c_5 (\theta_L - \theta_{CL}) + c_6 \dot{\gamma} + c_7 \int \dot{\gamma} dt$	
$\theta_d = [\theta_{dx}, \theta_{dy}]^T$	COMMANDED SECONDARY MIRROR ANGLES
$\theta_L = [\theta_x, \theta_y]^T$	SPACECRAFT LINE-OF-SIGHT VECTOR
$\dot{\gamma} = [\dot{\gamma}_x, \dot{\gamma}_y]^T$	FGS POSITION ERROR VECTOR
$c_6, c_7$	MATRICES OF CONTROL GAINS
$\theta_{CL} = [\theta_{CX}, \theta_{CY}]^T$	
$c_5$	SCALE FACTOR ERROR MATRIX

## CONTROL GAIN MATRIX STRUCTURE

This chart shows the C matrix for the 28 deg model. The matrices C1, C2, C3, C5, C6 and C7 are defined in the previous charts. The Z(I x J) matrices are zero matrices of I rows and J columns and correspond to states which are not fed back. For instance, C2 describes a feedback from the three attitude angles, but since no interbody angles are fed back in this particular control law, a 3x13 zero matrix is found following C2. In more complex control laws, as could be derived for instance from optimal control methods, this 3x13 matrix would be non-zero since the other states would be fed back. Similarly, in the bottom part of the C matrix (the AIS control laws) only certain states are used, and the zero matrices again describe the absence of feedback from some of the states.



**SIRTF**

# CONTROL GAIN MATRIX STRUCTURE

$$C = \begin{bmatrix} -C_1 & Z (3 \times 13) & - C_2 & Z (3 \times 13) & - C_3 & (3 \times 10) \\ Z (2 \times 3) & Z (2 \times 13) & C_5 & Z (2 \times 23) & - C_6 & C_7 \end{bmatrix}$$

Z: ZERO MATRIX

## NONLINEAR SIMULATION

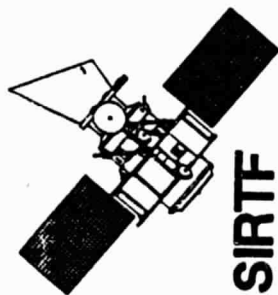
This chart shows a block diagram of the non-linear simulation as performed in the LISSA program. This diagram should not be construed as representing the control system, although it does include it. In particular, the output Y represents the output of the simulation, rather than only sensor measurements. The non-linear block is defined in the program by coding its equations in a special subroutine. This enables the imposition of non-linearities such as friction torque and maximum torque limits on the controller. The inclusion or the non-inclusion of the non-linear element is controlled by a single flag, thus linear simulations can be run easily when a particular performance evaluation does not require a non-linear model of the actuators.

The matrices H, K1 and K2 are used to provide any linear combination of X and U as an output. They do not affect the control design or performance. The command generator generates the feed-forward torque, the rate command, and attitude commands by assuming that the plant behaves as a rigid body.



# SIRTF





---

## SIMULATION RESULTS

---

PRECEDING PAGE BLANK NOT FILMED

131

PAGE 130 INTENTIONALLY BLANK

## SIMULATION CASES

Various operating conditions were simulated:

### 1. Small Angle Slew

This is an important maneuver for the SIRTf mission, in which the telescope must be pointed quickly from one part of the sky to another. The slew angle is relatively small (7 arcmin), but, because of structural flexibility and control system limitations, the system is not quiescent at the end of the prescribed slew time. Instead, damped oscillations are observed causing a pointing error which after some time (settling time) becomes smaller than the maximum allowable error (0.1 arcsec). This settling time is a function of both the time taken to perform the slew (slew time) and the torque profile used to slew the spacecraft.

### 2. Large Angle Slews

In these maneuvers, the spacecraft has to change its orientation by a relatively large angle. A particularly important case is for a 120 deg slew in 8 minutes (480 sec). For the same reasons as before, there may be some residual oscillations at the end of the slew and they depend upon the slew angle, the slew time and the torque profile. Some special conditions may occur in the SIRTf mission in which a faster slew is needed, i.e. 90 degrees in 90 seconds. This case has also been examined in the simulations.

### 3. Disturbance Response

These simulations address the evaluation of pointing errors due to either external disturbance torques (aerodynamic, gravity-gradient), or internally generated disturbance torques (momentum unload, cryogen slosh, CMG bearing stiction). The momentum unload is achieved through magnetic torques which are capable of continuously applying varying torques to the vehicle in order to keep the average momentum stored in the CMG system at a low value. However, it is more efficient to use them in a pulse mode in order to conserve energy. The liquid cryogen is superfluid Helium: inertial effects associated with its free rotation inside the tank cause small disturbance torques. Finally, the CMG bearing stiction is a non-linear effect causing limit cycling to occur.



## SIMULATION CASES

---

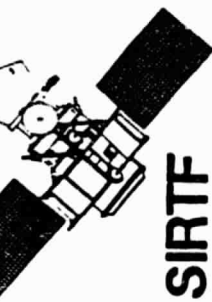
- SMALL ANGLE SLEWS
  - SETTLING TIME VS. COMMANDED SLEW TIME
  - SELECTED COMMAND PROFILES
- LARGE ANGLE SLEWS
  - 90/90 SEC USING SELECTED COMMAND PROFILES
  - 120°/480 SEC USING SELECTED COMMAND PROFILES
- DISTURBANCE RESPONSE
  - AERODYNAMIC TORQUE
  - AERODYNAMIC TORQUE AND MOMENTUM UNLOAD
  - CRYOGEN SLOSH
  - CHG BEARING STICTION

## SINE-VERSINE AND BANG-BANG TORQUE PROFILES

In a slew maneuver, the torque time history, or torque profile, has a strong impact on the modal excitation of the spacecraft and thus on the settling time. The "time optimal" torque profile is a profile which minimizes the maximum torque; it is also known as the "Bang-Bang" profile since it requires a full acceleration followed by a full deceleration. However, its spectrum is very rich in harmonics which can significantly excite vibration modes. In order to diminish this excitation, the torque profile must be modified in a such a way that its power spectrum decays rapidly with frequency. To meet this requirement, a very attractive profile, known as the "Sine-Versine", was developed by LMSC a few years ago. It is defined by the mathematical function:

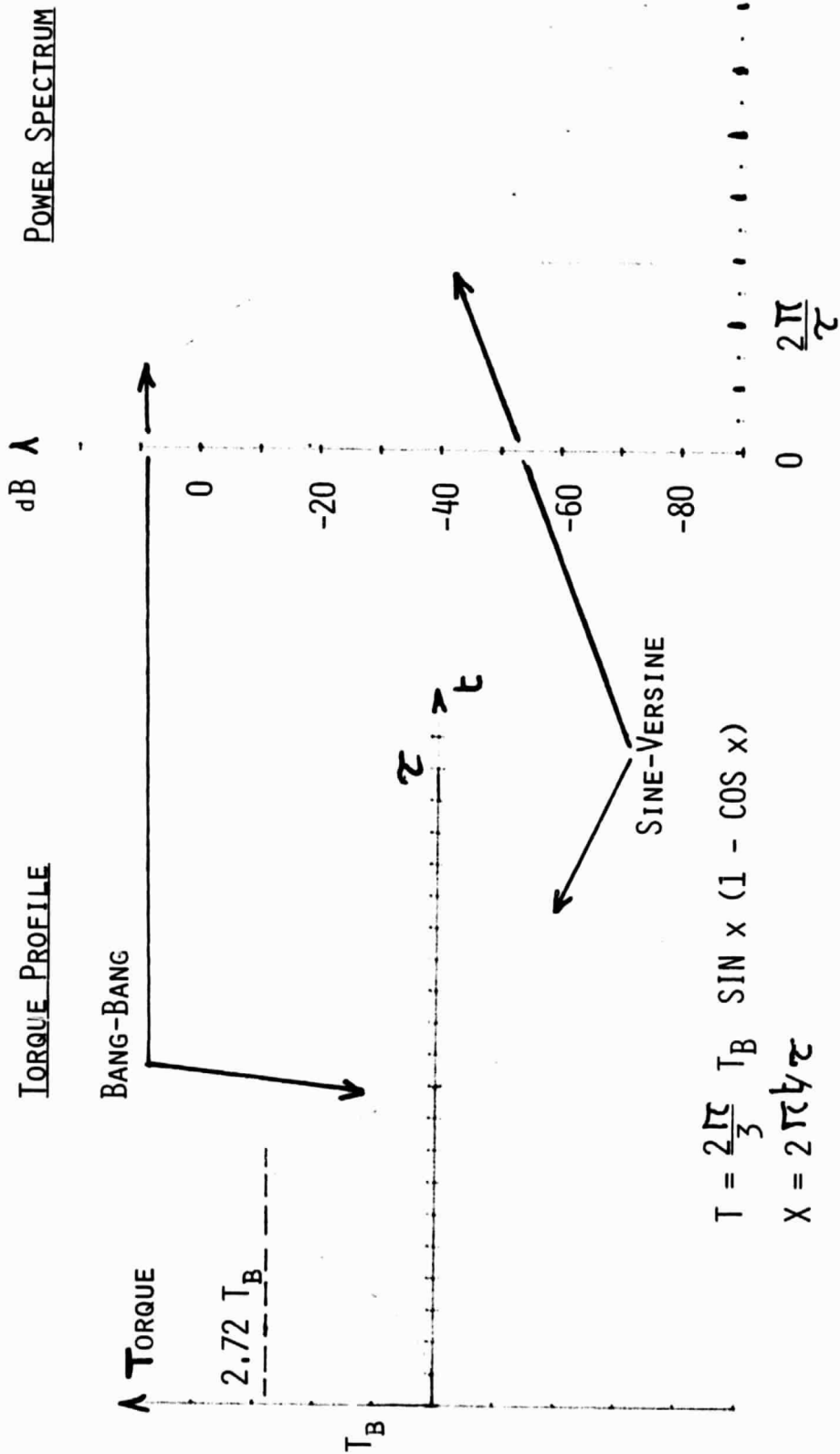
$T = T_{sv} \sin x (1 - \cos x)$  , where  $x = 2\pi t/\tau$  ,  $\tau$  is the slew time, and  $T_{sv}$  a constant.

The chart shows the two profiles and their corresponding power spectra. In order to make the comparison meaningful, the constant  $T_{sv}$  has been chosen to be  $(2\pi/3)T_b$ , so that the same slew angle be achieved in both cases. If the modal frequencies are greater than about  $2.3\pi/\tau$  , there is a significant advantage in using the Sine-Versine. For instance, with a first mode at 0.76 Hz (Solar Panel), and a slew time larger or equal to 3 seconds, the Sine-Versine results in better performance.



**SIRTF**

# SINE-VERSINE AND BANG-BANG TORQUE PROFILES



# BANG-BANG AND SINE-VERSINE SLEWS: TORQUE, RATE, AND ANGLE PROFILES.

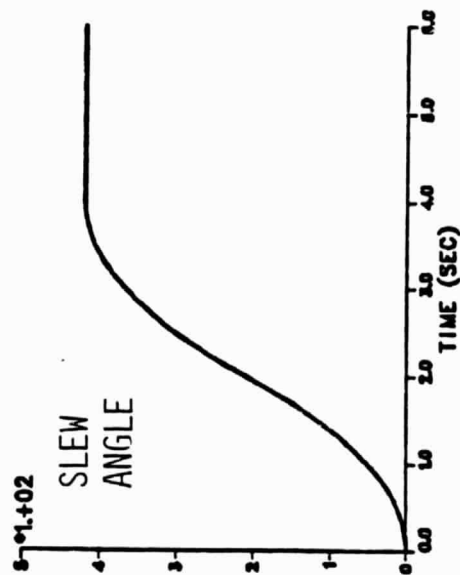
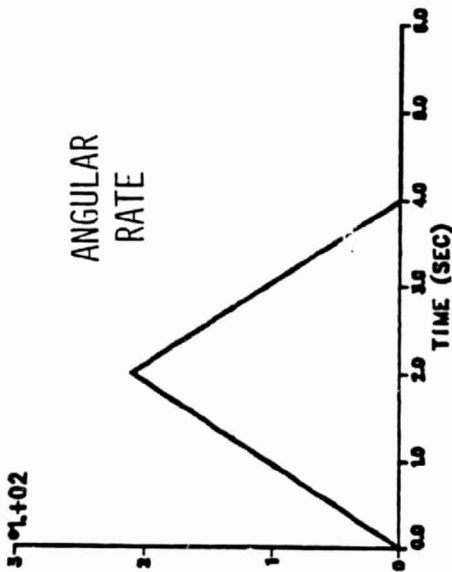
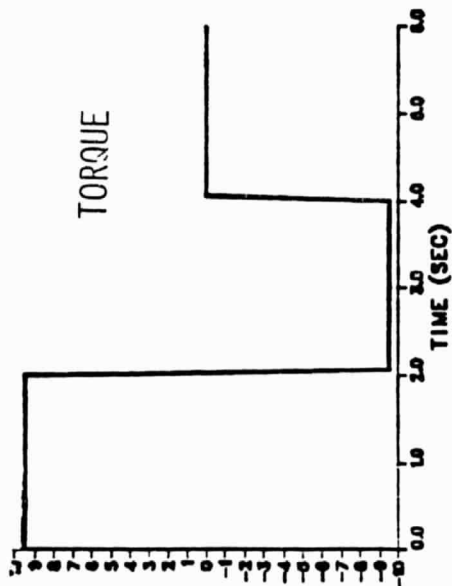
This chart shows the two torque profiles with the corresponding time histories of slew rate and slew angle. (These time histories are computed on the assumption of a rigid vehicle). While the torque profile (B-B or S-V) is used as a direct (feedforward) command to the CMGs, the computed angle and angular rate are subtracted from the corresponding actual vehicle angle and angular rate, so as to manufacture the error signals used in the feedback loop. These error signals, if different from zero, result in control torque increments which are added to the ideal torque profiles shown in the chart. Thus the actual torque applied to the vehicle may depart from the ideal bang-bang or sine-versine. This departure will be more pronounced if a given torque profile excites more natural vibrations, since the control system will have to compensate for these vibrations by applying more correcting torques. Thus, in general, it can be expected that the bang-bang profile will be strongly amended by the control system, and, even though its nominal peak torque is smaller than the sine-versine peak torque by a factor 2.7 or so, in reality the actual peak torque could be much higher.



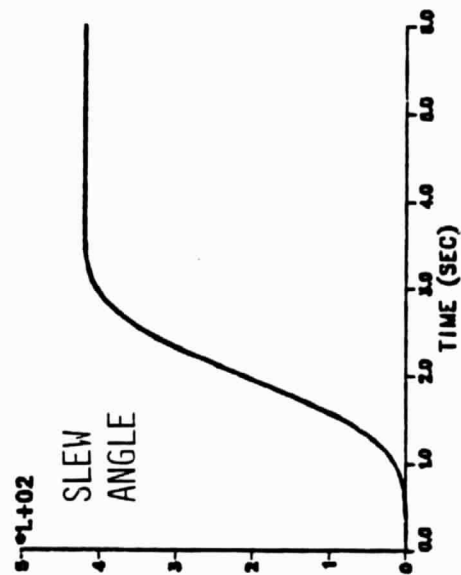
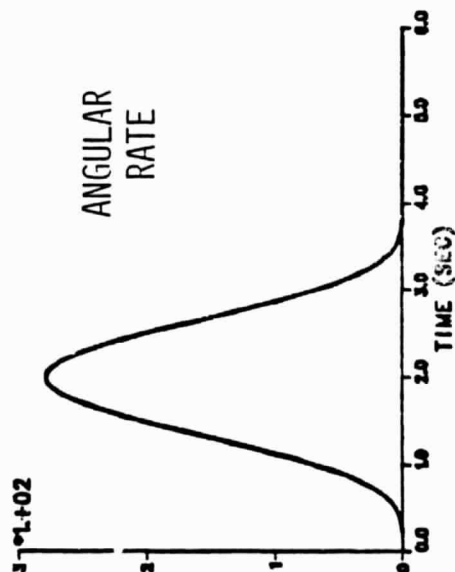
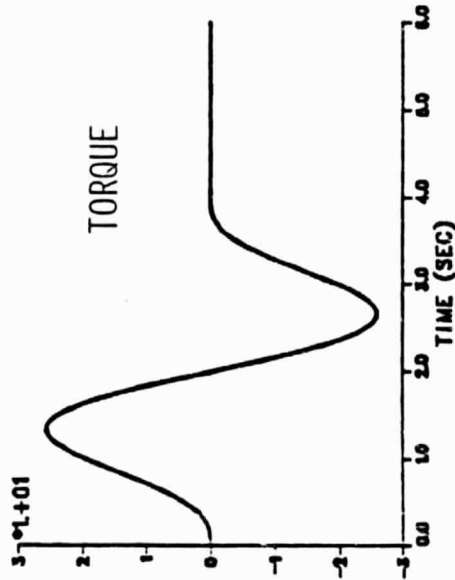
**SIRTF**

**BANG-BANG AND SINE-VERSINE SLEWS:  
TORQUE, RATE, AND ANGLE PROFILES**

**BANG-BANG SLEW**



**SINE-VERSINE SLEW**



## 28 DEG ORBIT OPEN AND CLOSED-LOOP ROOTS

This chart shows the eigenvalues of the dynamical model of the spacecraft (open loop roots) and those of the total system, i.e. when attitude and image stabilization control systems are activated (closed-loop roots). The corresponding modes or subsystems associated with a particular root are identified. The natural structural damping is usually low and has been adjusted in the model to be at or below 1 % of critical damping. Very little additional damping is introduced by the ACS in the roots corresponding to the telescope and the TDRSS antennae. However, up to 10 % is introduced in the three solar panel modes that couple with spacecraft rotations (antisymmetric modes). Symmetric modes are not affected by the ACS, and, conversely, do not cause pointing errors when excited. The ACS is primarily controlling the rigid body modes, introducing more than 50% damping in all three rotations with a bandwidth of about 1/2 Hz. The FGS bandwidth is less than 1/2 Hz (corresponding to a 1 Hz sampling rate). Finally, although the slosh frequency is truly zero, it was set at a very small value to avoid numerical instabilities in the simulation. This has no measurable effect on the results.



**SIRTF**

# 28° ORBIT OPEN AND CLOSED-LOOP ROOTS

## CLOSED LOOP

FREQUENCY	DAMPING	SLOSH
2.2450-03	.002962	SLASH
1.5481-01	1.000000	SLASH
1.5532-01	1.000000	SLASH
4.1575-01	1.000000	SLASH
4.4220-01	1.000000	SLASH
4.5755-01	1.000000	SLASH
5.2613-01	.583563	SLASH
5.5412-01	.505149	SLASH
5.6182-01	.550964	SLASH
7.5588-01	.008707	SLASH
7.6674-01	.107023	SLASH
7.8922-01	.009091	SLASH
8.0196-01	.108266	SLASH
1.0730+00	.008427	SLASH
1.0746+00	.010692	SLASH
1.1451+00	.078586	SLASH
1.1751+00	.076872	SLASH
1.4090+00	.005264	SLASH
1.4268+00	.027222	SLASH
1.4281+00	.005086	SLASH
1.4491+00	.022967	SLASH
1.3454+01	.490865	SLASH
1.3457+01	.496704	SLASH
1.9989+01	.009287	SLASH
2.0387+01	.009024	SLASH

## OPEN LOOP

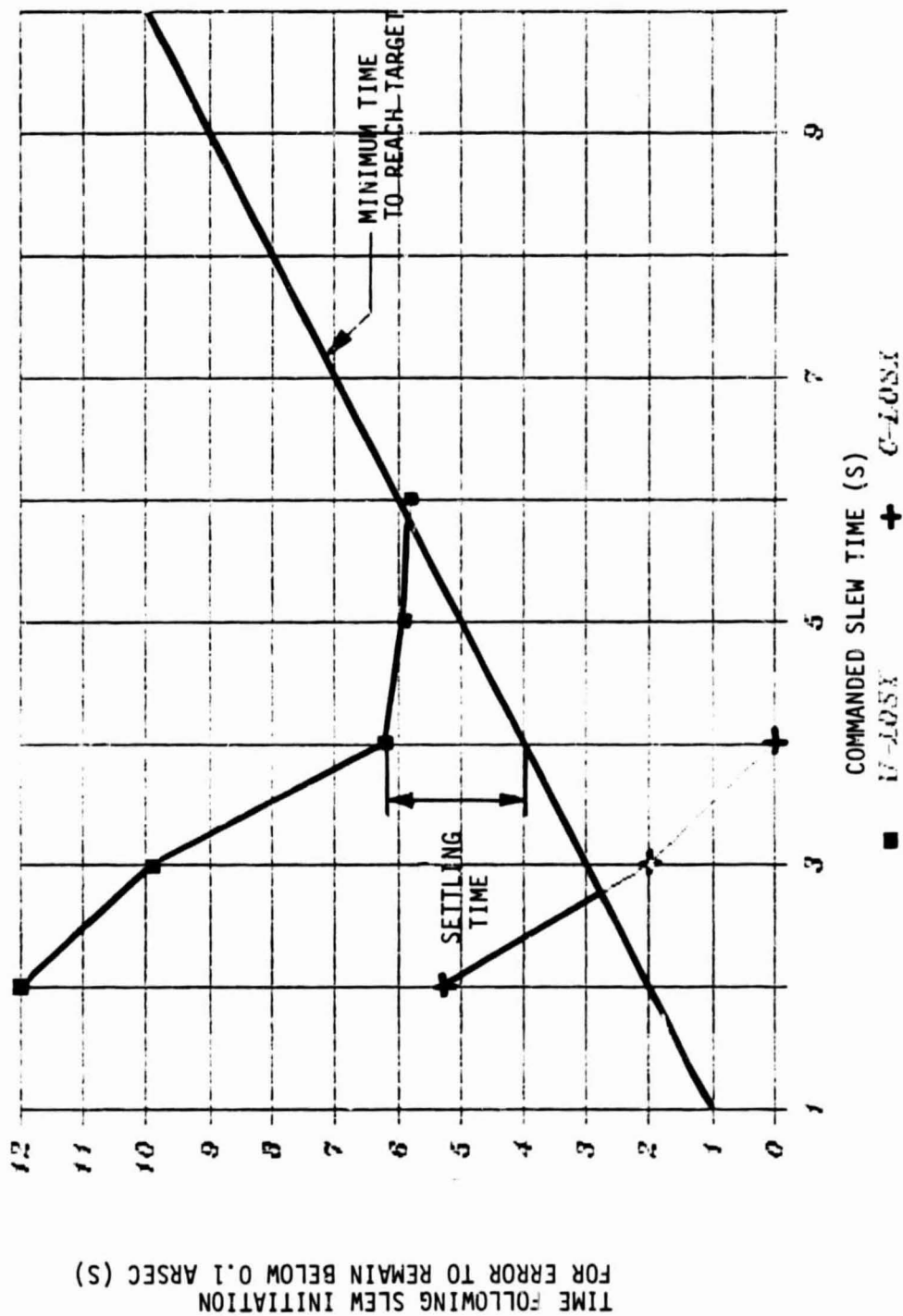
FREQUENCY	DAMPING	RIGID BODY
1.5755-05	.000000	RIGID BODY
1.8450-05	.000000	RIGID BODY
2.8483-05	.000000	RIGID BODY
2.2541-03	.002974	SLOSH
7.5588-01	.008707	SLOSH
7.8922-01	.009091	SLOSH
8.3272-01	.009591	SLOSH
8.7377-01	.010005	SLOSH
1.0730+00	.008427	SLOSH
1.0759+00	.008447	SLOSH
1.4091+00	.005155	SLOSH
1.4261+00	.005085	SLOSH
1.4462+00	.005368	SLOSH
1.4610+00	.005229	SLOSH
1.9992+01	.004499	SLOSH
2.0390+01	.004578	SLOSH

#### SETTLING TIME VS SLEW TIME FOR 28 DEG ORBIT (SINE-VERSINE SLEW)

This chart summarizes the main simulation results concerning small angle slews for the 28 deg orbit. These are 7 arcmin slews with a slew time varying from 2 to 6 seconds. The slew torque profile was a sine-versine. The chart shows plots of the time it takes after the start of the slew maneuver for the pointing error to decay to and remain below 0.1 arcsec. This pointing error is defined as the difference between the commanded and actual pointing angles. Thus, the error could settle below 0.1 arcsec before the end of the slew, i.e., the telescope could be tracking the prescribed attitude angle time history within 0.1 arcsec before being on the target. However, as long as the telescope line-of-sight is not on target, i.e., its attitude has not yet reached the prescribed final value, no observation can be made. Thus the minimum achievable time to reach the target is, by definition, equal to the prescribed slew time. This fact is graphically represented by a straight line. Points above this line mean that structural vibrations excited during the slew period need an extra time to damp out after the end of the slew (settling time). Points below the line mean that the telescope was already tracking the prescribed profile before the end of the slew.

The Time-To-Reach-Target (TTRT) has been plotted for the telescope Line-Of-Sight (U-LOSX) and for the actual focal plane error when Active Image Stabilization is used (C-LOSX). The TTRT first decreases, due to lessening of structural excitations, until about 6 seconds for U-LOSX (or 3 seconds for C-LOSX). Increasing the slew time beyond these values, will further reduce the residual oscillations, but will not improve the TTRT. The AIS will make it possible to achieve a 3 second TTRT instead of 6 seconds.

# SETTLING TIME VS SLEW TIME FOR 28° ORBIT (SINE-VERSINE)

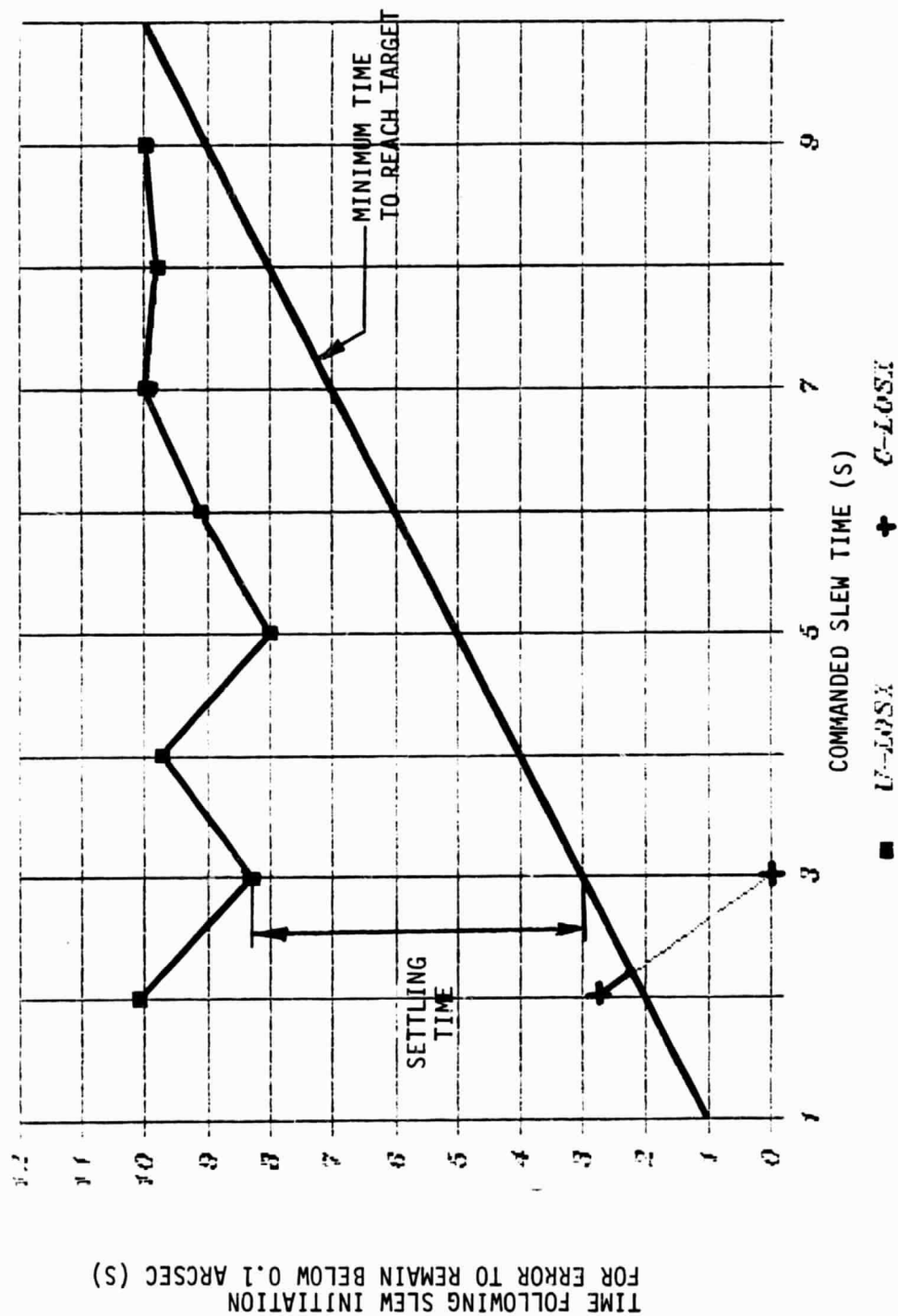


#### SETTLING TIME VS SLEW TIME FOR 28 DEG ORBIT (BANG-BANG SLEW)

This chart is analogous to the previous one, but corresponds to a Bang-Bang torque profile. In this case, lengthening the slew time does not significantly improve the TTRT. This results from the fact that the Bang-Bang power spectral density decreases only slowly with increased slew time, as was shown previously. The excitation of the solar panels and antennae is significant and is reoccurring at the very end of the slew, as the torque is abruptly turned-off. The settling time is therefore never zero when a Bang-Bang profile is used and the TTRT always exceeds the slew time. Slew times from 2 to 9 seconds were simulated. The dramatic effect of Active Image Stabilization is evident in this case in which the TTRT is reduced from 10 to 3 seconds.



# SETTLING TIME VS SLEW TIME FOR 28° ORBIT (BANG-BANG SLEW)



SIMULATION CASE: 28 DEG ORBIT (Small Angle Slews)

This table summarizes the main simulation results concerning the system performance for small slew maneuvers. The slews are about the X-axis and thus the main pointing error appears in U-LOSX. Errors in the other axes (U-LOSY and U-LOSZ) are much smaller. The pointing errors as well as the other quantities shown in the table are the maximum values during and beyond the slew time. The "mirror tilt" values correspond to the secondary mirror motion when AIS is turned on. They are very conservative since, in a real mission, there will be no need to activate AIS during the slew, but only at the end, where the required pointing corrections are much smaller. The TDRSS antenna and Solar Panel bending is expressed in terms of their global angular deflection. Several operating cases are shown. First are slews using the Sine-Versine torque profile for various slew times. The cases use the Bang-Bang profile. The effect of a 2 % error in the feed-forward torque command and of no feed-forward command are shown. Finally, the FGS feedback for AIS was turned off in the last case, resulting in an increase in settling times.



# SIMULATION CASE: 28 DEG ORBIT

SMALL ANGLE SLEWS (7 Arcmin in 2 s)

	Total Time to Settle on Target (s)		Maximum values During or After Slew					
	U-LOSx	C-LOSx	U-LOSy	C-LOSx	U-LOSy	MIRROR TORSS Tilt Rending	SP Rending Torque	CMG CRUISEN Velocity
SINE-VERSINE	12.0	5.4	3.0	20. AS	0.4 AS	0.4 AS	3. AS	220. AS
	2 sec slew	2.0	2.5	7.8 AS	0.15 AS	0.3 AS	5. AS	100. AS
	3 sec slew	-	-	7.8 AS	0.15 AS	0.3 AS	5. AS	100. AS
	4 sec slew	-	-	7.8 AS	0.15 AS	0.3 AS	5. AS	100. AS
	5 sec slew	-	-	7.8 AS	0.15 AS	0.3 AS	5. AS	100. AS
BANG-BANG	10.1	2.8	2.0	7.8 AS	0.15 AS	0.3 AS	5. AS	100. AS
	2 sec slew	-	-	7.8 AS	0.15 AS	0.3 AS	5. AS	100. AS
	3 sec slew	-	-	7.8 AS	0.15 AS	0.3 AS	5. AS	100. AS
	4 sec slew	-	-	7.8 AS	0.15 AS	0.3 AS	5. AS	100. AS
	5 sec slew	-	-	7.8 AS	0.15 AS	0.3 AS	5. AS	100. AS
BANG-BANG (2 sec) With: 2 x Scale Error in FF Command	10.1	2.8	2.0	7.8 AS	0.15 AS	0.3 AS	5. AS	100. AS
	2 sec slew	-	-	7.8 AS	0.15 AS	0.3 AS	5. AS	100. AS
	3 sec slew	-	-	7.8 AS	0.15 AS	0.3 AS	5. AS	100. AS
	4 sec slew	-	-	7.8 AS	0.15 AS	0.3 AS	5. AS	100. AS
	5 sec slew	-	-	7.8 AS	0.15 AS	0.3 AS	5. AS	100. AS
no FF command	10.3	3.8	3.2	40. AS	0.3 AS	0.4 AS	160. AS	55. AS
	2 sec slew	-	-	40. AS	0.3 AS	0.4 AS	160. AS	55. AS
	3 sec slew	-	-	40. AS	0.3 AS	0.4 AS	160. AS	55. AS
	4 sec slew	-	-	40. AS	0.3 AS	0.4 AS	160. AS	55. AS
	5 sec slew	-	-	40. AS	0.3 AS	0.4 AS	160. AS	55. AS
no FGS Feedback	10.1	3.5	2.0	7.8 AS	0.15 AS	0.3 AS	5. AS	100. AS
	2 sec slew	-	-	7.8 AS	0.15 AS	0.3 AS	5. AS	100. AS
	3 sec slew	-	-	7.8 AS	0.15 AS	0.3 AS	5. AS	100. AS
	4 sec slew	-	-	7.8 AS	0.15 AS	0.3 AS	5. AS	100. AS
	5 sec slew	-	-	7.8 AS	0.15 AS	0.3 AS	5. AS	100. AS

\*\*\* Abbreviations: AS = arcsec

SIMULATION CASE: 28 DEG ORBIT (Large Angle Slews)

The disposition of this chart is similar to that of the previous chart. The cases studied here concern various large angle slews. The nominal slew, as defined by the original system requirements, is a 120 degree in 8 minutes slew. Bang-Bang and Sine-Versine profiles were used. Note that the Sine-Versine results in an increase in maximum slew rate (0.7 vs 0.5 deg/s).

A 2.5 deg in 10 sec slew was studied. It also has a 1/4 deg/s average slew rate. However, because of the shorter time involved, the required torque is much higher and so is the corresponding excitation of structural vibration. Finally three torque profiles were studied for the 90 deg/90 sec case. The Bang-Cruise-Bang is the profile which results in the minimum possible slew rate. Thus reducing the momentum storage requirements. However it requires the highest torque (300 Nm). This torque is applied in one direction for one second, then turned off for 88 seconds, then applied in the other direction for another second to stop the spacecraft. The Sine-Versine profile does not excite vibrations (settling time = 0), but produces the highest rate (2.8 deg/s).

The cryogen velocity is maximum in the S-V 90 degree slew and reaches about 30 mrad/s. The CM of the cryogen is about 0.5 m from the vehicle axis, creating a centrifical force a little less than .1 N. Since the tank is also offset by about 1 m from the vehicle CM, a disturbance torque of about 0.1 Nm could thus be generated.



# SIMULATION CASE: 28 DEG ORBIT

## LARGE ANGLE SLEWS

	Time to Settle After End Of Slew (s)			Maximum Values During or After Slew .....						
	U-LUSX	C-LUSX	U-LOSY	U-LUSX	C-LOSX	U-LOSY	U-LOSZ	TDRSS Bending	SP Bending	CMG Torque Velocity
120 Deg/8 min ----- Bang-Bang (0.5 Deg/s max)	1.8	0.0	0.0	0.5 AS	20 mAS	-	-	50. mAS	1.8 AS	0.68 Nm 2. mrad/s
Sine-Versine (0.7 Deg/s max)	0.0	0.0	0.0	0.5 AS	30. mAS	-	-	60. mAS	1.5 AS	1.4 Nm 10. mrad/s
2.5 Deg/10 s ----- Sine-Versine (0.7 Deg/s max)	10.2	0.0	0.0	0.9 AS	35. mAS	-	-	2. AS	75. AS	67.2 Nm 10. mrad/s
90 Deg/30 s ----- Bang-Bang (2 deg/s max)	0.5	0.0	0.0	4.5 AS	0.07 AS	0.05 AS	0.1 AS	2. AS	45. AS	12. Nm 18. mrad/s
Sine-Versine (2.8 deg/s max)	0.0	0.0	0.0	1.2 AS	0.02 AS	0.01 AS	0.01 AS	1. AS	32. AS	38. Nm 30. mrad/s
Bang-Cruise-Bang (1.02 deg/s max)	7.5	5.5	1.5	35. AS	4. AS	0.72 AS	1.44 AS	20. AS	500. AS	320. Nm 12. mrad/s

\*\*\* Abbreviations: AS = arcsec, mAS = milliarcsec

#### SIMULATION CASE: 28 DEG ORBIT (Disturbances)

The disposition of this chart is the same as the previous chart. However, there is no mention of settling times since the pointing errors are more of a steady-state nature. The effect of an initial vehicle rate of 1 arcsec/s is first shown for two levels of CMG bearing stiction. Because of stiction on the gimbal bearing, the CMG gimbal rate cannot be made arbitrarily small, and the CMG gimbal motor is either at rest or rotating at or above this minimum rate. As a result the torque output cannot be made arbitrarily small. The minimum value for this torque is usually a given fraction of the maximum torque output. For a 300 Nm CMG, a ratio of 1 in 1000 will result in a 0.3 Nm minimum torque; for a 1/5000 ratio, much more difficult to obtain, it will be 0.06 Nm. On the other hand, if smaller CMGs are used, e.g. 25 Nm for the baseline medium performance design, then less than 0.06 Nm stiction can easily be obtained. The high and low stiction cases have been simulated and are shown in the table.

The stiction effect results in a limit cycle in which the CMG gimbal angle changes in an abrupt fashion, resulting in pulse-like torques disturbing the spacecraft. It also produces an apparent lag which reduces the system performance. In the low stiction case, the limit cycle effect is not sufficient to directly affect the pointing accuracy, but high stiction will require the use of AIS.

The momentum dump case corresponds to a pulse-shaped desaturation torque of 0.1 Nm magnitude applied for 10 seconds. Finally, a step torque equal to 0.025 Nm was applied to simulate a worst case aerodynamic torque. Again gimbal stiction primarily degrades the transient response, but limit cycle effects remain negligible for the low stiction case.



**SIRTF**

# SIMULATION CASE: 28 DEG ORBIT

## DISTURBANCES

	U-LOSX	C-LOSX	U-LOSX	U-LOSZ	MIRROR Tilt	TDRSS Bending	SP Bending	CMG Torque
1 AS/s Init. Rate								
Stiction 0.30 Nm	0.20 AS	2.0 mAS	-	0.6 mAS	0.80 AS	13. mAS	0.36 AS	0.6 Nm
0.06 Nm	0.04 AS	2.5 mAS	-	0.1 mAS	0.16 AS	17. mAS	0.38 AS	0.6 Nm
Momentum Dump (0.1 Nm)								
	70. mAS	0.60 mAS	0.30 mAS	0.6 mAS	0.280 AS	7.0 mAS	0.30 AS	0.25 Nm
Aero Torque (0.025 Nm)								
Stiction 0.30 Nm	120. mAS	1.20 mAS	0.15 mAS	0.25 mAS	0.480 AS	4.5 mAS	0.15 AS	0.50 Nm
0.06 Nm	25. mAS	0.45 mAS	-	0.16 mAS	0.100 AS	2.2 mAS	0.08 AS	0.10 Nm
No Stiction	17. mAS	0.13 mAS	-	0.15 mAS	0.060 AS	1.5 mAS	0.06 AS	0.05 Nm

\*\*\* Abbreviations : AS = arcsec , mAS = milliarcsec .

## 98 DEG ORBIT OPEN AND CLOSED-LOOP ROOTS

This chart shows the eigenvalues of the dynamical model of the spacecraft (open loop roots) and those of the total system, i.e. when attitude and image stabilization control systems are activated (closed-loop roots). The corresponding modes or subsystems associated to a particular root are identified. The natural structural damping is usually low and has been adjusted in the model to be at or below 1 % of critical damping. Very little additional damping is introduced by the ACS in the roots corresponding to the telescope (0.8 %) and about 2 % in those TDRSS antenna modes that couple with spacecraft rotations (antisymmetric modes). Symmetric modes are not affected by the ACS, and, conversely, do not cause pointing errors when excited. The ACS is mainly controlling the rigid body modes, introducing more than 60% damping in all three rotations and with a bandwidth of about 1/2 Hz. The FGS bandwidth is less than 1/2 Hz (corresponding to a 1 Hz sampling rate).

Finally, although the slosh frequency is truly zero, it was set at a very small value to avoid numerical instabilities in the simulation, but had no measurable effect on the results.



# 98° ORBIT OPEN AND CLOSED-LOOP ROOTS

## CLOSED LOOP

FREQUENCY	DAMPING	
1.3417-03	.001770	SLOSH
1.5481-01	1.000000	ALS INTEGRATOR
1.5532-01	1.000000	
4.6544-01	1.000000	RIGID BODY
5.0880-01	1.000000	INTEGRAL CONTROL
5.1141-01	.681724	
5.1658-01	.650632	RIGID BODY
5.2409-01	.605742	
5.5679-01	1.000000	RIGID BODY INTEGRAL CONTROL
1.1451+00	.078586	MIRROR SERVO
1.1751+00	.076872	
1.4729+00	.005967	
1.4930+00	.005757	TDRSS ANTENNA
1.4931+00	.022131	
1.5168+00	.023402	
1.3454+01	.490865	MIRROR DYNAMICS
1.3457+01	.496704	
1.9478+01	.008736	TELESCOPE
1.9644+01	.008297	

## OPEN LOOP

FREQUENCY	DAMPING	
3.0331-05	.000000	RIGID BODY
5.0411-05	.000000	
6.4621-05	.000000	
1.3527-03	.001785	SLOSH
1.4727+00	.005436	
1.4927+00	.005362	
1.5062+00	.005522	TDRSS ANTENNA
1.5297+00	.005485	
1.9481+01	.004901	TELESCOPE
1.9646+01	.005141	

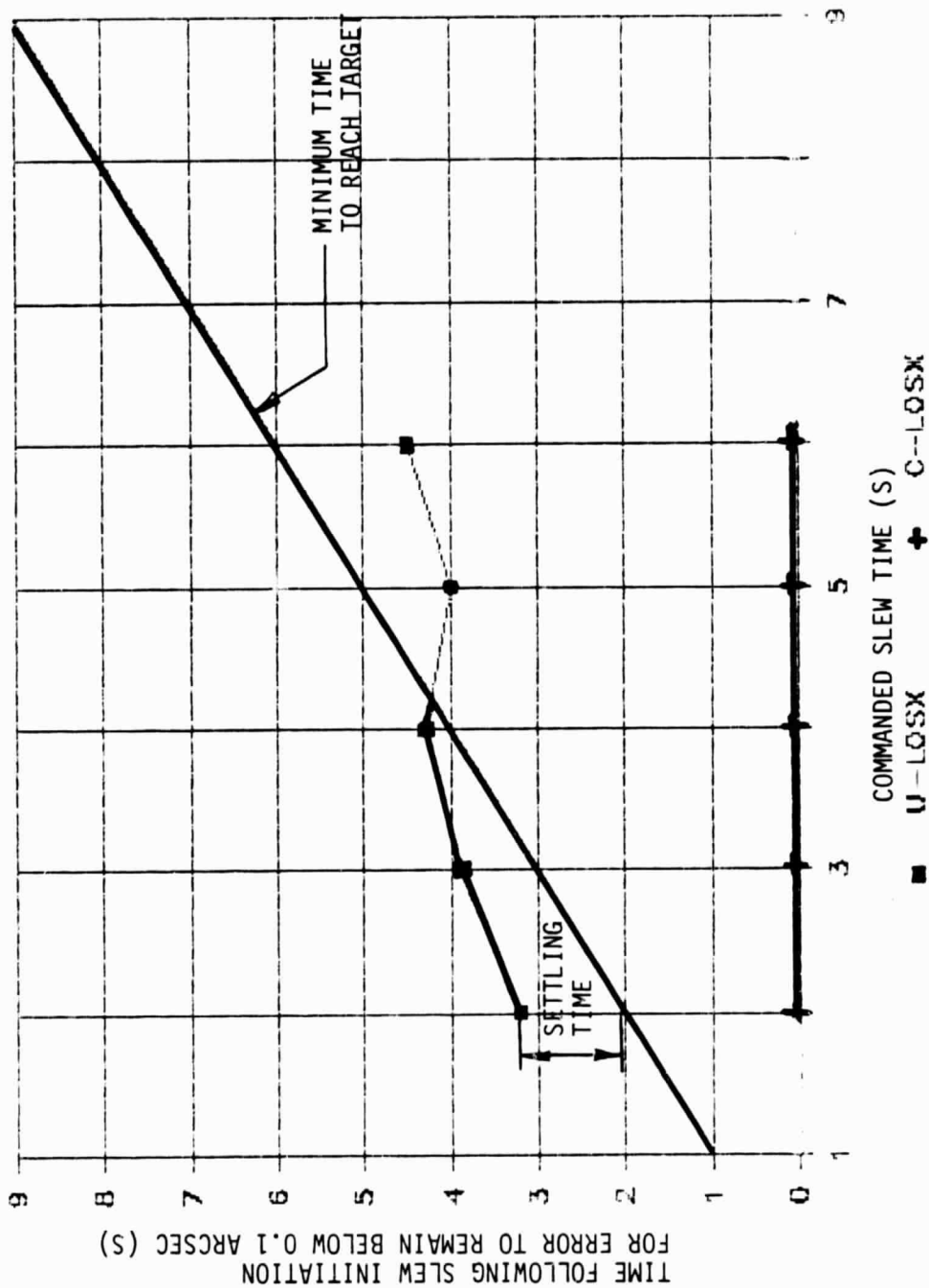
#### SETTLING TIME VS SLEW TIME FOR 98 DEG ORBIT (SINE-VERSINE SLEW)

This chart summarizes the main simulation results concerning small angle slews for the 98 deg orbit. These are 7 arcmin slews with a slew time varying from 2 to 6 seconds. The slew torque profile was a sine-versine. The chart shows plots of the time it takes after the start of the slew maneuver for pointing error to decay to and remain below 0.1 arcsec. This pointing error is defined as the difference between the commanded and actual pointing angles. The error could settle below 0.1 arcsec before the end of the slew, i.e., the telescope could be tracking the prescribed attitude angle time history within 0.1 arcsec before being on target. However, as long as the telescope line-of-sight is not on target, i.e., its attitude has not yet reached the prescribed final value, no observation can be made. Thus the minimum achievable time to reach the target is, by definition, equal to the prescribed slew time. This fact is graphically represented by a straight line. Points above this line mean that structural vibrations excited during the slew period need an extra time to damp out after the end of the slew (settling time). Points below the line mean that the telescope was already tracking the prescribed profile before the end of the slew.

The telescope Line-Of-Sight (U-LOSX) and the focal plane pointing error after correction by the AIS (C-LOSX) are shown on the chart. In contrast with the 28 degree case, the Time-To-Reach-Target (TTRT) quickly approaches its minimum value, i.e. the slew time. Since the structural vibration problem is not as severe, it is possible to be on target in about 3 seconds without AIS, and 2 seconds with AIS, the tracking error being below 0.1 arcsec during the entire slew maneuver in the latter case.



# SETTLING TIME VS SLEW TIME FOR 98° ORBIT



#### SIMULATION CASE: 98 DEG ORBIT (Small Angle Slews)

This table summarizes the main simulation results concerning the system performance for small slew maneuvers. The slews are about the X-axis and thus the main pointing error appears in U-LOSX. Errors in the other axes (U-LOS<sub>Y</sub> and U-LOS<sub>Z</sub>) are much smaller. The pointing errors as well as the other quantities shown in the table are the maximum values during and beyond the slew time. The times shown for the U-LOS<sub>X</sub>, C-LOS<sub>X</sub> and U-LOS<sub>Y</sub> are the TTRTs corresponding to the various slews simulated.

The "mirror tilt" values correspond to the secondary mirror motion when the AIS is turned on. They are very conservative since, in a real mission, there will be no need to activate AIS during the slew, but only at the end where the required pointing corrections are much smaller. The TDRSS antenna bending is expressed in terms of its global angular deflection. Several operating cases are shown. First are two Sine-Versine slews using 2 and 3 second slew times. Results for corresponding Bang-Bang slews are shown next. The next four cases also use a Bang-Bang torque profile. The effect of a 2 % error in the feed-forward torque command and of no feed-forward command are shown. In the last case, the FGS feedback for the AIS was turned off, showing an increase in the settling time of about 1 second.



**SIRT**

# SIMULATION CASE: 98 DEG ORBIT

## SMALL ANGLE SLEWS (7 arcmin)

Total time to Settle  
on Target (s)

Maximum Values During or After the Slew Period .....

	U-LOSX	C-LOSX	U-LOSX	U-LOSZ	MIRROR	TDRSS	CMG	CRYOGEN
	U-LOSX	C-LOSX	U-LOSX	U-LOSZ	Tilt	Bending	Torque	Velocity
SINE-VERSE								
2 sec slew	3.2	0.0	0.0	0.0	1.5 AS	0.03 AS	30. mAS	0.37 AS
3 sec slew	3.9	0.0	0.0	0.0	6. AS	3. AS	90. Nm	0.1 mrad/s
BANG-BANG								
2 sec slew	4.1	1.5	0.0	0.0	4.2 AS	0.11 AS	21. mAS	18. mAS
					16.8 AS	4. AS	53. Nm	0.1 mrad/s
BANG-BANG (2 sec)								
with :								
2 % Scale Error	4.1	2.0	0.0	0.0	4.1 AS	0.12 AS	21. mAS	18. mAS
in FF Command					16.4 AS	4. AS	53. Nm	0.1 mrad/s
no FF Command	4.8	2.0	0.0	0.0	28. AS	0.90 AS	25. AS	14. mAS
					112. AS	3. AS	53. Nm	0.1 mrad/s
no FGS Feedback	4.5	2.5	0.0	0.0	5.6 AS	0.15 AS	6.0 mAS	0.2 AS
					22.4 AS	4. AS	60. Nm	0.1 mrad/s

\*\*\* Abbreviations : AS = arcsec , mAS = milliarcsec .

#### SIMULATION CASE: 98 DEG ORBIT (Large Angle Slews)

The disposition of this chart is similar to that of the previous chart. The cases studied here concern various large angle slews. The nominal slew, as defined by the original system requirements, is 120 degrees in 8 minutes. Bang-Bang and Sine-Versine profiles were used. Note that the Sine-Versine results in an increase in maximum slew rate (0.7 vs 0.5 deg/s).

A 2.5 deg in 10 sec slew was studied. It also has a  $1/4$  deg/s average slew rate. However, because of the shorter time involved, the required torque is much higher and so is the corresponding excitation of structural vibration. Finally, three torque profiles were studied for the 90 deg/90 sec case. The Bang-Cruise-Bang is the profile which results in the minimum possible slew rate, thus reducing the momentum storage requirements. However it requires the highest torque (300 Nm). This torque is applied in one direction for one second, then turned off for 88 seconds, then applied in the other direction for another second to stop the spacecraft. The Sine-Versine profile does not excite vibrations (settling time = 0), but produces the highest rate (2.8 deg/s).

Compared with the 28 degree orbit cases, the cryogen velocity is remarkably small. This is because in the polar orbit design the helium tank is very close to the CM of the vehicle and thus, even though the cryogen mass is larger, much less dynamic interaction takes place.



# SIMULATION CASE: 98 DEG ORBIT

## LARGE ANGLE SLEWS

		Time to Settle After End of Slew (s)						Maximum Values During and After Slew Period .....		
		U-LOSX	C-LOSX	U-LOSX	U-LOSX	C-LOSX	U-LOSX	TDRSS Bending Torque	CMG Torque	CRYOGEN Velocity
120 Deg/8 min ----- Bang-Bang (0.5 Deg/s max)		1.5	0.0	0.0	0.0	0.4 AS	30. mAS	1. mAS	-	40. mAS 0.6 Nm 0.4 mrad/s
	Sine-Versine (0.7 Deg/s max)	0.0	0.0	0.0	0.0	0.5 AS	40. mAS	1. mAS	-	50. mAS 0.9 Nm 0.4 mrad/s
2.5 Deg/10s ----- Sine-Versine (0.7 Deg/s max)		0.0	0.0	0.0	0.0	5.5 AS	80. mAS	20. mAS	18. AS	1.7 AS 70. Nm 0.5 mrad/s
90 Deg/90 s SLEW ----- Bang-Bang (2 deg/s max)		2.0	0.0	0.0	0.0	2.5 AS	80. mAS	9. mAS	7. mAS	1.0 AS 23. Nm 1.3 mrad/s
	Sine-Versine (2.8 deg/s max)	0.0	0.0	0.0	0.0	1.4 AS	30. mAS	1. mAS	1. mAS	0.6 AS 32. Nm 2.0 mrad/s
Bang-Cruise-Bang (1.02 deg/s max)		10.0	4.0	0.0	0.0	50. AS	0.8 AS	90. mAS	90. mAS	18. AS 360. Nm 0.7 mrad/s

\*\*\* Abbreviations : AS = arcsec , mAS = milliarccsec .

SIMULATION CASE: 98 DEG ORBIT (Disturbances)

The disposition of this chart is the same as the previous chart. However, there is no mention of settling times since the pointing errors are more of a steady-state nature. The effect of an initial vehicle rate of 1 arcsec/s is first shown for two levels of CMG bearing stiction. Because of stiction on the gimbal bearing, the CMG gimbal rate cannot be made arbitrarily small, and the CMG gimbal motor is either at rest or rotating at or above this minimum rate. As a result the torque output cannot be made arbitrarily small. The minimum value for this torque is usually a given fraction of the maximum torque output. For a 300 Nm CMG, a ratio of 1 in 1000 will result in a 0.3 Nm minimum torque; for a 1/5000 ratio, much more difficult to obtain, it will be 0.06 Nm. On the other hand, if smaller CMGs are used, e.g. 25 Nm for the baseline medium performance design, then less than 0.06 Nm stiction can easily be obtained. The high and low stiction cases have been simulated and are shown in the table.

The stiction effect results in a limit cycle in which the CMG gimbal angle changes in an abrupt fashion, resulting in pulse-like torques disturbing the spacecraft. It also produces an apparent lag which reduces the system performance. In the low stiction case, the limit cycle effect is not sufficient however to directly affect the pointing accuracy. In all cases, limit cycle effects are less pronounced than in the 28 deg orbit vehicle because of lower flexibility.

The momentum dump case corresponds to a pulse-shaped desaturation torque of 0.1 Nm magnitude applied for 10 seconds. Finally, a step torque equal to 0.025 Nm was applied to simulate a worst case aerodynamic torque. Again gimbal stiction primarily degrades the transient response, but limit cycle effects remain negligible for the low stiction case.

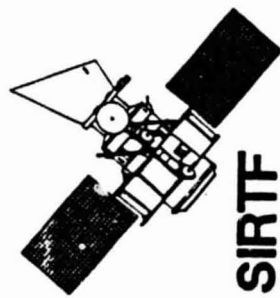


# SIMULATION CASE: 98 DEG ORBIT

## DISTURBANCES

	U-LOSX	C-LOSX	U-LOSX	U-LOSZ	MIRROR	LDPS	CMG
					Tilt	Heading	Torque
1 AS/s Init. Rate							
Stiction 0.30 Nm	0.16 AS	6.0 mAS	-	0.5 mAS	0.6 AS	0.15 AS	0.60 Nm
0.06 Nm	0.04 AS	7.0 mAS	-	0.7 mAS	0.16 AS	0.15 AS	0.80 Nm
Momentum Dump (0.1 Nm)							
	50. mAS	0.6 mAS	-	0.4 mAS	0.20 AS	6.0 mAS	0.18 Nm
Aero Torque (0.025 Nm)							
Stiction 0.30 Nm	100. mAS	2.0 mAS	-	0.10 mAS	0.40 AS	4.0 mAS	0.50 Nm
0.06 Nm	22. mAS	0.3 mAS	-	0.09 mAS	0.09 AS	2.0 mAS	0.07 Nm
No Stiction	12. mAS	0.13 mAS	-	0.08 mAS	0.05 AS	1.3 mAS	0.04 Nm

\*\*\* Abbreviations : AS = arcsec , mAS = milliarcsec .



---

REPRESENTATIVE SIMULATION  
TIME HISTORIES

---

PRECEDING PAGE BLANK NOT FILMED

161

28 DEG ORBIT 7 ARCMIN/2S BANG-BANG SLEW

This chart shows time histories corresponding to the following conditions:

Slew direction: about the X axis  
Slew angle : 7 arcmin  
Slew time : 2 sec  
Torque profile: BANG-BANG

The following quantities are displayed:

Top left: Solar Panel bending about the slew axis.	(arcsec)
Top Right: TDRSS antenna bending about the slew axis.	(arcsec)
Bottom Left: Telescope pointing error	(arcsec)
Bottom Right: Focal Plane pointing error after correction by AIS.	(arcsec)

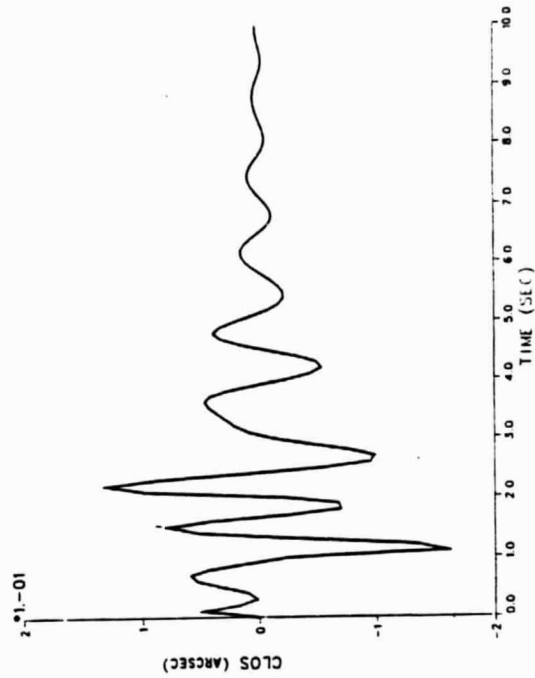
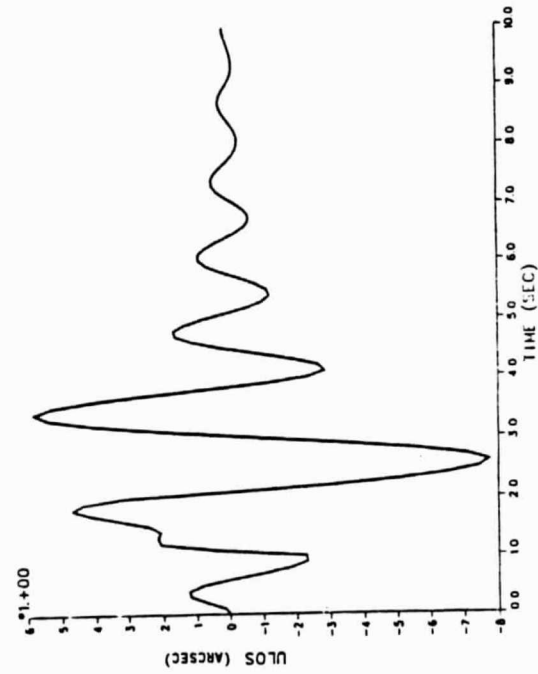
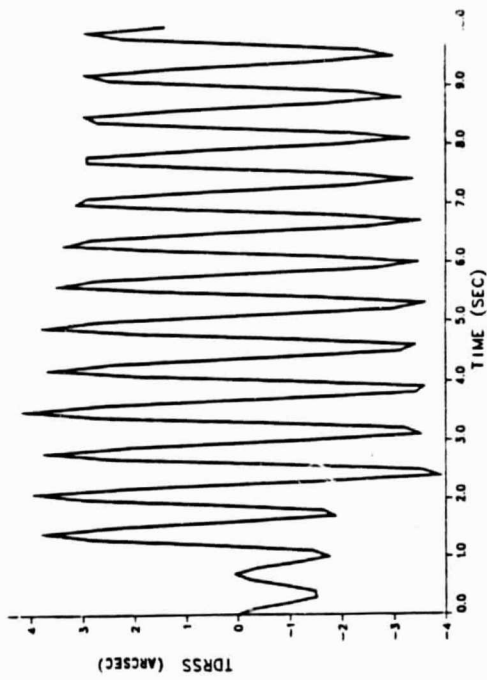
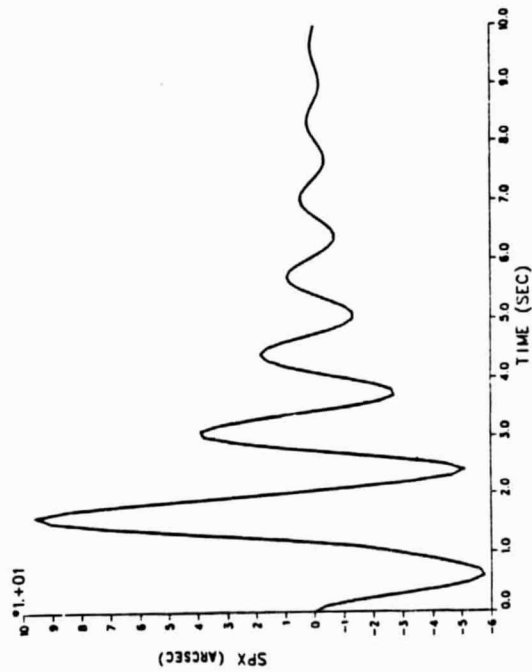
Remarks: Note the lightly damped vibration of the TDRSS antenna



**SIRTf**

28° ORBIT 7 ARCMIN/2S

BANG-BANG SLEW



28 DEG ORBIT 7 ARCMIN/2S SINE-VERSINE SLEW

This chart shows time histories corresponding to the following conditions:

Slew direction: about the X axis  
Slew angle : 7 arcmin  
Slew time : 2 sec  
Torque profile: SINE-VERSINE

The following quantities are displayed:

Top left: Solar Panel bending about the slew axis. (arcsec)

Top Right: TDRSS antenna bending about the slew axis. (arcsec)

Bottom Left: Telescope pointing error (arcsec)

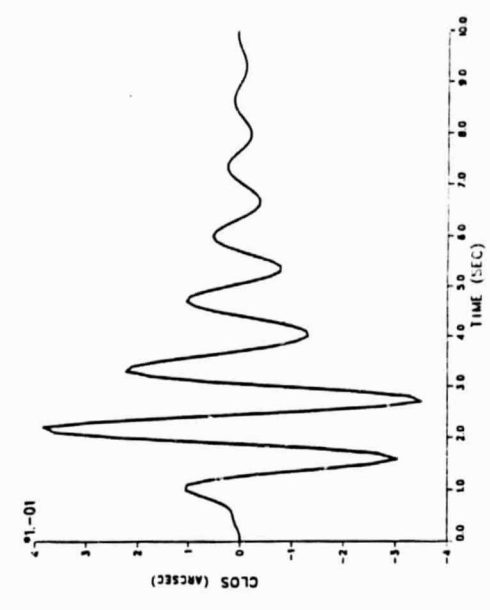
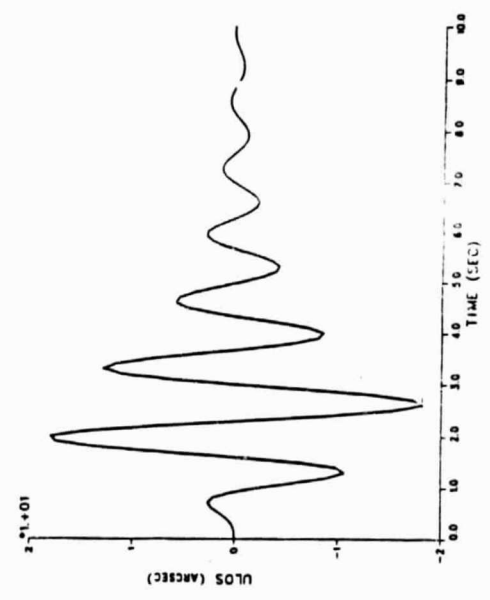
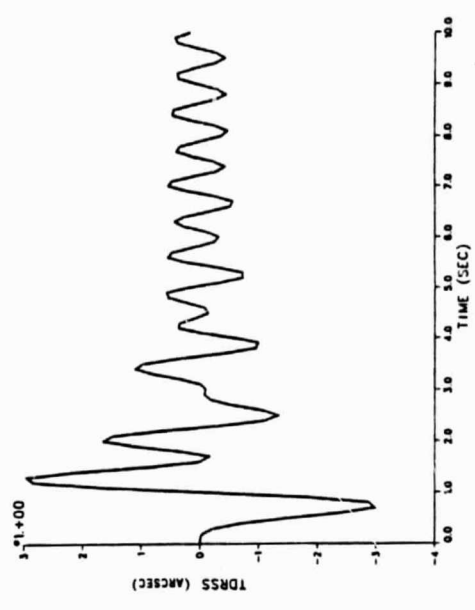
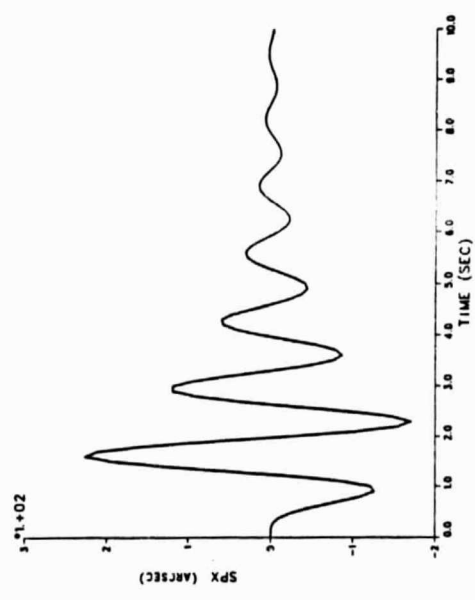
Bottom Right: Focal Plane pointing error after  
correction by AIS. (arcsec)

Remarks: Compare the vibration of the TDRSS with the previous chart. The choice of the torque profile greatly influences the amount of structural vibration excited for frequencies larger than the reciprocal of the slew time. The solar panel has a greater excitation than in previous cases because of its lower natural resonance and also because higher peak torques are required for this torque profile.



SIRTF

28° ORBIT 7 ARCMIN/2S SINE-VERSINE SLEW



98 DEG ORBIT 7 ARCMIN/2S SINE-VERSINE SLEW

This chart shows time histories corresponding to the following conditions:

Slew direction: about the X axis  
Slew angle : 7 arcmin  
Slew time : 2 sec  
Torque profile: SINE-VERSINE

The following quantities are displayed:

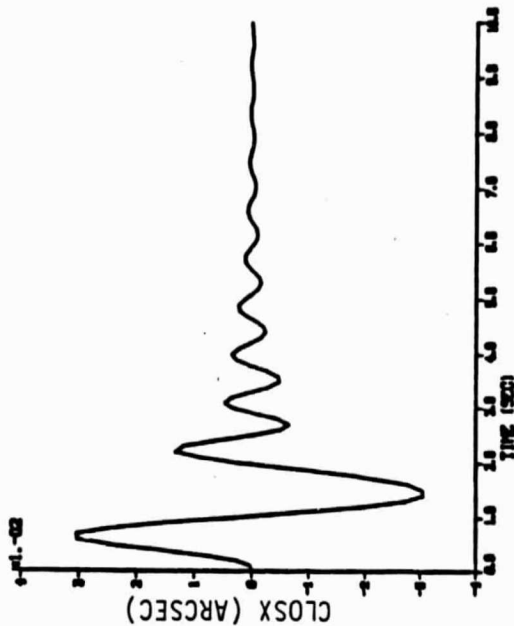
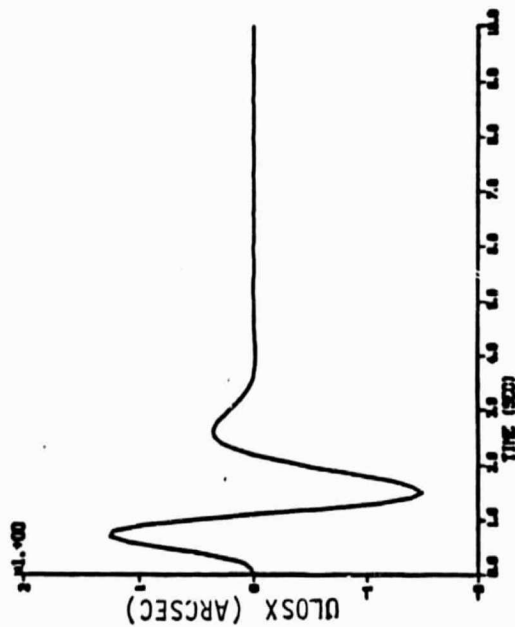
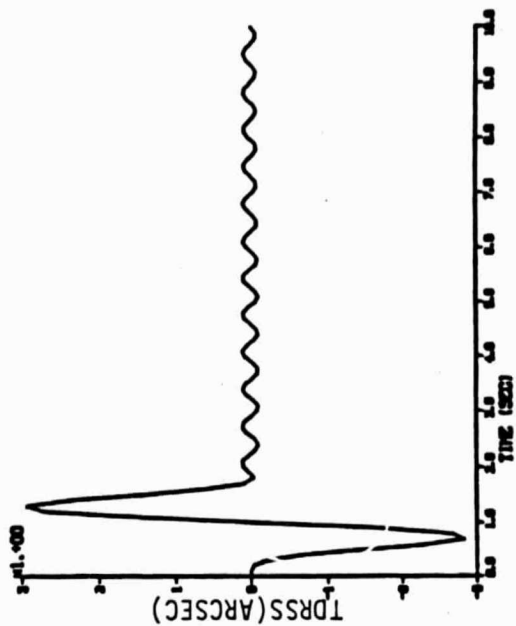
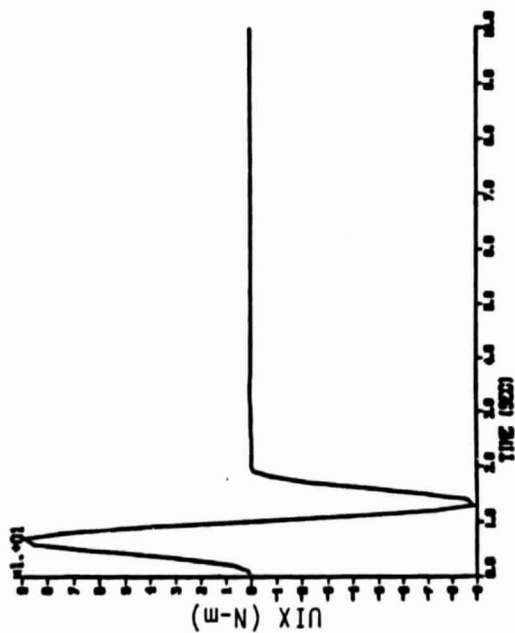
Top left: Total control torque (feedforward + feedback) (N-m)  
Top Right: TDRSS antenna bending about the slew axis. (arcsec)  
Bottom Left: Telescope pointing error (arcsec)  
Bottom Right: Focal Plane pointing error after  
correction by AIS. (arcsec)

Remarks: The absence of solar panel dynamics clearly improves the performance as can be seen for this 98 deg orbit case.



**SIRTF**

98° ORBIT 7 ARCMIN/2S SINE-VERSINE SLEW



28 DEG ORBIT 2.5 DEGREES/10S SINE-VERSINE SLEW

This chart shows time histories corresponding to the following conditions:

Slew direction: about the X axis  
Slew angle : 2.5 deg  
Slew time : 10 sec  
Torque profile: SINE-VERSINE

The following quantities are displayed:

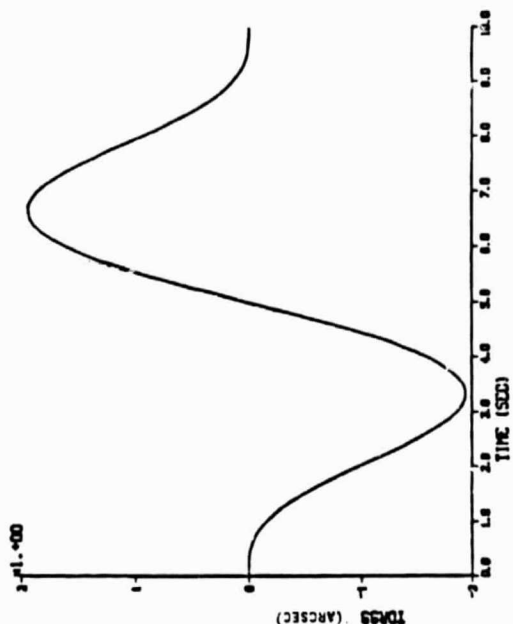
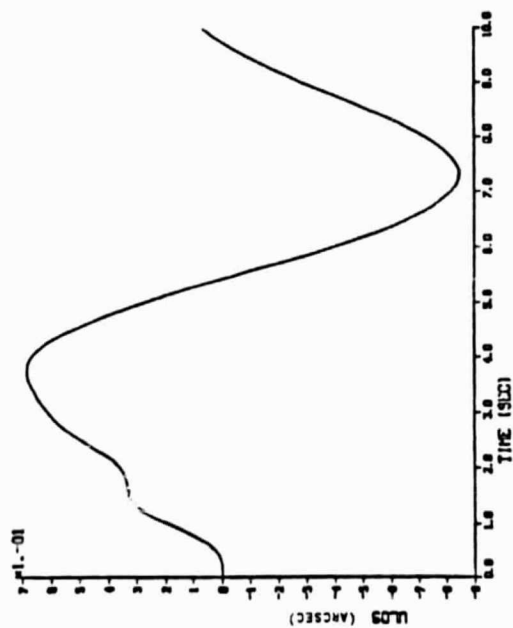
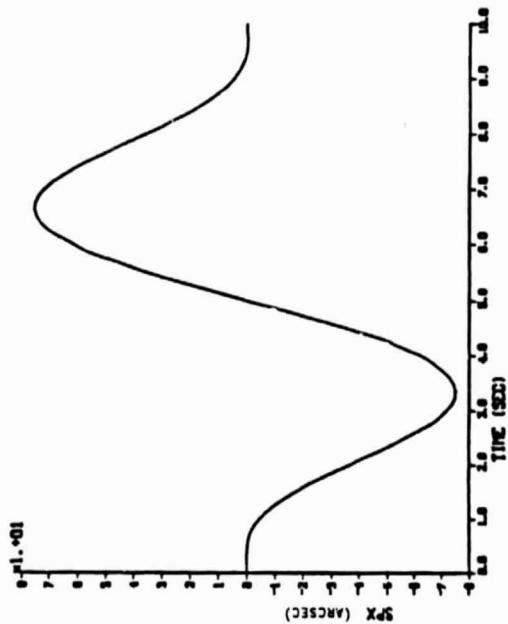
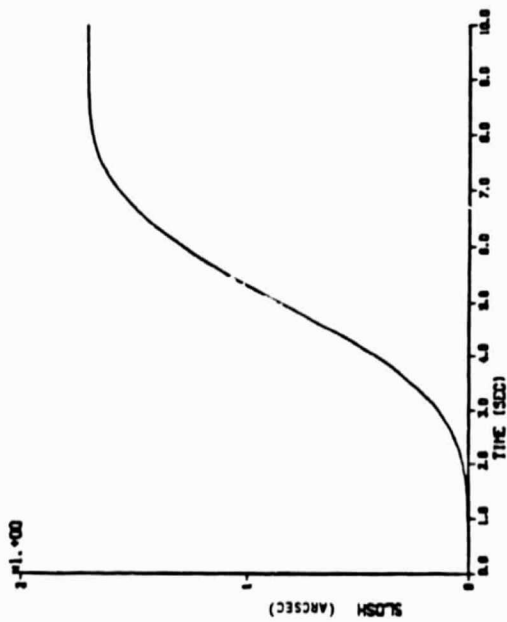
Top left: Cryogen slosh angle about the Z axis. (arcsec)  
Top Right: Solar Panel bending about the slew axis. (arcsec)  
Bottom Left: Telescope pointing error (arcsec)  
Bottom Right: TDRSS antenna bending about the slew axis (arcsec)

Remarks: Because of the longer slew time, and of the smooth torque profile used, deformations are quasi-static and no "ringing" is observed.



SIRTF

28° ORBIT 2.5°/10S SINE-VERSINE SLEW



This chart shows time histories corresponding to the following conditions:

The following quantities are displayed:

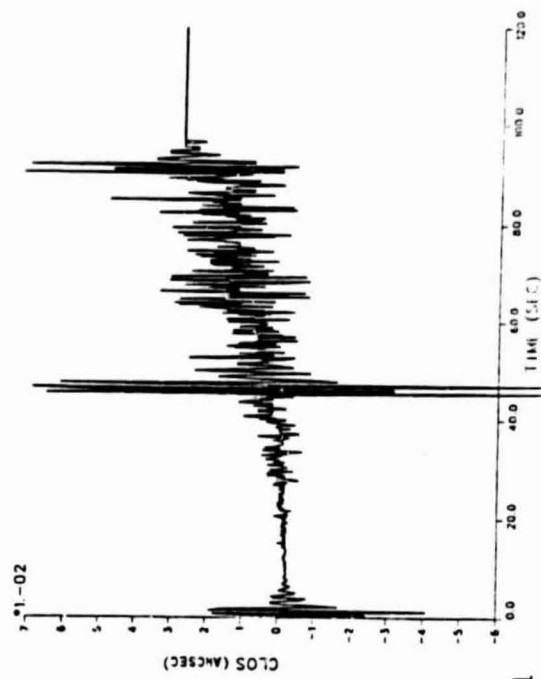
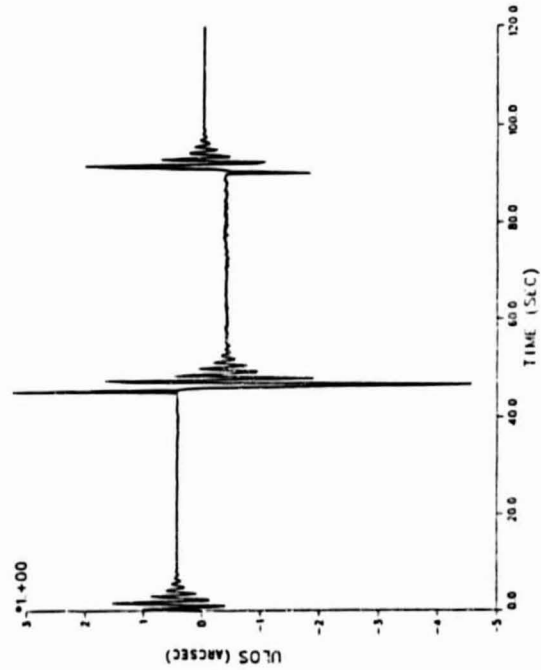
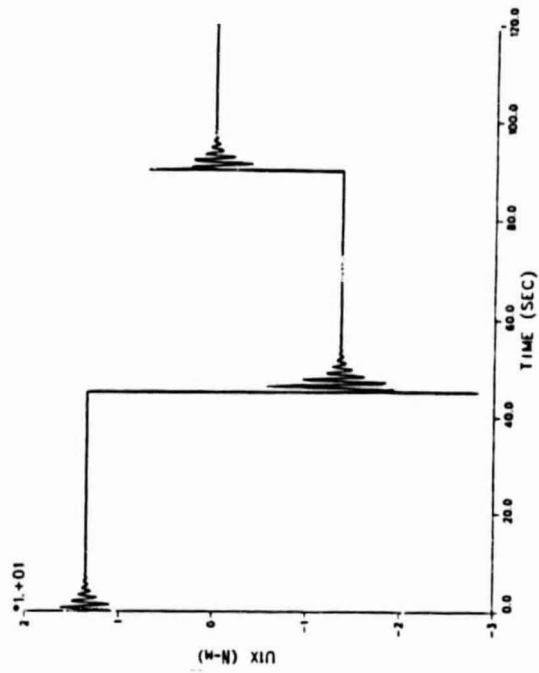
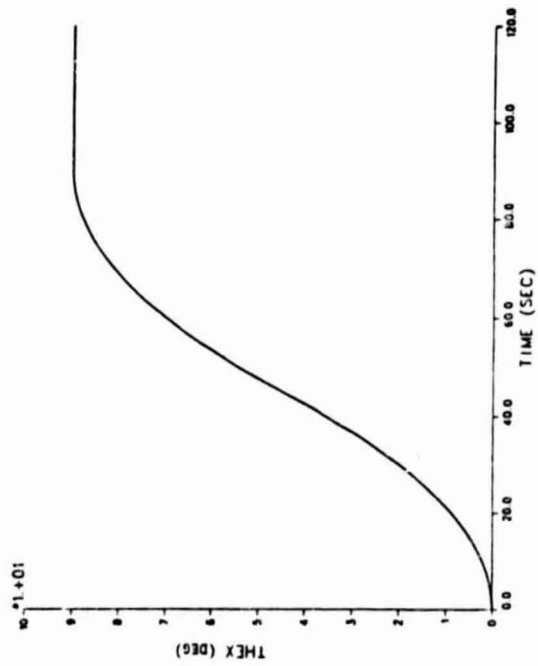
Remarks: Note the strong structural excitation due to the sharp reversal in the torque. The control system does try to compensate and applies oscillatory torques resulting in about 10% damping ratio. The noisy behavior of the focal plane pointing error is a result of the finite word length in the digital simulation. Although the UNIVAC computer uses a 36-bit word, it is not sufficient to accurately compute the pointing error (about 1 part in 10 million since the final slew angle is 90 deg and the pointing error about .05 arcsec), thus the toggling of the LSB in the data word which appears as noise on the pointing error.



SIRTF

28° ORBIT 90°/90S

BANG-BANG SLEW



28 DEG ORBIT 90 degrees/90 s SINE-VERSINE SLEW

This chart shows time histories corresponding to the following conditions:

Slew direction: about the X axis  
Slew angle : 90 deg  
Slew time : 90 sec  
Torque profile: SINE-VERSINE

The following quantities are displayed:

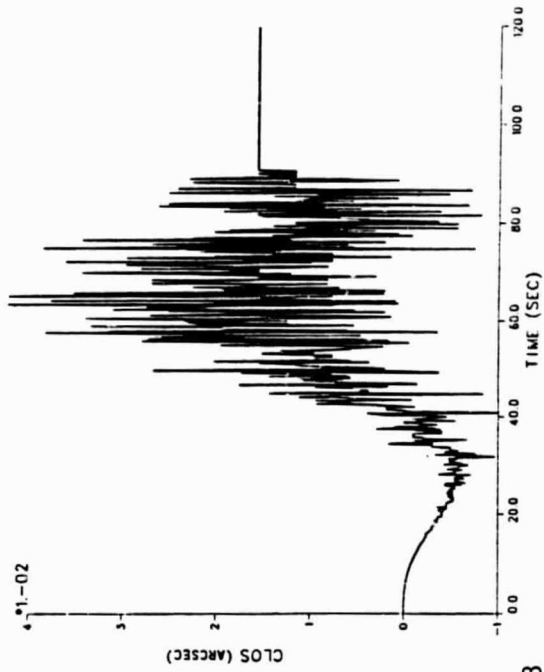
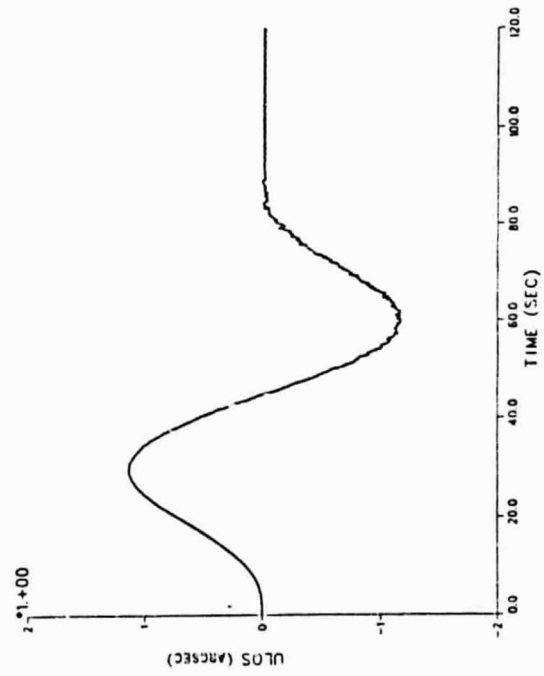
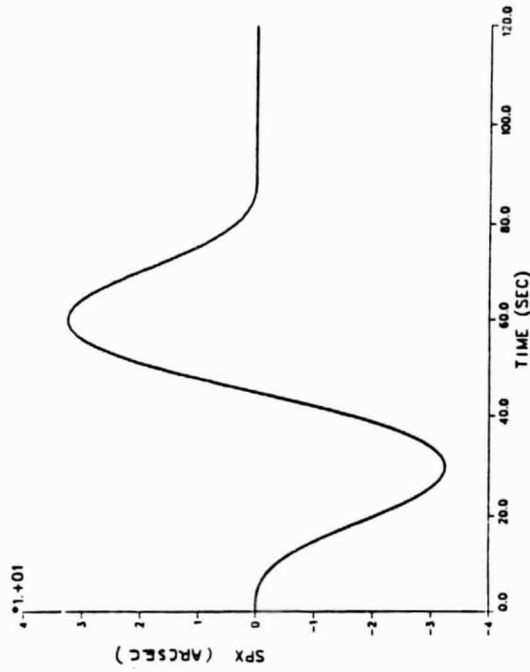
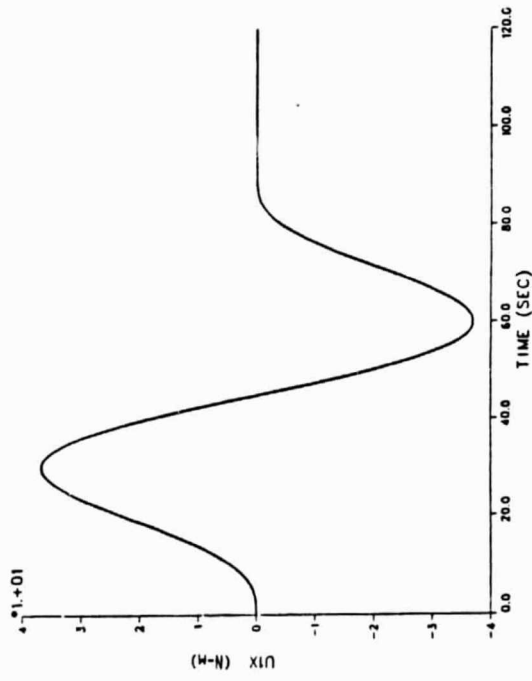
Top i ft:	Total control torque about the slew axis.	(N-m)
Top Right:	Solar Panel bending about the slew axis.	(arcsec)
Bottom Left:	Telescope pointing error	(arcsec)
Bottom Right:	Focal Plane pointing error after correction by AIS.	(arcsec)

Remarks: Again the computer word length is producing some noise in the compensated pointing error (CLOS). The actual dynamics of this slew are very smooth.



**SIRTf**

28° ORBIT 90°/90S SINE-VERSINE SLEW



28 DEG ORBIT 90 degrees/90 s BANG-CRUISE-BANG SLEW

This chart shows the time histories corresponding the following conditions:

Slew direction: about the X axis  
Slew angle : 90 deg  
Slew time : 90 sec  
Torque profile: BANG-CRUISE-BANG

The following quantities are displayed:

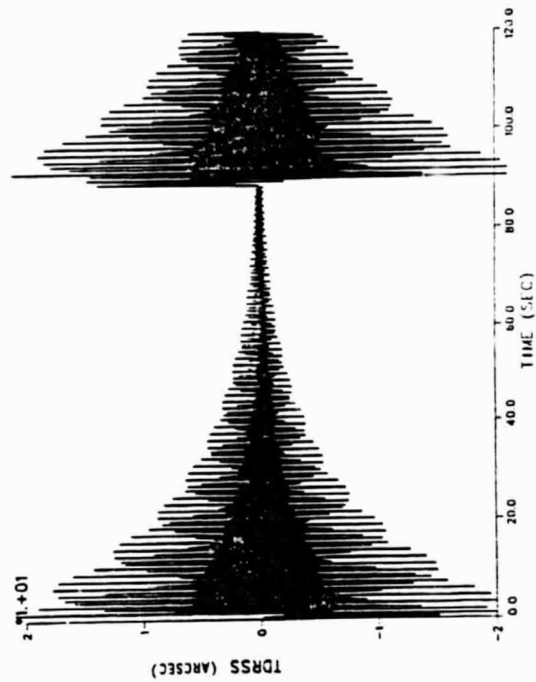
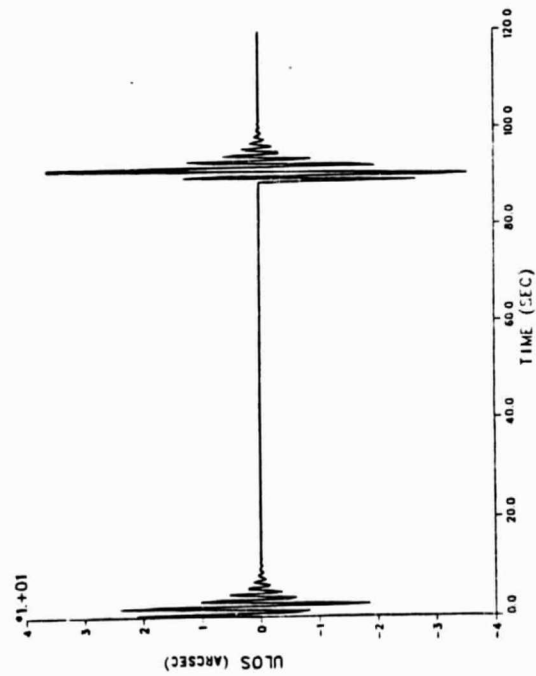
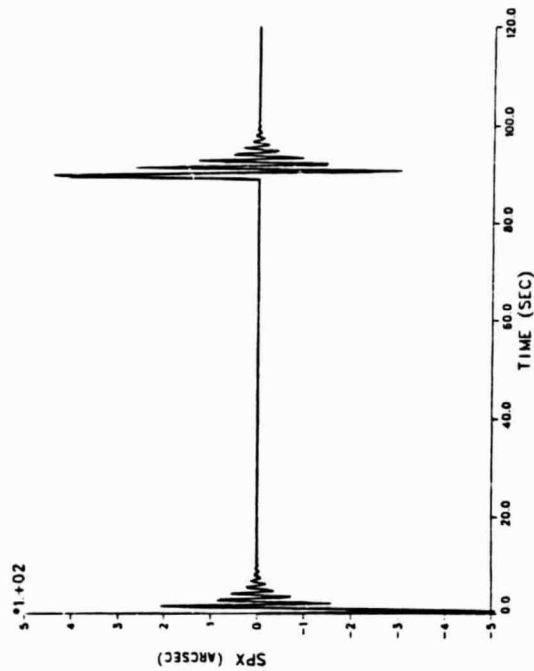
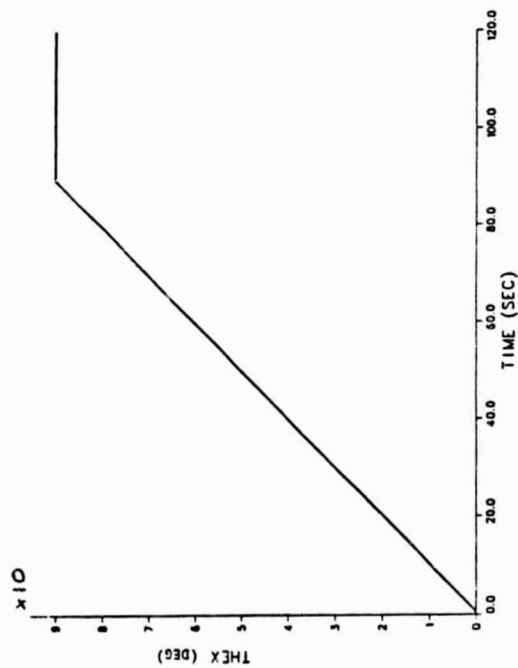
Top left: Spacecraft attitude angle about slew axis. (deg)  
Top Right: Solar Panel bending about the slew axis. (arcsec)  
Bottom Left: Telescope pointing error (arcsec)  
Bottom Right: TDRSS bending about the slew axis (arcsec)

Remarks: Note the linear motion of the attitude angle (CRUISE part of the slew). The acceleration and deceleration is quite large in this type of slew, resulting in larger solar panel and TDRSS antenna excitation.



**SIRTf**

28° ORBIT 90°/90S BANG-CRUISE-BANG SLEW



## 28 DEG ORBIT ROTATING CRYOGEN EFFECT

This chart shows time histories corresponding to the following conditions:

Cryogen mass rotating about the vehicle Z-axis at a rate of 0.03 radians per second

The following quantities are displayed:

Top left: Telescope pointing error (arcsec)

Bottom Left: Focal Plane pointing error after correction by AIS. (arcsec)

Top Right : Total control torque delivered by CMGs (N-m)

Bottom Right: Angle between Spacecraft and Telescope (arcsec)

Remarks: This simulation was run to demonstrate the capability of the control system to deal with worst case cryogen slosh. The maximum slosh rate measured in any of the preceding simulation cases never exceeded 0.030 radians per second. The rotation rate of 0.03 radians per second used in the present simulation corresponds to an equivalent rotating torque of magnitude 0.15 N-m. This value is for the 28 degree orbit spacecraft in which the liquid cryogen tank is significantly offset from the center of mass. The uncompensated pointing error remains well below 0.1 arcsec.

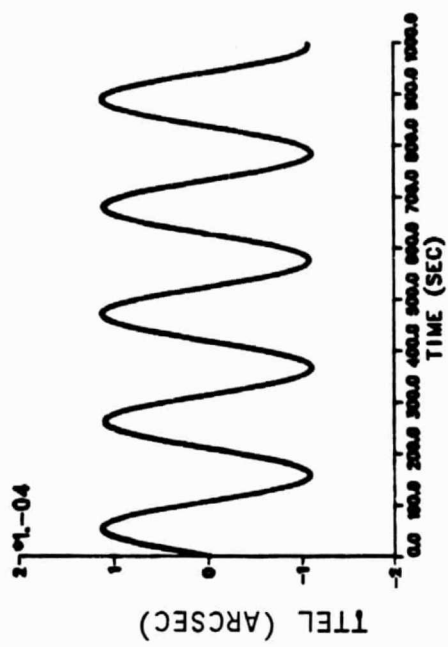
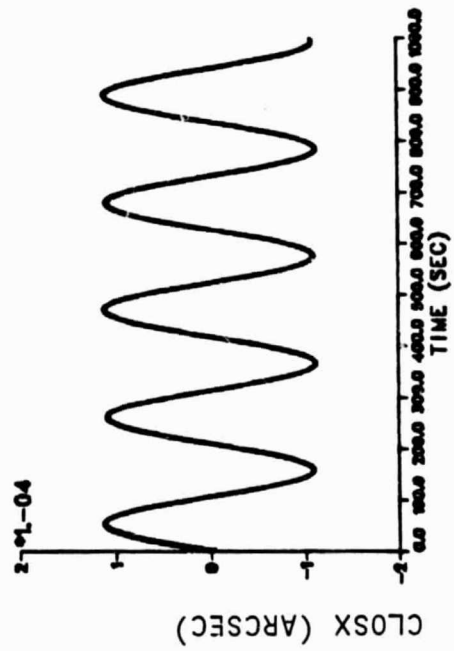
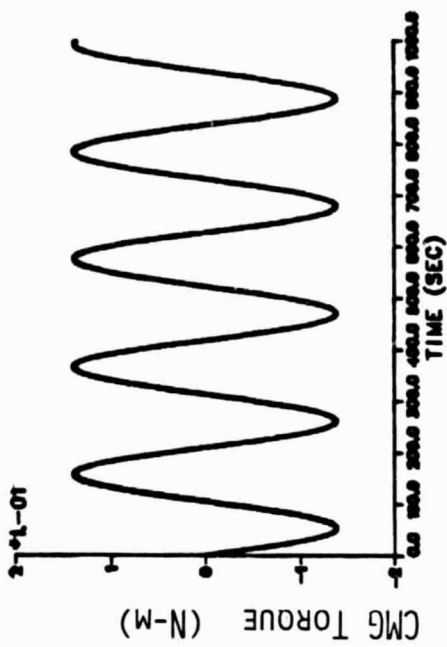
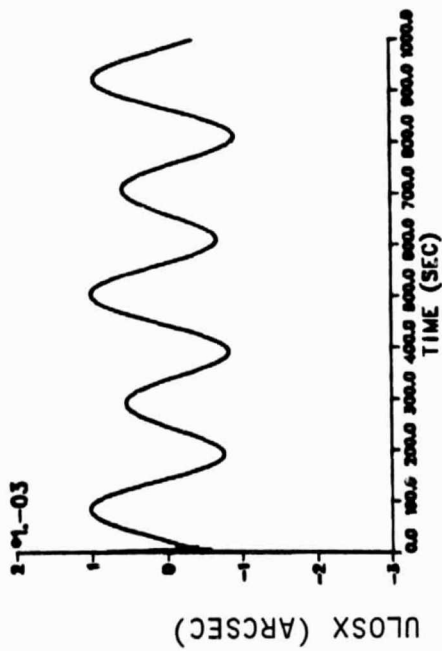
In this simulation, the AIS used feedforward compensation only, which should have brought the pointing error from 1.E-3 to 2.E-5 arcsec (assuming 2% error in scaling factor). However, the observed compensated error (CLOSX) is about 1.E-4 arcsec. This is because the gyros are mounted on the spacecraft and not on the telescope, thus the pointing error due to the angle between the spacecraft and the telescope cannot be compensated for by the AIS feedforward loop. This is confirmed by comparing CLOSX with the telescope angle (TTEL).



**SIRTf**

# 28° ORBIT    ROTATING CRYOGEN EFFECT

ROTATION RATE : 0.03 RAD/S



## 28 DEG ORBIT CMG STICTION EFFECTS

This chart shows time histories corresponding to the following conditions:

Initial conditions: 0.1 arcsec/s rate about X-axis  
Stiction torque: 0.06 N-m

The following quantities are displayed:

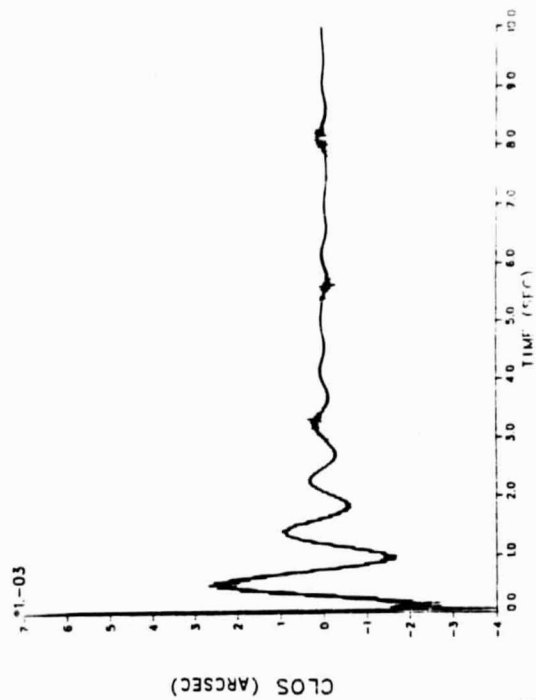
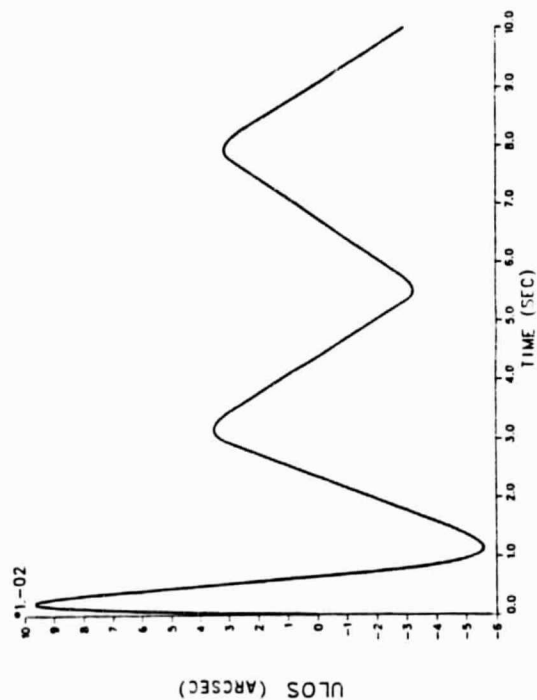
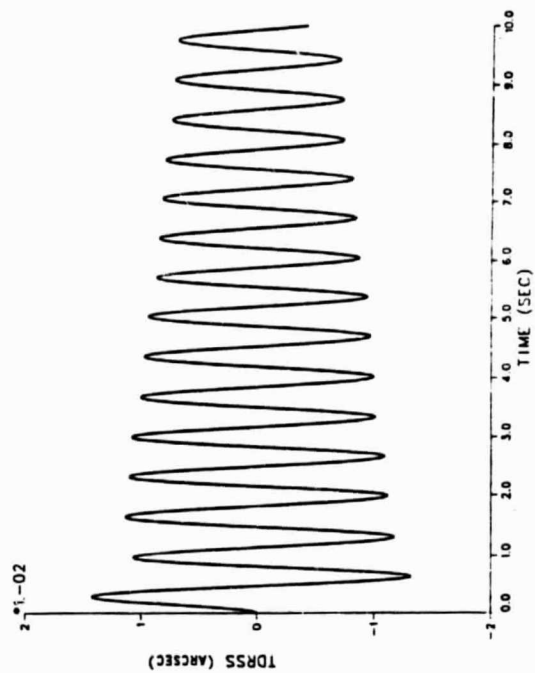
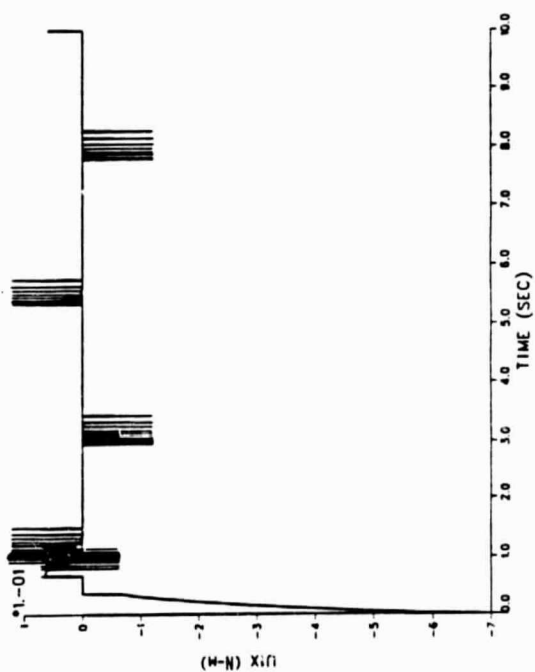
Top left: Total control torque about the slew axis.	(arcsec)
Top Right: TDRSC antenna bending about the slew axis.	(arcsec)
Bottom Left: Telescope pointing error	(arcsec)
Bottom Right: Focal Plane pointing error after correction by AIS.	(arcsec)

Remarks: Note the limit cycling after the control system  
has removed the effects of the initial rate.



SIRTF

# 28° ORBIT CMG STICKION EFFECTS



## 28 DEG ORBIT N-BODY NON-LINEAR SIMULATION

This chart shows time histories corresponding to the following conditions:

Slew direction: about the X axis  
Slew angle : 120 deg  
Slew time : 480 s (8 minutes)  
Torque profile: BANG-CRUISE-BANG

The following quantities are displayed:

Top left: Slosh angle	(between 0 and 2 s)	(rad)
Top Right: Slosh angle	(between 0 and 70 s)	(rad)
Bottom Left: Spacecraft pointing angle		(rad)
Bottom Right: Spacecraft pointing angle		(rad)

Remarks: This non-linear dynamic simulation was made using the N-BODY program. The purpose of these simulation runs was to precisely evaluate the slosh motion of the cryogen. Note that because there is no friction between the dewar wall and the cryogen, the mass of the cryogen tends to remain inertially fixed and acts as an angle indicator for the motion of the spacecraft.

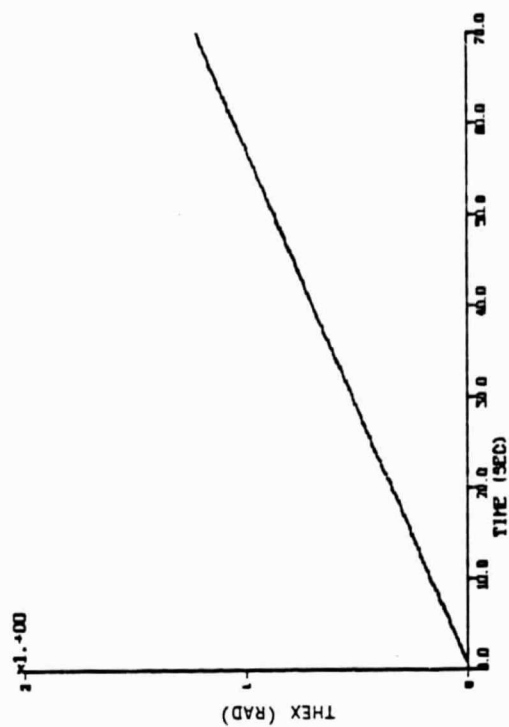
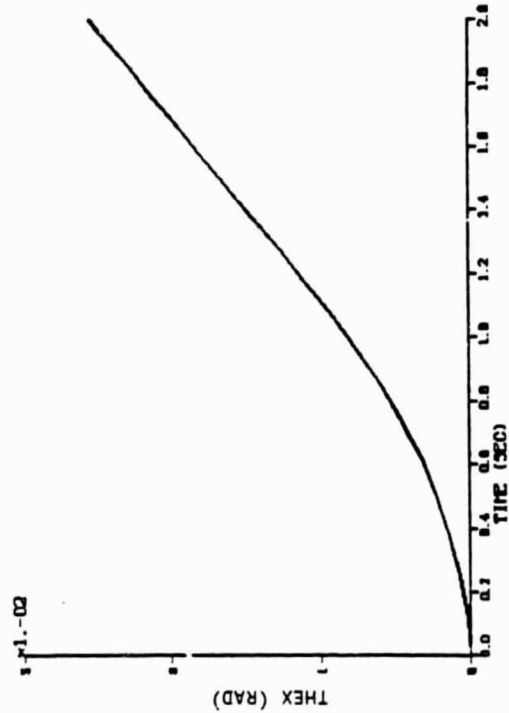
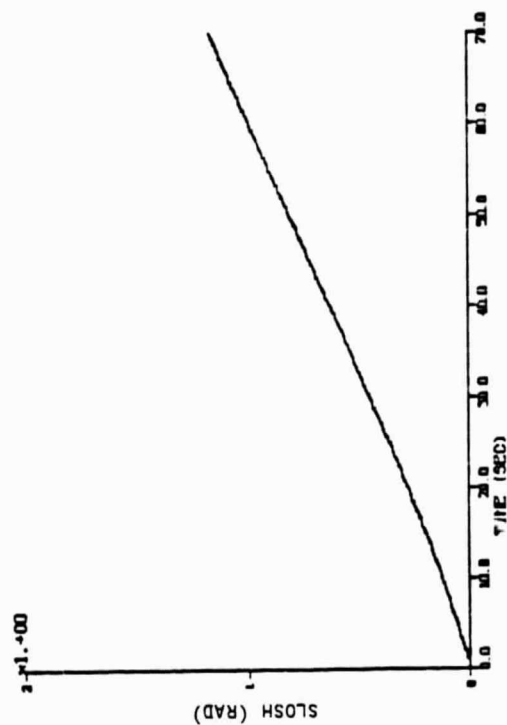
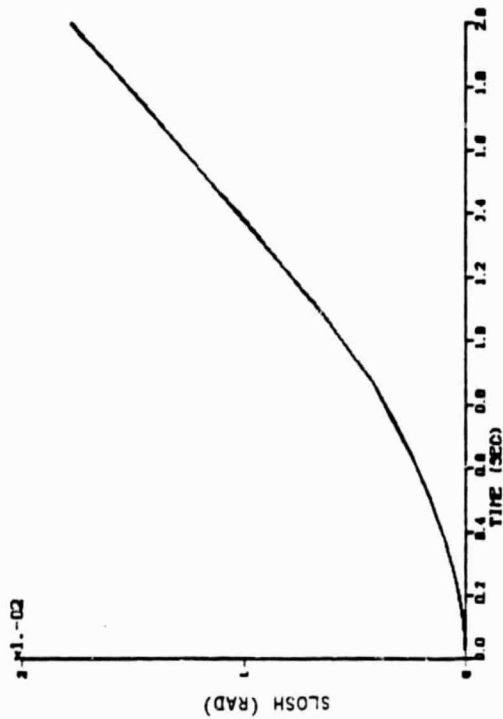


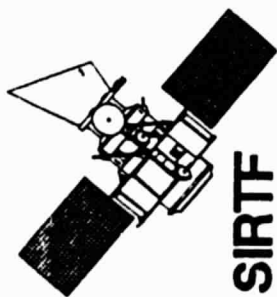
SIRTF

28° ORBIT

N-BODY NON-LINEAR SIMULATION

DCB SLEW NON-LINEAR SIMULATION





---

## CONCLUSIONS

---

PRECEDING PAGE BLANK NOT FILLED

## GENERAL (1)

- CRYOGEN SLOSH IS NOT A SIGNIFICANT DISTURBANCE
- ANTENNA REACTION TORQUES CAUSED BY TRACKING THE TDRSS WILL NOT DISTURB OBSERVATION
- REQUIREMENTS ON COMMANDED SLEW TIME FOR SMALL ANGLE SLEWS DRIVE ACTUATOR SIZING
- TORQUE PROFILES SUCH AS SINE-VERSINE MAY SUBSTANTIALLY IMPROVE SMALL ANGLE SLEW PERFORMANCE BECAUSE
  - TOTAL MANEUVER TIME (SLEW PLUS SETTling) IS GENERALLY SHORTER
  - CAN GET FASTER RESPONSE WITHOUT RESORTING TO AIS



## CONCLUSIONS

### GENERAL (2)

- THE  $120^{\circ}/8$  MIN SLEW REQUIREMENT IS VERY WEAK AND A SYSTEM SIZED WITH THIS AS THE MAXIMUM CAPABILITY WILL REQUIRE  $> 15$  SEC FOR A 7 ARCMINUTE SMALL ANGLE SLEW
- NONE OF THE DISTURBANCE TORQUES WERE SIGNIFICANT IN TERMS OF DRIVING THE SYSTEM DESIGN

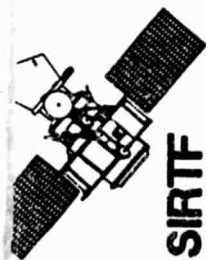


**SIRTF**

## CONCLUSIONS

### 28 DEGREE ORBIT SPACECRAFT

- FLEXIBLE SOLAR PANELS DRIVE PERFORMANCE OF THE SYSTEM DURING SLEW MANEUVERS
- A 90°/90 SEC HIGH PERFORMANCE EARTH-SUN AVOIDANCE MANEUVER REQUIRES A MAXIMUM CAPABILITY SYSTEM, BUT DOES NOT CAUSE UNACCEPTABLE STRUCTURAL DYNAMICS
- AIS CAN MAKE SUBSTANTIAL IMPROVEMENT IN SMALL ANGLE SLEW PERFORMANCE (TOTAL TIME REQUIRED FOR MANEUVER)
  - 2.2 SEC VS. 10 SEC FOR BANG-BANG TORQUE PROFILE
  - 2.7 SEC VS. 5.3 SEC FOR SINE-VERSINE TORQUE PROFILE

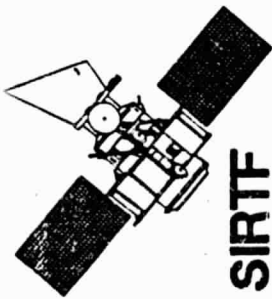


## CONCLUSIONS

---

### 98 DEGREE ORBIT SPACECRAFT

- SPACECRAFT MUCH MORE RIGID THAN 28 DEGREE ORBIT SPACECRAFT BECAUSE
  - ONLY SINGLE SOLAR PANEL
  - SOLAR PANEL RIGIDLY ATTACHED TO SPACECRAFT
- AIS IMPROVES SMALL ANGLE SLEW PERFORMANCE, BUT NOT AS DRAMATICALLY AS FOR 28 DEGREE ORBIT SPACECRAFT
  - 2 SEC VS. 4.2 SEC FOR SINE-VERSINE TORQUE PROFILE
- SINCE NO 90<sup>0</sup>/90 SEC EARTH-SUN AVOIDANCE MANEUVER WILL BE REQUIRED, THE "MEDIUM CAPABILITY" SYSTEM IS SUFFICIENT



---

APPENDIX A  
IRAS SLOSH MEMO

---

DOCUMENTATION OF LIQUID HELIUM SLOSH MODELS DEVELOPED FOR  
THE IRAS ACS SIMULATION

By K. R. Lorell, Research Scientist

I. INTRODUCTION

This report describes the equations used to model the motion of superfluid liquid helium inside the IRAS telescope dewar. Relative motion between the superfluid and the dewar wall is important because of the potentially significant disturbing forces generated during wall-fluid interactions. Additionally, there exists the possibility of energy exchange between the satellite and the liquid helium through the medium of the attitude control subsystem. Under worst-case conditions a resonance may develop, should the natural frequencies of any of the modes of fluid motion and the ACS be sufficiently well matched.

In order to study the behavior of the attitude control subsystem and the resultant effect on pointing accuracy in the presence of disturbing torques induced by helium motion, three rather simple lumped-parameter models were developed. The models are all mechanical analogs utilizing either a pendulum or spring-mass-damper system. The rationale for not employing fluid-mechanical techniques is threefold: 1) our primary concern is the large-scale interaction of the superfluid helium and the satellite attitude dynamics, not the actual detailed fluid motion, 2) fluid motion in general and superfluid helium in particular has proved to be very difficult to model, and 3) experiments by Mason, Collins, and Petrac (unpublished) have shown that the simple models are adequate for worst-case analyses.

## II. CASE I-SIMPLE SPRING-MASS-DAMPER

During the initial phases of the flight, the dewar will be almost completely filled with helium. Lorell, DeBra, and Collins have concluded that with the dewar nearly filled, the motion of the fluid relative to the tank will resemble that of a lightly damped spring-mass system. Figure 1 shows a single-axis two degree-of-freedom system. The equations describing the motion of the slosh mass and the resulting forces acting on the walls of the dewar can be obtained by approximating the slosh mass and satellite as damped linear harmonic oscillators. For the slosh mass we have

$$mL^2 \ddot{\theta}_m + KL(\theta_m - \theta_s) + BL(\dot{\theta}_m - \dot{\theta}_s) = 0 \quad (1)$$

and for the satellite,

$$I_s \ddot{\theta}_s - KL(\theta_m - \theta_s) - BL(\dot{\theta}_m - \dot{\theta}_s) = M_D + M_C \dot{\theta}_s \quad (2)$$

where  $K$  is the spring constant,  $B$  is the damping constant, and the small-angle approximation has been used.  $M_D$  and  $M_C$  are disturbing and control moments respectively. In order to select appropriate initial values for the parameters  $K$  and  $B$ , we use the equation

$$m \ddot{\theta}_m + K \theta_m + B \dot{\theta}_m = 0 \quad (3)$$

or, for the LaPlace transform of (3), the LaPlace variable  $S$  is given by

$$S = -\frac{B}{2m} \pm j \frac{[4Km - B^2]^{1/2}}{2m} \quad (4)$$

From experimental work by Collins, we can select

$$\frac{B}{2\pi n} = 0.2 \cdot \text{sec}^{-1} \text{ and } \left| j \left[ 4Km - B^2 \right]^{1/2} / 2m \right| = 30 \text{ rad/sec} \quad (5)$$

$$\text{if } m = 100 \text{ kg, then } K = 9 \times 10^4 \text{ N}\cdot\text{m/m, } B = 40 \text{ N}\cdot\text{m/sec}$$

Similarly, if the natural frequency is only 3 rad/sec then

$$K = 9 \times 10^2 \text{ N}\cdot\text{m/m} \quad (7)$$

### III. CASE II - SINGLE ROTATING PENDULUM

As the level of cryogen in the dewar decreases during the flight, a transition occurs from a nearly full state, with the fluid wetting all of the dewar walls, to a nearly empty state with the fluid confined to a small volume. This concentrated mass of fluid interacts with the dewar walls in response to satellite attitude motions which in turn are influenced by the fluid motion. It is easy to imagine a situation in which either an extended series of slewing maneuvers or continued limit cycle activity might excite a resonant mode in the dewar-fluid system. DeBra, Marquies, and Karsten have all independently suggested modeling the depleted cryogen case with a rotating pendulum whose axis of rotation is coincident with the dewar axis of symmetry. In this model the pendulum is of fixed mass and length and rotates in a plane which lies parallel with the Y-Z plane of the satellite. Figure 2 illustrates the pendulum arrangement inside the dewar while Figure 3 is a diagram of forces acting on the mass and rod.

Our goal is to compute  $F_p$ . Thus, summing components of forces acting on  $m$  along the direction of  $F_p$ , we can immediately write

$$F_p = -mR\dot{\phi}^2 + mL\ddot{\theta}_y \cos\phi + mL\ddot{\theta}_z \sin\phi \quad (8)$$

For torques acting about the axis of rotation (equivalent to forces perpendicular to  $F_p$ ), we can write

$$mR^2\ddot{\phi} + B'\dot{\phi} = mLR\ddot{\theta}_z \cos\phi - mLR\ddot{\theta}_y \sin\phi \quad (9)$$

thus providing a means to calculate the motion of the pendulum.

The reaction of the satellite to  $F_p$  (that is, the force generated by the rotating pendulum mass) is

$$I_{yy}\ddot{\theta}_y = -(-F_p)L\cos\phi \quad (10)$$

$$I_{zz}\ddot{\theta}_z = -(-F_p)L\sin\phi$$

or

$$I_{yy}\ddot{\theta}_y = -m[R\dot{\phi}^2 - L\ddot{\theta}_y \cos\phi - L\ddot{\theta}_z \sin\phi]L\cos\phi + Mc_y + \tau$$

$$I_{zz}\ddot{\theta}_z = -m[R\dot{\phi}^2 - L\ddot{\theta}_y \cos\phi - L\ddot{\theta}_z \sin\phi]L\sin\phi + Mc_z + \tau$$

Expressions (9) and (11) form a set of second-order non-linear differential equations which must be solved numerically in the context of the ACS simulation. Aside from programming the equations themselves, all that is needed is appropriate initial conditions for  $\phi$  and  $\dot{\phi}$ . However, a range of values for  $\phi$  and  $\dot{\phi}$  should be explored (with particular attention to  $\dot{\phi}$ ) in order to determine any areas of ACS sensitivity.

In order to calculate an approximate starting value for  $B'$ , assume a time constant of  $.2 \text{ sec}^{-1}$  as before with  $m = 20 \text{ kg}$ ,  $R = 75 \text{ cm}$ . Then a LaPlace transform of the left side of (9) yields

$$\Phi(s) = \dot{\phi}(0) / s(mR^2s + B') \quad (12)$$

or

$$\frac{B'}{mR^2} = 0.2 \text{ and } B' = 2.25 \text{ Nt-m/rad/sec} \quad (13)$$

It is suggested that since  $B'$  is a rather critical value to the outcome of the investigation, it be varied by an order of magnitude both higher and lower.

#### IV. CASE III - DOUBLE (OR MULTIPLE) ROTATING PENDULA

Margulies' has developed a model for fuel slosh in a Lockheed Agena which uses a multiple pendulum concept. This idea relates to the possibility of more than one slosh mass being excited during maneuvering or under dewar fill-level conditions wherein the fluid condenses into several units. While this model is probably more appropriate for a vehicle with high maneuvering rates such as the Agena, it could be useful to describe the cryogen behavior in a 25% to 75% fill situation in the IRAS dewar.

Figure 4 indicates the generalized location of two pendulums in the IRAS dewar. Using notation identical with that of Case II, it is immediately possible to write down a set of governing equations analogous to (3), (9), (10), and (11).

$$\begin{aligned} F_{P1} &= -m_1 R_1 \dot{\phi}_1^2 + m_1 L_1 \ddot{\theta}_y \cos \phi_1 + m_1 L_1 \ddot{\theta}_z \sin \phi_1 \\ F_{P2} &= -m_2 R_2 \dot{\phi}_2^2 + m_2 L_2 \ddot{\theta}_y \cos \phi_2 + m_2 L_2 \ddot{\theta}_z \sin \phi_2 \end{aligned} \quad (14)$$

where

$$m_1 R_1 \ddot{\phi}_1 + m_1 L_1 \ddot{\theta}_y \sin \phi_1 - m_1 L_1 \ddot{\theta}_z \cos \phi_1 + \frac{B'}{R_1} \dot{\phi}_1 = 0$$

$$m_2 R_2 \ddot{\phi}_2 + m_2 L_2 \ddot{\theta}_y \sin \phi_2 - m_2 L_2 \ddot{\theta}_z \cos \phi_2 + \frac{B'}{R_2} \dot{\phi}_2$$

and

$$I_{yy} \ddot{\theta}_y = - \sum_{i=1}^2 \left\{ m_i [R_i \dot{\phi}_i^2 - L_i \ddot{\theta}_y \cos \phi_i - L_i \ddot{\theta}_z \sin \phi_i] L_i \cos \phi_i \right\} + M_{cy} +$$

$$I_{zz} \ddot{\theta}_z = - \sum_{i=1}^2 \left\{ m_i [R_i \dot{\phi}_i^2 - L_i \ddot{\theta}_y \cos \phi_i - L_i \ddot{\theta}_z \sin \phi_i] L_i \sin \phi_i \right\} +$$

$B'$  can be selected as in Case II.

Equations (15) and (16) may clearly be extended indefinitely to include any arbitrary number of pendulums. However, the resultant computational load required to perform an iterative solution of the coupled non-linear equations rapidly becomes unmanageable, so that probably three separate masses is a practical limit.

#### V. IMPLEMENTATION IN THE IRAS ACS SIMULATION

Equations for the three slosh models may be implemented into the IRAS ACS simulation through the addition of the appropriate state variables. The slosh equations essentially model a disturbing moment which contains its own dynamics. The slosh state-variables thus require inputs from the vehicle state-variables for their computation. After the slosh state has been computed,  $F_p$  may be determined and included in the next iteration of the vehicle state.

Figure 5 illustrates a simplified block diagram of the IRAS ACS simulation without the slosh model. Basically, the cryogen slosh is a dynamic disturbance moment which is a function of the vehicle states. Figure 6 indicates this configuration.

The computation sequence for the ACS simulation with slosh dynamics is shown in Figure 7. The reason for computing the value of  $F_p$  first is that non-zero initial values of  $\phi$  and  $\dot{\phi}$  define a non-zero initial value of  $F_p$  which affects the initial conditions of the attitude computation. This sequence permits the examination of ACS/slosh interaction for other than quiescent start-up conditions, e.g., simulation of pointing mode operation following a series of scans or slews.

## VI. CONCLUSIONS

Equations of motion of three models of liquid helium motion within the IRAS dewar are described. The models are all simple mechanical analogs, and no attempt has been made to describe the detailed motion of the fluid. One of the models is suitable for fluid motion with the dewar nearly full, while the other two are representative of intermediate fill levels, including an almost empty dewar.

Values for natural frequency and damping coefficients have been derived from experiments performed in zero gravity conditions with superfluid helium. These values should be used only as a starting point; however. Simulations should be done with critical parameters, such as initial conditions, damping coefficients, and natural frequencies varied by as much as an order of magnitude. This technique makes it possible to bound the slosh state-variable regimes, if any, which adversely affect the ACS.

VII. REFERENCES

1. Collins, D., Notes on Calculations Based on Zero Gravity Superfluid He Experiments, private correspondence, Jet Propulsion Laboratory, Pasadena, CA, Feb. 1973.
2. DeBra, D., Notes on IRAS Slosh Discussions, Palo Alto, CA, Oct-Nov 1977.
3. Karsten, L., The Effects of Liquid Helium on the Attitude Control of IP S, IRAS Report No. R-ACS-76-02, Fokker Space Division, Amsterdam, The Netherlands, March 1976.
4. Lomen, D. O., Digital Analysis of Liquid Propellant Sloshing in Mobile Tanks with Rotational Symmetry, NASA Contractor Report CR230, National Aeronautics and Space Administration, Washington, D.C., May 1965.
5. Lorell, J., Forces Produced by Fuel Oscillations, Progress Report No. 20-149, Jet Propulsion Laboratory, Pasadena, CA, Oct. 1951.
6. Margulies, G., Space Tug Technical Proposal, Folder 1, Lockheed Missiles and Space Co., Inc., Sunnyvale, CA, April 1975.
7. Mason, P., and Havens, W., Minutes of Discussion of Effect of Slosh on IRAS ACS with Prof. DeBra, Jet Propulsion Laboratory, Interoffice Memorandum, Jet Propulsion Laboratory, Pasadena, CA, April 1978.
8. NASA, Propellant Slosh Loads, NASA Space Vehicle Design Criteria Monograph SP8009, National Aeronautics and Space Administration, Washington, D.C., August 1968.
9. NASA, Slosh Suppression, NASA Space Vehicle Design Criteria Monograph SP-3031, National Aeronautics and Space Administration, Washington, D.C., May 1969.

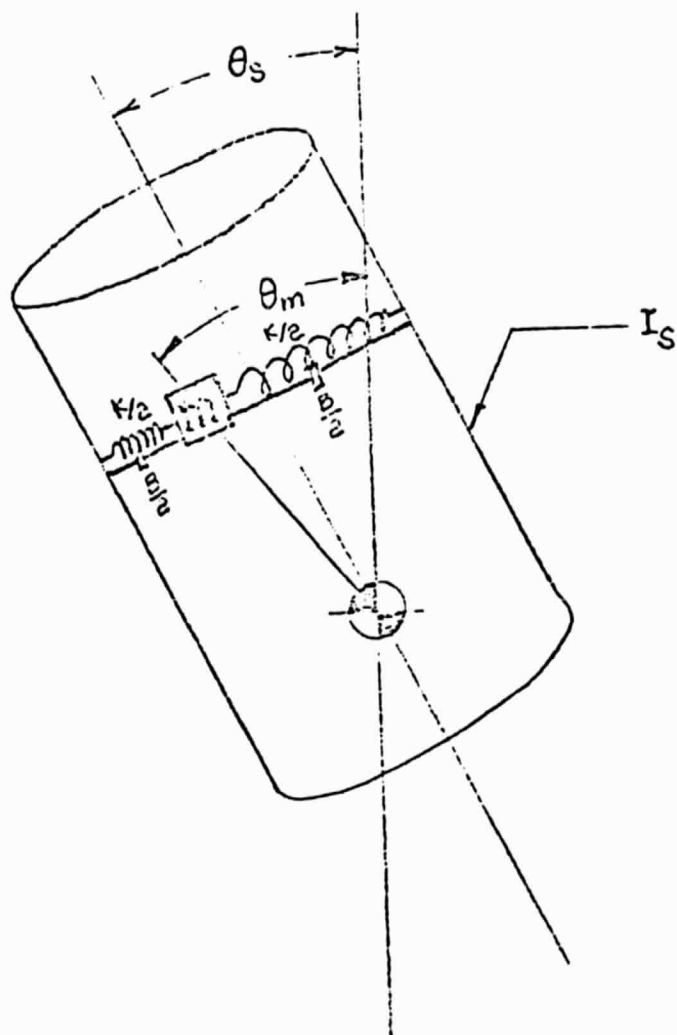


Figure 1. Simple Spring-Mass-Damper System

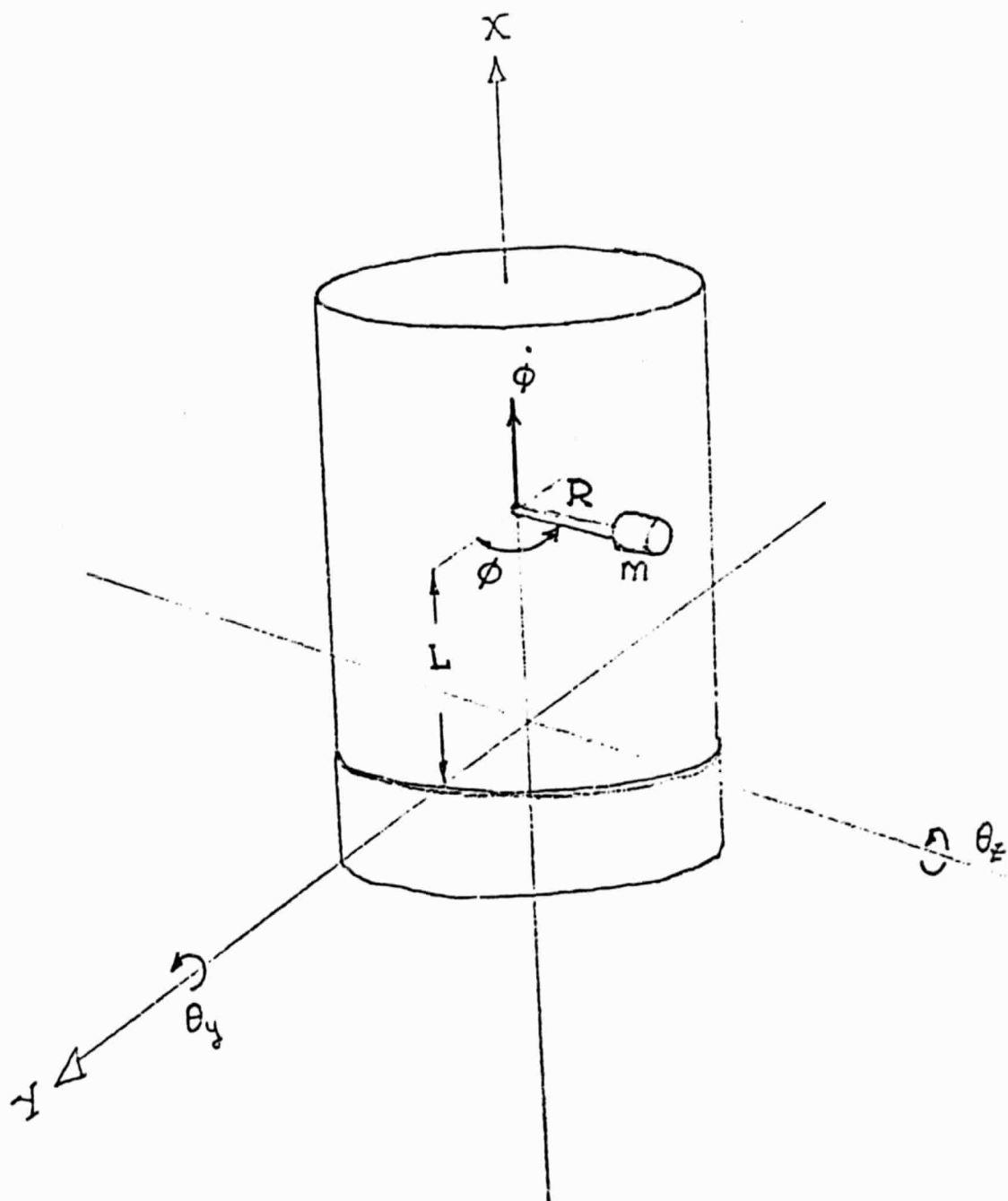


Figure 2. Rotating Pendulum Geometry

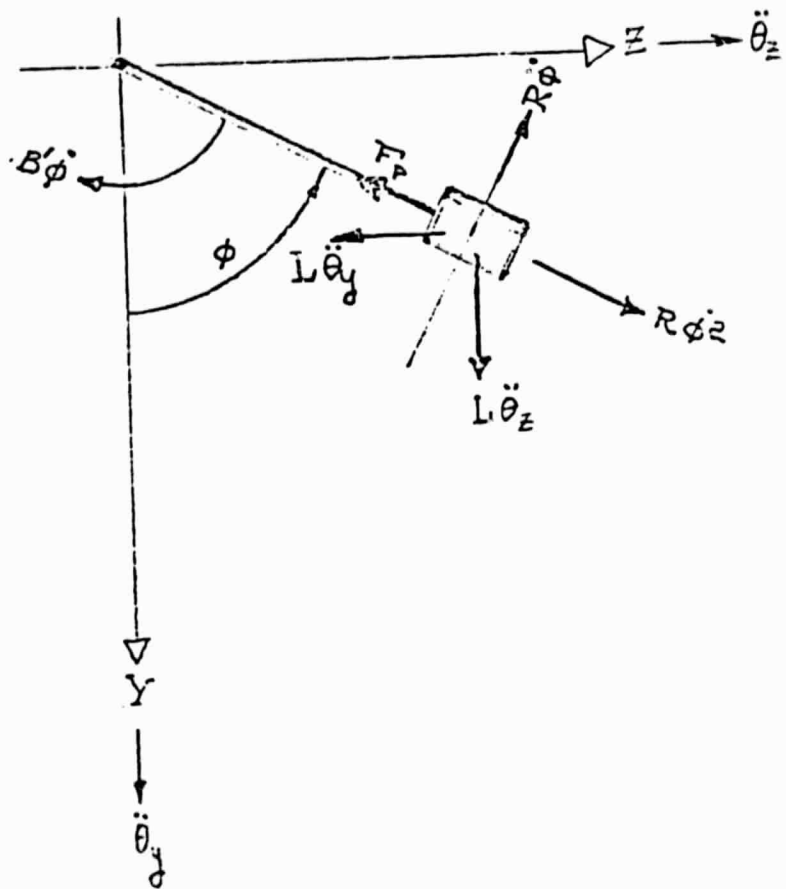


Figure 3. Force Diagram for Rotating Pendulum

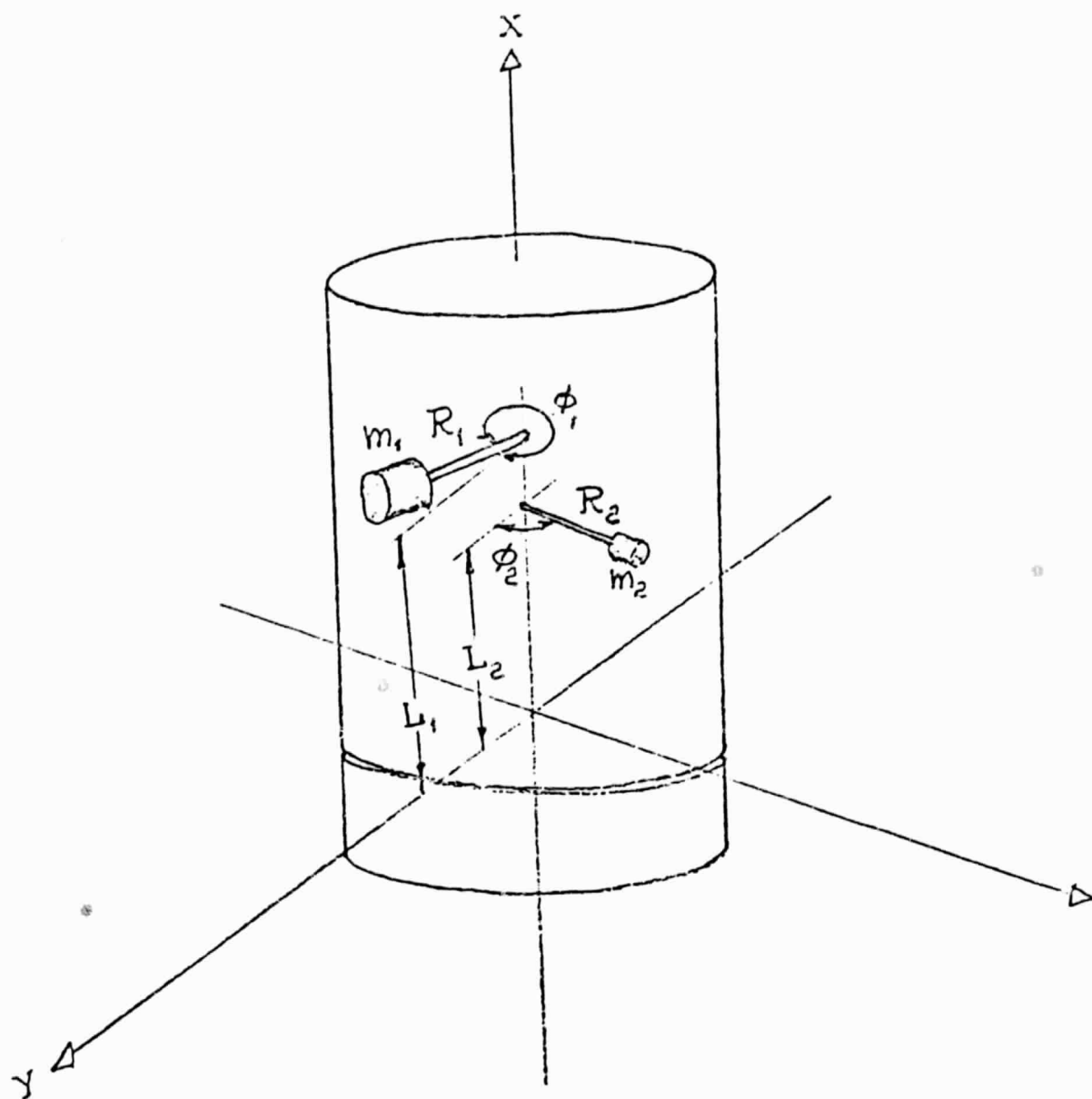


Figure 4. Double Rotating Pendulum System

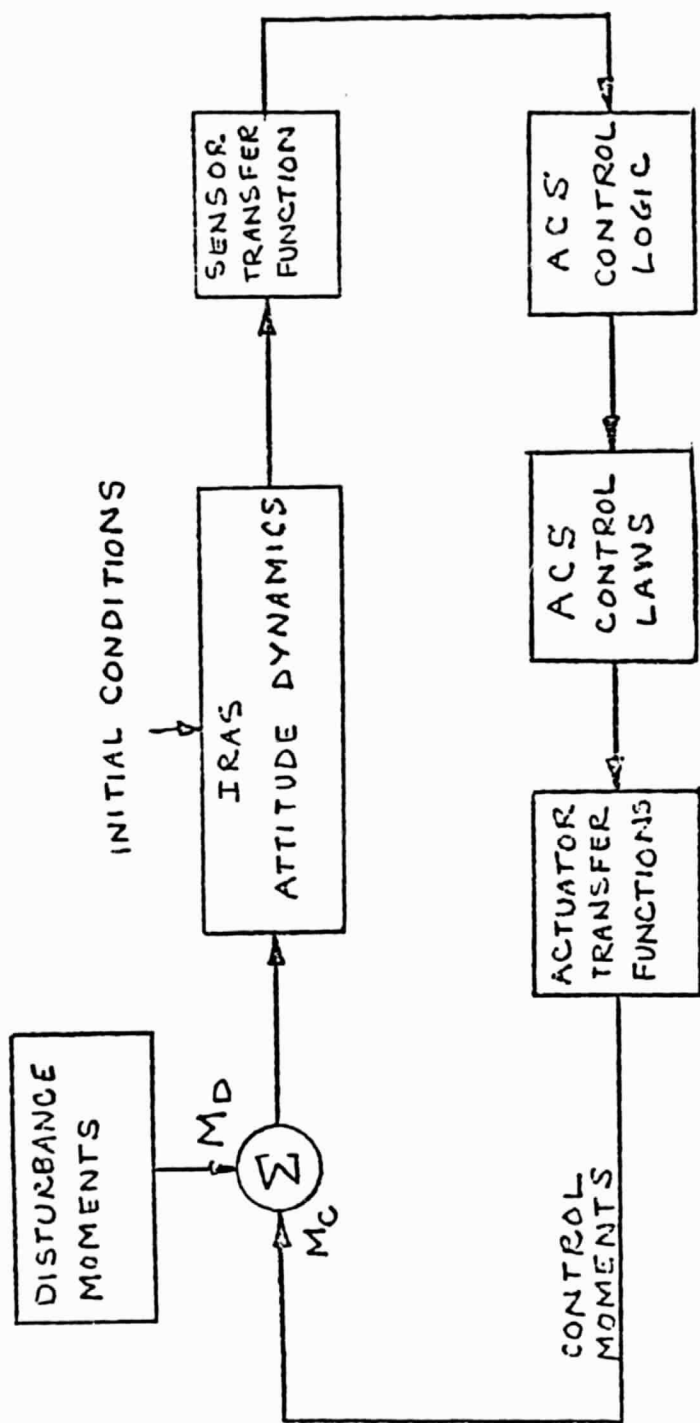


Figure 5. Block Diagram of the IRAS ACS Simulation

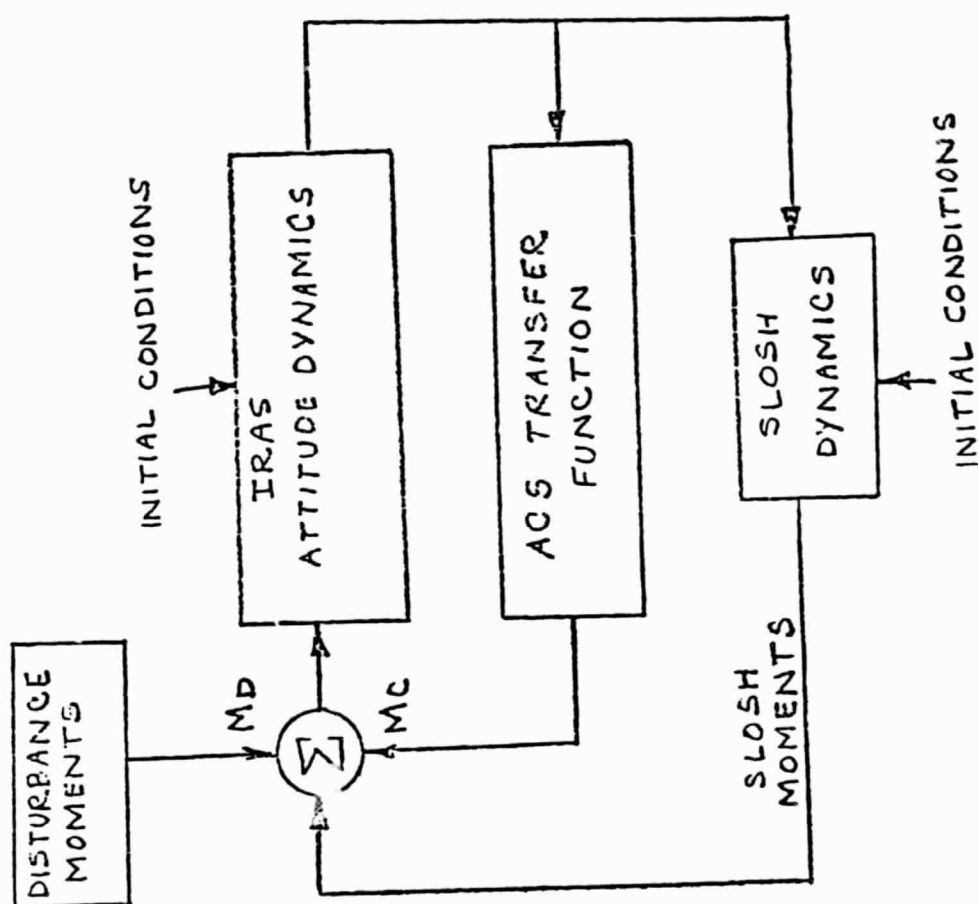


Figure 6. IRAS ACS Simulation with slosh dynamics included

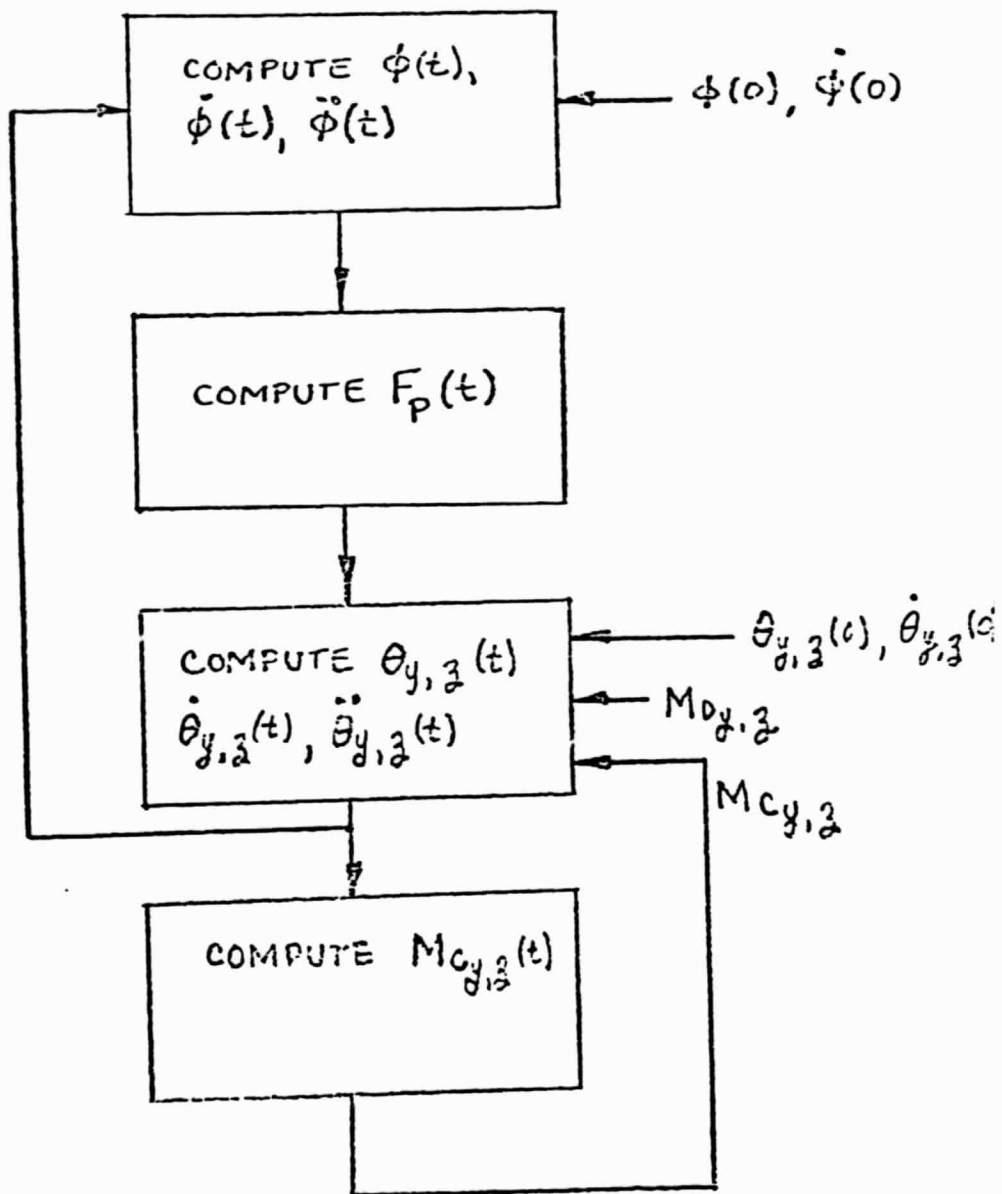
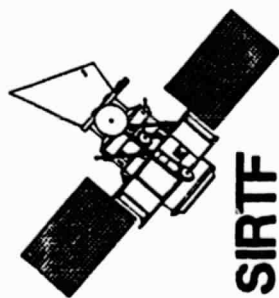


Figure 7. Suggested computation sequence



APPENDIX B  
SYSTEM MATRICES

PRECEDING PAGE BLANK NOT FILMED

## VEHICLE AND SYSTEM MATRICES FOR 28 and 98 DEG CASES

This appendix contains the numerical values for the matrices used in the various simulations of the 28 degree and 98 degree orbit vehicles. Two sets of matrices are presented for each vehicle :

- 1) The matrices  $F_v$  and  $G_v$  corresponding to the vehicle dynamics only, as obtained through the NBODY/TERFLEX program.
- 2) The matrices  $F$ ,  $G$ ,  $C$  and  $B$  corresponding to the whole system, i.e., that include the various control loops for attitude control as well as for AIS. This set of matrices was used directly in the LISSA program for all the linear simulations and the simulations of the CMG gimbal stiction. This latter effect requires a special code in LISSA to make explicit the dependency between the commanded torque and the torque delivered by the CMGs.

The matrices  $H$  and  $K$  used by the LISSA program to tailor the output are not displayed in this appendix because they are basically scaling factors and are therefore generated ad-hoc and of no fundamental value.

All matrices are given in the same standard format : each and only non-zero matrix element is printed, preceded by two integers representing the row and column indices respectively. The name and dimension of each matrix is printed first, followed by the value of the non-zero elements and their indices.

In the  $C$  matrices, for both cases, one may note the quantity 1.02 which corresponds to the feedforward scale factor error used in the simulations for both AIS and attitude control system.

214 INTENTIONALLY BLANK

\*\*\*\*\* VEHICLE DYNAMICS MATRICES FOR 28 DEG ORBIT (1 of 3)\*\*\*\*\*

\*\* Fv IS 32X32

1, 4	1.565-01	1, 5	-2.643-04	1, 6	-1.936-08	1, 7	8.994-05
1, 8	4.346-06	1, 9	9.062-05	1, 10	-4.265-06	1, 11	5.546-03
1, 12	1.198-08	1, 13	1.488-06	1, 14	5.546-03	1, 15	1.198-08
1, 16	1.488-06	1, 17	-4.449-08	1, 18	-3.833-13	1, 19	-4.423-12
1, 20	2.220+03	1, 21	-3.650+00	1, 22	-4.610-08	1, 23	7.724-02
1, 24	3.835-03	1, 25	7.782-02	1, 26	-3.764-03	1, 27	1.513+00
1, 28	4.791-06	1, 29	4.059-04	1, 30	1.513+00	1, 31	4.791-06
1, 32	4.059-04	2, 4	-4.295-04	2, 5	1.695-01	2, 6	5.875-08
2, 7	-1.599-04	2, 8	1.354-03	2, 9	1.594-04	2, 10	1.353-03
2, 11	-7.461-07	2, 12	4.004-04	2, 13	3.360-04	2, 14	-7.461-07
2, 15	4.004-04	2, 16	3.360-04	2, 17	-1.437-12	2, 18	-1.281-08
2, 19	-2.078-09	2, 20	-6.095+00	2, 21	2.341+03	2, 22	1.399-07
2, 23	-1.373-01	2, 24	1.194+00	2, 25	1.369-01	2, 26	1.194+00
2, 27	-2.035-04	2, 28	1.601-01	2, 29	9.165-02	2, 30	-2.035-04
2, 31	1.601-01	2, 32	9.165-02	3, 4	-3.605-03	3, 5	2.344-02
3, 6	4.483-07	3, 7	-1.278-03	3, 8	1.618-04	3, 9	1.274-03
3, 10	1.575-04	3, 11	-6.262-06	3, 12	4.723-05	3, 13	5.814-03
3, 14	-6.262-06	3, 15	4.723-05	3, 16	5.814-03	3, 17	-1.206-11
3, 18	-1.511-09	3, 19	-1.661-08	3, 20	-5.115+01	3, 21	3.237+02
3, 22	1.067-06	3, 23	-1.098+00	3, 24	1.427-01	3, 25	1.094+00
3, 26	1.390-01	3, 27	-1.708-03	3, 28	1.889-02	3, 29	1.586+00
3, 30	-1.708-03	3, 31	1.889-02	3, 32	1.586+00	4, 4	-1.136+00
4, 5	-2.256-02	4, 6	-2.819-06	4, 7	-7.996-05	4, 8	-1.418-05
4, 9	-2.194-05	4, 10	2.110-05	4, 11	-5.523-03	4, 12	1.023-06
4, 13	1.271-04	4, 14	-5.523-03	4, 15	1.023-06	4, 16	1.271-04
4, 17	4.470-08	4, 18	-3.272-11	4, 19	-3.776-10	4, 20	-1.612+04
4, 21	-3.116+02	4, 22	-6.712-06	4, 23	-6.867-02	4, 24	-1.251-02
4, 25	-1.884-02	4, 26	1.861-02	4, 27	-1.506+00	4, 28	4.091-04
4, 29	3.466-02	4, 30	-1.506+00	4, 31	4.091-04	4, 32	3.466-02
5, 4	-2.256-02	5, 5	-1.163+00	5, 6	-2.942-06	5, 7	1.765-04
5, 8	-1.351-03	5, 9	-2.008-04	5, 10	-1.378-03	5, 11	-3.925-05
5, 12	-4.036-04	5, 13	-6.873-04	5, 14	-3.925-05	5, 15	-4.036-04
5, 16	-6.873-04	5, 17	-7.552-11	5, 18	1.292-08	5, 19	2.456-09
5, 20	-3.202+02	5, 21	-1.607+04	5, 22	-7.004-06	5, 23	1.516-01
5, 24	-1.192+00	5, 25	-1.725-01	5, 26	-1.216+00	5, 27	-1.071-02
5, 28	-1.615-01	5, 29	-1.874-01	5, 30	-1.071-02	5, 31	-1.615-01
5, 32	-1.874-01	6, 4	-7.048-01	6, 5	-7.354-01	6, 6	-8.796-05
6, 7	5.212-04	6, 8	-5.306-04	6, 9	-1.283-03	6, 10	2.942-04
6, 11	1.695-03	6, 12	-3.497-05	6, 13	-4.268-03	6, 14	1.695-03
6, 15	-3.497-05	6, 16	-4.268-03	6, 17	-1.383-09	6, 18	1.119-09
6, 19	1.174-08	6, 20	-1.000+04	6, 21	-1.016+04	6, 22	-2.094-04
6, 23	4.476-01	6, 24	-4.682-01	6, 25	-1.102+00	6, 26	2.596-01
6, 27	4.622-01	6, 28	-1.399-02	6, 29	-1.164+00	6, 30	4.622-01
6, 31	-1.399-02	6, 32	-1.164+00	7, 4	-1.975-02	7, 5	4.360-02
7, 6	5.151-07	7, 7	-9.354-02	7, 8	3.197-04	7, 9	2.262-03
7, 10	3.161-04	7, 11	-8.002-04	7, 12	9.405-05	7, 13	1.158-02
7, 14	-8.002-04	7, 15	9.405-05	7, 16	1.158-02	7, 17	6.349-09
7, 18	-3.009-09	7, 19	-3.308-08	7, 20	-2.803+02	7, 21	6.021+02
7, 22	1.226-06	7, 23	-8.033+01	7, 24	2.821-01	7, 25	1.943+00
7, 26	2.789-01	7, 27	-2.182-01	7, 28	3.762-02	7, 29	3.157+00
7, 30	-2.182-01	7, 31	3.762-02	7, 32	3.157+00	8, 4	-3.504-03

\*\*\*\*\* VEHICLE DYNAMICS MATRICES FOR 28 DEG ORBIT (2 of 3) \*\*\*\*

Matrix Fv (continued)

8, 5	-3.338-01	8, 6	-5.243-07	8, 7	3.197-04	8, 8	-9.367-02
8, 9	-3.236-04	8, 10	-2.424-03	8, 11	9.471-04	8, 12	-7.962-04
8, 13	-6.864-04	8, 14	9.471-04	8, 15	-7.962-04	8, 16	-6.864-04
8, 17	3.068-10	8, 18	2.548-08	8, 19	4.187-09	8, 20	-4.972+01
8, 21	-4.610+03	8, 22	-1.248-06	8, 23	2.746-01	8, 24	-8.265+01
8, 25	-2.779-01	8, 26	-2.139+00	8, 27	2.583-01	8, 28	-3.185-01
8, 29	-1.872-01	8, 30	2.583-01	8, 31	-3.185-01	8, 32	-1.872-01
9, 4	-5.420-03	9, 5	-4.962-02	9, 6	-1.268-06	9, 7	2.262-03
9, 8	-3.236-04	9, 9	-9.352-02	9, 10	-3.104-04	9, 11	-7.753-04
9, 12	-9.377-05	9, 13	-1.154-02	9, 14	-7.753-04	9, 15	-9.377-05
9, 16	-1.154-02	9, 17	6.397-09	9, 18	3.001-09	9, 19	3.298-08
9, 20	-7.692+01	9, 21	-6.852+02	9, 22	-3.018-06	9, 23	1.943+00
9, 24	-2.855-01	9, 25	-8.032+01	9, 26	-2.739-01	9, 27	-2.114-01
9, 28	-3.751-02	9, 29	-3.148+00	9, 30	-2.114-01	9, 31	-3.751-02
9, 32	-3.148+00	10, 4	5.212-03	10, 5	-3.404-01	10, 6	2.907-07
10, 7	3.161-04	10, 8	-2.424-03	10, 9	-3.104-04	10, 10	-9.367-02
10, 11	-9.442-04	10, 12	-7.959-04	10, 13	-6.497-04	10, 14	-9.442-04
10, 15	-7.959-04	10, 16	-6.497-04	10, 17	-3.011-10	10, 18	2.547-08
10, 19	4.078-09	10, 20	7.396+01	10, 21	-4.700+03	10, 22	6.922-07
10, 23	2.715-01	10, 24	-2.139+00	10, 25	-2.666-01	10, 26	-8.265+01
10, 27	-2.575-01	10, 28	-3.184-01	10, 29	-1.772-01	10, 30	-2.575-01
10, 31	-3.184-01	10, 32	-1.772-01	11, 4	-2.636-01	11, 5	-1.873-03
11, 6	3.235-07	11, 7	-1.546-04	11, 8	1.830-04	11, 9	-1.498-04
11, 10	-1.824-04	11, 11	-9.283-02	11, 12	8.478-08	11, 13	1.054-05
11, 14	-1.013-02	11, 15	8.478-08	11, 16	1.054-05	11, 17	7.563-08
11, 18	-2.713-12	11, 19	-3.131-11	11, 20	-3.741+03	11, 21	-2.587+01
11, 22	7.703-07	11, 23	-1.328-01	11, 24	1.614-01	11, 25	-1.286-01
11, 26	-1.609-01	11, 27	-2.532+01	11, 28	3.391-05	11, 29	2.873-03
11, 30	-2.762+00	11, 31	3.391-05	11, 32	2.873-03	12, 4	4.295-04
12, 5	-1.695-01	12, 6	-5.875-08	12, 7	1.599-04	12, 8	-1.354-03
12, 9	-1.594-04	12, 10	-1.353-03	12, 11	7.461-07	12, 12	-1.140-01
12, 13	-3.360-04	12, 14	7.461-07	12, 15	-4.004-04	12, 16	-3.360-04
12, 17	1.437-12	12, 18	1.281-08	12, 19	2.078-09	12, 20	6.095+00
12, 21	-2.341+03	12, 22	-1.399-07	12, 23	1.373-01	12, 24	-1.194+00
12, 25	-1.369-01	12, 26	-1.194+00	12, 27	2.035-04	12, 28	-4.561+01
12, 29	-9.165-02	12, 30	2.035-04	12, 31	-1.601-01	12, 32	-9.165-02
13, 4	6.065-03	13, 5	-3.280-02	13, 6	-8.147-07	13, 7	2.236-03
13, 8	-1.326-04	13, 9	-2.230-03	13, 10	-1.255-04	13, 11	1.054-05
13, 12	-3.819-05	13, 13	-1.012-01	13, 14	1.054-05	13, 15	-3.819-05
13, 16	-1.104-02	13, 17	2.030-11	13, 18	1.222-09	13, 19	2.907-08
13, 20	8.607+01	13, 21	-4.530+02	13, 22	-1.940-06	13, 23	1.921+00
13, 24	-1.170-01	13, 25	-1.915+00	13, 26	-1.107-01	13, 27	2.873-03
13, 28	-1.527-02	13, 29	-2.760+01	13, 30	2.873-03	13, 31	-1.527-02
13, 32	-3.012+00	14, 4	-2.636-01	14, 5	-1.873-03	14, 6	3.235-07
14, 7	-1.546-04	14, 8	1.830-04	14, 9	-1.498-04	14, 10	-1.824-04
14, 11	-1.013-02	14, 12	8.478-08	14, 13	1.054-05	14, 14	-9.283-02
14, 15	8.478-08	14, 16	1.054-05	14, 17	7.563-08	14, 18	-2.713-12
14, 19	-3.131-11	14, 20	-3.741+03	14, 21	-2.587+01	14, 22	7.703-07
14, 23	-1.328-01	14, 24	1.614-01	14, 25	-1.286-01	14, 26	-1.609-01
14, 27	-2.762+00	14, 28	3.391-05	14, 29	2.873-03	14, 30	-2.532+01
14, 31	3.391-05	14, 32	2.873-03	15, 4	4.295-04	15, 5	-1.695-01

\*\*\*\*\* VEHICLE DYNAMICS MATRICES FOR 28 DEG ORBIT (3 of 3)\*\*\*\*\*

Matrix Fv (continued)

15, 6	-5.875-08	15, 7	1.599-04	15, 8	-1.354-03	15, 9	-1.594-04
15, 10	-1.353-03	15, 11	7.461-07	15, 12	-4.004-04	15, 13	-3.360-04
15, 14	7.461-07	15, 15	-1.140-01	15, 16	-3.360-04	15, 17	1.437-12
15, 18	1.281-08	15, 19	2.078-09	15, 20	6.095+00	15, 21	-2.341+03
15, 22	-1.399-07	15, 23	1.373-01	15, 24	-1.194+00	15, 25	-1.369-01
15, 26	-1.194+00	15, 27	2.035-04	15, 28	-1.601-01	15, 29	-9.165-02
15, 30	2.035-04	15, 31	-4.561+01	15, 32	-9.165-02	16, 4	6.065-03
16, 5	-3.280-02	16, 6	-8.147-07	16, 7	2.236-03	16, 8	-1.326-04
16, 9	-2.230-03	16, 10	-1.255-04	16, 11	1.054-05	16, 12	-3.819-05
16, 13	-1.104-02	16, 14	1.054-05	16, 15	-3.819-05	16, 16	-1.012-01
16, 17	2.030-11	16, 18	1.222-09	16, 19	2.907-08	16, 20	8.607+01
16, 21	-4.530+02	16, 22	-1.940-06	16, 23	1.921+00	16, 24	-1.170-01
16, 25	-1.915+00	16, 26	-1.107-01	16, 27	2.873-03	16, 28	-1.527-02
16, 29	-3.012+00	16, 30	2.873-03	16, 31	-1.527-02	16, 32	-2.760+01
17, 1	1.000+00	18, 2	1.000+00	19, 3	1.000+00	20, 4	1.000+00
21, 5	1.000+00	22, 6	1.000+00	23, 7	1.000+00	24, 8	1.000+00
25, 9	1.000+00	26, 10	1.000+00	27, 11	1.000+00	28, 12	1.000+00
29, 13	1.000+00	30, 14	1.000+00	31, 15	1.000+00	32, 16	1.000+00

\*\* Gv IS 32X 3

1	7.416-05	2.395-09	2.010-08
2	2.395-09	8.007-05	9.446-06
3	2.010-08	9.446-06	7.550-05
4	-7.451-05	2.045-07	1.716-06
5	1.259-07	-8.073-05	-1.116-05
6	2.305-06	-6.994-06	-5.337-05
7	-1.058-05	1.881-05	1.504-04
8	-5.113-07	-1.592-04	-1.903-05
9	-1.066-05	-1.875-05	-1.499-04
10	5.018-07	-1.592-04	-1.853-05
11	-1.260-04	1.696-08	1.423-07
12	-2.395-09	-8.007-05	-9.446-06
13	-3.383-08	-7.637-06	-1.321-04
14	-1.260-04	1.696-08	1.423-07
15	-2.395-09	-8.007-05	-9.446-06
16	-3.383-08	-7.637-06	-1.321-04

\*\*\*\*\* SYSTEM MATRICES FOR 28 DEG ORBIT ( 1 of 3 ) \*\*\*\*\*

\*\* F IS 45X45

1, 4	1.565-01	1, 5	-2.643-04	1, 6	-1.936-08	1, 7	8.994-05
1, 8	4.346-06	1, 9	9.062-05	1, 10	-4.265-06	1, 11	5.546-03
1, 12	1.198-08	1, 13	1.488-06	1, 14	5.546-03	1, 15	1.198-08
1, 16	1.488-06	1, 17	-4.449-08	1, 18	-3.833-13	1, 19	-4.423-12
1, 20	2.220+03	1, 21	-3.650+00	1, 22	-4.610-08	1, 23	7.724-02
1, 24	3.835-03	1, 25	7.742-02	1, 26	-3.764-03	1, 27	1.513+00
1, 28	4.791-06	1, 29	4.059-04	1, 30	1.513+00	1, 31	4.791-06
1, 32	4.059-04	2, 4	-4.295-04	2, 5	1.695-01	2, 6	5.875-08
2, 7	-1.599-04	2, 8	1.354-03	2, 9	1.594-04	2, 10	1.353-03
2, 11	-7.461-07	2, 12	4.004-04	2, 13	3.360-04	2, 14	-7.461-07
2, 15	4.004-04	2, 16	3.360-04	2, 17	-1.437-12	2, 18	-1.281-08
2, 19	-2.078-09	2, 20	-6.095+00	2, 21	2.341+03	2, 22	1.399-07
2, 23	-1.373-01	2, 24	1.194+00	2, 25	1.369-01	2, 26	1.194+00
2, 27	-2.035-04	2, 28	1.601-01	2, 29	9.165-02	2, 30	-2.035-04
2, 31	1.601-01	2, 32	9.165-02	3, 4	-3.605-03	3, 5	2.344-02
3, 6	4.483-07	3, 7	-1.278-03	3, 8	1.618-04	3, 9	1.274-03
3, 10	1.575-04	3, 11	-6.262-06	3, 12	4.723-05	3, 13	5.814-03
3, 14	-6.262-06	3, 15	4.723-05	3, 16	5.814-03	3, 17	-1.206-11
3, 18	-1.511-09	3, 19	-1.661-08	3, 20	-5.115+01	3, 21	3.237+02
3, 22	1.067-06	3, 23	-1.098+00	3, 24	1.427-01	3, 25	1.094+00
3, 26	1.390-01	3, 27	-1.708-03	3, 28	1.889-02	3, 29	1.586+00
3, 30	-1.708-03	3, 31	1.889-02	3, 32	1.586+00	4, 4	-1.136+00
4, 5	-2.256-02	4, 6	-2.819-06	4, 7	-7.996-05	4, 8	-1.418-05
4, 9	-2.194-05	4, 10	2.110-05	4, 11	-5.523-03	4, 12	1.023-06
4, 13	1.271-04	4, 14	-5.523-03	4, 15	1.023-06	4, 16	1.271-04
4, 17	4.470-08	4, 18	-3.272-11	4, 19	-3.776-10	4, 20	-1.612+04
4, 21	-3.116+02	4, 22	-6.712-06	4, 23	-6.867-02	4, 24	-1.251-02
4, 25	-1.884-02	4, 26	1.861-02	4, 27	-1.506+00	4, 28	4.091-04
4, 29	3.466-02	4, 30	-1.506+00	4, 31	4.091-04	4, 32	3.466-02
5, 4	-2.256-02	5, 5	-1.163+00	5, 6	-2.942-06	5, 7	1.765-04
5, 8	-1.351-03	5, 9	-2.008-04	5, 10	-1.378-03	5, 11	-3.925-05
5, 12	-4.036-04	5, 13	-6.873-04	5, 14	-3.925-05	5, 15	-4.036-04
5, 16	-6.873-04	5, 17	-7.552-11	5, 18	1.292-08	5, 19	2.456-09
5, 20	-3.202+02	5, 21	-1.607+04	5, 22	-7.004-06	5, 23	1.516-01
5, 24	-1.192+00	5, 25	-1.725-01	5, 26	-1.216+00	5, 27	-1.071-02
5, 28	-1.615-01	5, 29	-1.874-01	5, 30	-1.071-02	5, 31	-1.615-01
5, 32	-1.874-01	6, 4	-7.048-01	6, 5	-7.354-01	6, 6	-8.796-05
6, 7	5.212-04	6, 8	-5.306-04	6, 9	-1.283-03	6, 10	2.942-04
6, 11	1.695-03	6, 12	-3.497-05	6, 13	-4.268-03	6, 14	1.695-03
6, 15	-3.497-05	6, 16	-4.268-03	6, 17	-1.383-09	6, 18	1.119-09
6, 19	1.174-08	6, 20	-1.000+04	6, 21	-1.016+04	6, 22	-2.094-04
6, 23	4.476-01	6, 24	-4.682-01	6, 25	-1.102+00	6, 26	2.596-01
6, 27	4.622-01	6, 28	-1.399-02	6, 29	-1.164+00	6, 30	4.622-01
6, 31	-1.399-02	6, 32	-1.164+00	7, 4	-1.975-02	7, 5	4.360-02
7, 6	5.151-07	7, 7	-9.354-02	7, 8	3.197-04	7, 9	2.262-03
7, 10	3.161-04	7, 11	-8.002-04	7, 12	9.405-05	7, 13	1.158-02
7, 14	-8.002-04	7, 15	9.405-05	7, 16	1.158-02	7, 17	6.349-09
7, 18	-3.009-09	7, 19	-3.308-08	7, 20	-2.803+02	7, 21	6.021+02
7, 22	1.226-06	7, 23	-8.033+01	7, 24	2.821-01	7, 25	1.943+00
7, 26	2.789-01	7, 27	-2.182-01	7, 28	3.762-02	7, 29	3.157+00
7, 30	-2.182-01	7, 31	3.762-02	7, 32	3.157+00	8, 4	-3.504-03
8, 5	-3.338-01	8, 6	-5.243-07	8, 7	3.197-04	8, 8	-9.367-02
8, 9	-3.236-04	8, 10	-2.424-03	8, 11	9.471-04	8, 12	-7.962-04
8, 13	-6.864-04	8, 14	9.471-04	8, 15	-7.962-04	8, 16	-6.864-04

\*\*\*\*\* SYSTEM MATRICES FOR 28 DEG ORBIT ( 2 of 3 ) \*\*\*\*\*

Matrix F (continued)

8, 17	3.068-10	8, 18	2.548-08	8, 19	4.187-09	8, 20	-4.972+01
8, 21	-4.610+03	8, 22	-1.248-06	8, 23	2.746-01	8, 24	-8.265+01
8, 25	-2.779-01	8, 26	-2.139+00	8, 27	2.583-01	8, 28	-3.185-01
8, 29	-1.872-01	8, 30	2.583-01	8, 31	-3.185-01	8, 32	-1.872-01
9, 4	-5.420-03	9, 5	-4.962-02	9, 6	-1.268-06	9, 7	2.262-03
9, 8	-3.236-04	9, 9	-9.352-02	9, 10	-3.104-04	9, 11	-7.753-04
9, 12	-9.377-05	9, 13	-1.154-02	9, 14	-7.753-04	9, 15	-9.377-05
9, 16	-1.154-02	9, 17	6.397-09	9, 18	3.001-09	9, 19	3.298-08
9, 20	-7.692+01	9, 21	-6.852+02	9, 22	-3.018-06	9, 23	1.943+00
9, 24	-2.855-01	9, 25	-8.032+01	9, 26	-2.739-01	9, 27	-2.114-01
9, 28	-3.751-02	9, 29	-3.148+00	9, 30	-2.114-01	9, 31	-3.751-02
9, 32	-3.148+00	10, 4	5.212-03	10, 5	-3.404-01	10, 6	2.907-07
10, 7	3.161-04	10, 8	-2.424-03	10, 9	-3.104-04	10, 10	-9.357-02
10, 11	-9.442-04	10, 12	-7.959-04	10, 13	-6.497-04	10, 14	-9.442-04
10, 15	-7.959-04	10, 16	-6.497-04	10, 17	-3.011-10	10, 18	2.547-08
10, 19	4.078-09	10, 20	7.396+01	10, 21	-4.700+03	10, 22	6.922-07
10, 23	2.715-01	10, 24	-2.139+00	10, 25	-2.666-01	10, 26	-8.265+01
10, 27	-2.575-01	10, 28	-3.184-01	10, 29	-1.772-01	10, 30	-2.575-01
10, 31	-3.184-01	10, 32	-1.772-01	11, 4	-2.636-01	11, 5	-1.873-03
11, 6	3.235-07	11, 7	-1.546-04	11, 8	1.830-04	11, 9	-1.498-04
11, 10	-1.824-04	11, 11	-9.283-02	11, 12	8.478-08	11, 13	1.054-05
11, 14	-1.013-02	11, 15	8.478-08	11, 16	1.054-05	11, 17	7.563-08
11, 18	-2.713-12	11, 19	-3.131-11	11, 20	-3.741+03	11, 21	-2.587+01
11, 22	7.703-07	11, 23	-1.328-01	11, 24	1.614-01	11, 25	-1.609-01
11, 26	-1.609-01	11, 27	-2.532+01	11, 28	3.391-05	11, 29	2.873-03
11, 30	-2.762+00	11, 31	3.391-05	11, 32	2.873-03	12, 4	4.295-04
12, 5	-1.695-01	12, 6	-5.875-08	12, 7	1.599-04	12, 8	-1.354-03
12, 9	-1.594-04	12, 10	-1.353-03	12, 11	7.461-07	12, 12	-1.140-01
12, 13	-3.360-04	12, 14	7.461-07	12, 15	-4.004-04	12, 16	-3.360-04
12, 17	1.437-12	12, 18	1.281-08	12, 19	2.078-09	12, 20	6.095+00
12, 21	-2.341+03	12, 22	-1.399-07	12, 23	1.373-01	12, 24	-1.194+00
12, 25	-1.369-01	12, 26	-1.194+00	12, 27	2.035-04	12, 28	-4.561+01
12, 29	-9.165-02	12, 30	2.035-04	12, 31	-1.601-01	12, 32	-9.165-02
13, 4	6.065-03	13, 5	-3.280-02	13, 6	-8.147-07	13, 7	2.236-03
13, 8	-1.326-04	13, 9	-2.230-03	13, 10	-1.255-04	13, 11	1.054-05
13, 12	-3.819-05	13, 13	-1.012-01	13, 14	1.054-05	13, 15	-3.819-05
13, 16	-1.104-02	13, 17	2.030-11	13, 18	1.222-09	13, 19	2.907-08
13, 20	8.607+01	13, 21	-4.530+02	13, 22	-1.940-06	13, 23	1.921+00
13, 24	-1.170-01	13, 25	-1.915+00	13, 26	-1.107-01	13, 27	2.873-03
13, 28	-1.527-02	13, 29	-2.760+01	13, 30	2.873-03	13, 31	-1.527-02
13, 32	-3.012+00	14, 4	-2.636-01	14, 5	-1.873-03	14, 6	3.235-07
14, 7	-1.546-04	14, 8	1.830-04	14, 9	-1.498-04	14, 10	-1.824-04
14, 11	-1.013-02	14, 12	8.478-08	14, 13	1.054-05	14, 14	-9.283-02
14, 15	8.478-08	14, 16	1.054-05	14, 17	7.563-08	14, 18	-2.713-12
14, 19	-3.131-11	14, 20	-3.741+03	14, 21	-2.587+01	14, 22	7.703-07
14, 23	-1.328-01	14, 24	1.614-01	14, 25	-1.286-01	14, 26	-1.609-01
14, 27	-2.762+00	14, 28	3.391-05	14, 29	2.873-03	14, 30	-2.532+01
14, 31	3.391-05	14, 32	2.873-03	15, 4	4.295-04	15, 5	-1.695-01
15, 6	-5.875-08	15, 7	1.599-04	15, 8	-1.354-03	15, 9	-1.594-04
15, 10	-1.353-03	15, 11	7.461-07	15, 12	-4.004-04	15, 13	-3.360-04
15, 14	7.461-07	15, 15	-1.140-01	15, 16	-3.360-04	15, 17	1.437-12
15, 18	1.281-08	15, 19	2.078-09	15, 20	6.095+00	15, 21	-2.341+03
15, 22	-1.399-07	15, 23	1.373-01	15, 24	-1.194+00	15, 25	-1.369-01
15, 26	-1.194+00	15, 27	2.035-04	15, 28	-1.601-01	15, 29	-9.165-02
15, 30	2.035-04	15, 31	-4.561+01	15, 32	-9.165-02	16, 4	6.065-03

\*\*\*\*\* SYSTEM MATRICES FOR 28 DEG ORBIT ( 3 of 3 ) \*\*\*\*\*

Matrix F (continued)

16, 5	-3.280-02	16, 6	-8.147-07	16, 7	2.236-03	16, 8	-1.326-04
16, 9	-2.230-03	16, 10	-1.255-04	16, 11	1.054-05	16, 12	-3.819-05
16, 13	-1.104-02	16, 14	1.054-05	16, 15	-3.819-05	16, 16	-1.012-01
16, 17	2.030-11	16, 18	1.222-09	16, 19	2.907-08	16, 20	8.607+01
16, 21	-4.530+02	16, 22	-1.940-06	16, 23	1.921+00	16, 24	-1.170-01
16, 25	-1.915+00	16, 26	-1.107-01	16, 27	2.873-03	16, 28	-1.527-02
16, 29	-3.012+00	16, 30	2.873-03	16, 31	-1.527-02	16, 32	-2.760+01
17, 1	1.000+00	18, 2	1.000+00	19, 3	1.000+00	20, 4	1.000+00
21, 5	1.000+00	22, 6	1.000+00	23, 7	1.000+00	24, 8	1.000+00
25, 9	1.000+00	26, 10	1.000+00	27, 11	1.000+00	28, 12	1.000+00
29, 13	1.000+00	30, 14	1.000+00	31, 15	1.000+00	32, 16	1.000+00
33, 17	1.000+00	34, 18	1.000+00	35, 19	1.000+00	36, 36	-8.400+01
36, 38	-7.200+03	37, 37	-8.300+01	37, 39	-7.200+03	38, 36	1.000+00
39, 37	1.000+00	40, 17	-2.500+00	40, 36	2.500+00	40, 40	-2.100+00
40, 42	-2.500+00	41, 18	-2.400+00	41, 37	2.400+00	41, 41	-2.100+00
41, 43	-2.400+00	42, 40	1.000+00	43, 41	1.000+00	44, 42	1.000+00
45, 43	1.000+00						

\*\* G IS 45X17

1, 1	7.416-05	1, 2	2.395-09	1, 3	2.010-08	1, 15	7.416-05
1, 16	2.395-09	1, 17	2.010-08	2, 1	2.395-09	2, 2	8.007-05
2, 3	9.446-06	2, 15	2.395-09	2, 16	8.007-05	2, 17	9.446-06
3, 1	2.010-08	3, 2	9.446-06	3, 3	7.550-05	3, 15	2.010-08
3, 16	9.446-06	3, 17	7.550-05	4, 1	-7.451-05	4, 2	2.045-07
4, 3	1.716-06	5, 1	1.259-07	5, 2	-8.073-05	5, 3	-1.116-05
6, 1	2.305-06	6, 2	-6.994-06	6, 3	-5.337-05	7, 1	-1.058-05
7, 2	1.881-05	7, 3	1.504-04	8, 1	-5.113-07	8, 2	-1.592-04
8, 3	-1.903-05	9, 1	-1.066-05	9, 2	-1.875-05	9, 3	-1.499-04
10, 1	5.018-07	10, 2	-1.592-04	10, 3	-1.853-05	11, 1	-1.260-04
11, 2	1.696-08	11, 3	1.423-07	12, 1	-2.395-09	12, 2	-8.007-05
12, 3	-9.446-06	13, 1	-3.383-08	13, 2	-7.637-06	13, 3	-1.321-04
14, 1	-1.260-04	14, 2	1.696-08	14, 3	1.423-07	15, 1	-2.395-09
15, 2	-8.007-05	15, 3	-9.446-06	16, 1	-3.383-08	16, 2	-7.637-06
16, 3	-1.321-04	33, 12	-1.000+00	34, 13	-1.000+00	35, 14	-1.000+00
36, 4	8.400+01	37, 5	8.400+01	38, 4	-1.000+00	39, 5	-1.000+00
40, 12	2.500+00	41, 13	2.500+00				

\*\* C IS 5X45

1, 1	-1.106+05	1, 2	-1.677-01	1, 3	2.946+01	1, 17	-3.582+05
1, 18	-5.432-01	1, 19	9.543+01	1, 33	-5.018+05	1, 34	-7.610-01
1, 35	1.337+02	2, 1	-1.677-01	2, 2	-1.039+05	2, 3	1.300+04
2, 17	-5.432-01	2, 18	-3.367+05	2, 19	4.212+04	2, 33	-7.611-01
2, 34	-4.717+05	2, 35	5.901+04	3, 1	2.946+01	3, 2	1.300+04
3, 3	-1.102+05	3, 17	9.543+01	3, 18	4.212+04	3, 19	-3.570+05
3, 33	1.337+02	3, 34	5.901+04	3, 35	-5.002+05	4, 17	1.020+00
4, 42	-2.000+01	4, 44	-2.000+01	5, 18	1.122+00	5, 43	-2.200+01
5, 45	-2.200+01						

\*\* B IS 5X12

1, 1	1.020+00	1, 4	1.106+05	1, 5	1.677-01	1, 6	-2.946+01
1, 7	3.582+05	1, 8	5.432-01	1, 9	-9.543+01	2, 2	1.020+00
2, 4	1.677-01	2, 5	1.039+05	2, 6	-1.300+04	2, 7	5.432-01
2, 8	3.367+05	2, 9	-4.212+04	3, 3	1.020+00	3, 4	-2.946+01
3, 5	-1.300+04	3, 6	1.102+05	3, 7	-9.543+01	3, 8	-4.212+04
3, 9	3.570+05	4, 7	-1.020+00	5, 8	-1.122+00		

\*\* Fv IS 20X20

1, 4	1.205-01	1, 5	-2.943-04	1, 6	-1.308-08	1, 7	8.703-05
1, 8	-1.673-08	1, 9	8.771-05	1, 10	1.562-07	1, 11	-4.014-08
1, 12	-6.446-12	1, 13	-4.317-11	1, 14	1.446+03	1, 15	-3.679+00
1, 16	-3.115-08	1, 17	7.474-02	1, 18	-1.476-05	1, 19	7.429-02
1, 20	1.360-04	2, 4	-5.451-05	2, 5	1.339-01	2, 6	1.014-07
2, 7	-2.702-04	2, 8	1.423-03	2, 9	2.689-04	2, 10	1.422-03
2, 11	-2.417-12	2, 12	-1.315-07	2, 13	-3.426-08	2, 14	-6.542-01
2, 15	1.674+03	2, 16	2.414-07	2, 17	-2.321-01	2, 18	1.256+00
2, 19	2.278-01	2, 20	1.238+00	3, 4	-2.655-04	3, 5	3.621-02
3, 6	4.908-07	3, 7	-1.312-03	3, 8	2.728-04	3, 9	1.305-03
3, 10	2.663-04	3, 11	-1.177-11	3, 12	-2.492-08	3, 13	-1.663-07
3, 14	-3.186+00	3, 15	4.527+02	3, 16	1.169-06	3, 17	-1.127+00
3, 18	2.407-01	3, 19	1.106+00	3, 20	2.318-01	4, 4	-1.269+00
4, 5	-2.212-03	4, 6	-9.834-08	4, 7	-8.482-05	4, 8	-1.258-07
4, 9	-7.972-05	4, 10	1.174-06	4, 11	4.016-08	4, 12	-4.846-11
4, 13	-3.245-10	4, 14	-1.523+04	4, 15	-2.766+01	4, 16	-2.341-07
4, 17	-7.285-02	4, 18	-1.110-04	4, 19	-6.752-02	4, 20	1.022-03
5, 4	-2.489-03	5, 5	-1.199+00	5, 6	-4.087-06	5, 7	3.616-04
5, 8	-1.418-03	5, 9	-4.220-04	5, 10	-1.479-03	5, 11	-1.104-10
5, 12	1.339-07	5, 13	4.979-08	5, 14	-2.987-01	5, 15	-1.498+04
5, 16	-9.731-06	5, 17	3.106-01	5, 18	-1.251+00	5, 19	-3.574-01
5, 20	-1.288+00	6, 4	-2.107-02	6, 5	-7.785-01	6, 6	-3.302-05
6, 7	7.560-04	6, 8	-4.272-04	6, 9	-1.267-03	6, 10	9.328-06
6, 11	-9.344-10	6, 12	1.931-08	6, 13	1.286-07	6, 14	-2.529+02
6, 15	-9.731+03	6, 16	-7.862-05	6, 17	6.492-01	6, 18	-3.769-01
6, 19	-1.073+00	6, 20	8.121-03	7, 4	-1.796-02	7, 5	6.807-02
7, 6	7.471-07	7, 7	-1.029-01	7, 8	5.552-04	7, 9	2.357-03
7, 10	5.453-04	7, 11	6.143-09	7, 12	-5.086-08	7, 13	-3.395-07
7, 14	-2.155+02	7, 15	8.508+02	7, 16	1.779-06	7, 17	-8.835+01
7, 18	4.899-01	7, 19	1.997+00	7, 20	4.748-01	8, 4	-2.663-05
8, 5	-2.670-01	8, 6	-4.222-07	8, 7	5.552-04	8, 8	-1.031-01
8, 9	-5.558-04	8, 10	-2.603-03	8, 11	-1.181-12	8, 12	2.679-07
8, 13	7.060-08	8, 14	-3.196-01	8, 15	-3.337+03	8, 16	-1.005-06
8, 17	4.768-01	8, 18	-9.095+01	8, 19	-4.708-01	8, 20	-2.266+00
9, 4	-1.688-02	9, 5	-7.943-02	9, 6	-1.252-06	9, 7	2.357-03
9, 8	-5.558-04	9, 9	-1.028-01	9, 10	-5.393-04	9, 11	6.191-09
9, 12	5.061-08	9, 13	3.378-07	9, 14	-2.026+02	9, 15	-9.929+02
9, 16	-2.981-06	9, 17	2.024+00	9, 18	-4.904-01	9, 19	-8.711+01
9, 20	-4.695-01	10, 4	2.487-04	10, 5	-2.784-01	10, 6	9.219-09
10, 7	5.453-04	10, 8	-2.603-03	10, 9	-5.393-04	10, 10	-1.031-01
10, 11	1.103-11	10, 12	2.677-07	10, 13	6.893-08	10, 14	2.984+00
10, 15	-3.480+03	10, 16	2.195-08	10, 17	4.683-01	10, 18	-2.297+00
10, 19	-4.568-01	10, 20	-8.973+01	11, 1	1.000+00	12, 2	1.000+00
13, 3	1.000+00	14, 4	1.000+00	15, 5	1.000+00	16, 6	1.000+00
17, 7	1.000+00	18, 8	1.000+00	19, 9	1.000+00	20, 10	1.000+00

\*\* Gv IS 20X 3

1	6.690-05	4.029-09	1.962-08
2	4.029-09	8.219-05	1.557-05
3	1.962-08	1.557-05	7.559-05
4	-6.693-05	3.029-08	1.475-07
5	1.840-07	-8.369-05	-2.263-05
6	1.557-06	-1.207-05	-5.843-05
7	-1.024-05	3.179-05	1.543-04
8	1.968-09	-1.675-04	-3.209-05
9	-1.032-05	-3.163-05	-1.536-04
10	-1.838-08	-1.673-04	-3.133-05

\*\*\*\*\* SYSTEM MATRICES FOR THE 98 DEG ORBIT (1 OF 2)\*\*\*\*\*

\*\* F IS 33X33

1, 4	1.205-01	1, 5	-2.943-04	1, 6	-1.308-08	1, 7	8.703-05
1, 8	-1.673-08	1, 9	8.771-05	1, 10	1.562-07	1, 11	-4.014-08
1, 12	-6.446-12	1, 13	-4.317-11	1, 14	1.446+03	1, 15	-3.679+00
1, 16	-3.115-08	1, 17	7.474-02	1, 18	-1.476-05	1, 19	7.429-02
1, 20	1.360-04	2, 4	-5.451-05	2, 5	1.339-01	2, 6	1.014-07
2, 7	-2.702-04	2, 8	1.423-03	2, 9	2.689-04	2, 10	1.422-03
2, 11	-2.417-12	2, 12	-1.315-07	2, 13	-3.426-08	2, 14	-6.542-01
2, 15	1.674+03	2, 16	2.414-07	2, 17	-2.321-01	2, 18	1.256+00
2, 19	2.278-01	2, 20	1.238+00	3, 4	-2.655-04	3, 5	3.621-02
3, 6	4.908-07	3, 7	-1.312-03	3, 8	2.728-04	3, 9	1.305-03
3, 10	2.663-04	3, 11	-1.177-11	3, 12	-2.492-08	3, 13	-1.663-07
3, 14	-3.186+00	3, 15	4.527+02	3, 16	1.169-06	3, 17	-1.127+00
3, 18	2.407-01	3, 19	1.106+00	3, 20	2.318-01	4, 4	-1.269+00
4, 5	-2.212-03	4, 6	-9.834-08	4, 7	-8.482-05	4, 8	-1.258-07
4, 9	-7.972-05	4, 10	1.174-06	4, 11	4.016-08	4, 12	-4.846-11
4, 13	-3.245-10	4, 14	-1.523+04	4, 15	-2.766+01	4, 16	-2.341-07
4, 17	-7.285-02	4, 18	-1.110-04	4, 19	-6.752-02	4, 20	1.022-03
5, 4	-2.489-03	5, 5	-1.199+00	5, 6	-4.087-06	5, 7	3.616-04
5, 8	-1.418-03	5, 9	-4.227-04	5, 10	-1.479-03	5, 11	-1.104-10
5, 12	1.339-07	5, 13	4.979-08	5, 14	-2.987+01	5, 15	-1.498+04
5, 16	-9.731-06	5, 17	3.106-01	5, 18	-1.251+00	5, 19	-3.574-01
5, 20	-1.288+00	6, 4	-2.107-02	6, 5	-7.785-01	6, 6	-3.302-05
6, 7	7.560-04	6, 8	-4.272-04	6, 9	-1.267-03	6, 10	9.328-06
6, 11	-9.344-10	6, 12	1.931-08	6, 13	1.286-07	6, 14	-2.529+02
6, 15	-9.731+03	6, 16	-7.862-05	6, 17	6.492-01	6, 18	-3.769-01
6, 19	-1.073+00	6, 20	8.121-03	7, 4	-1.796-02	7, 5	6.807-02
7, 6	7.471-07	7, 7	-1.029-01	7, 8	5.552-04	7, 9	2.357-03
7, 10	5.453-04	7, 11	6.143-09	7, 12	-5.086-08	7, 13	-3.395-07
7, 14	-2.155+02	7, 15	8.508+02	7, 16	1.779-06	7, 17	-8.835+01
7, 18	4.899-01	7, 19	1.997+00	7, 20	4.748-01	8, 4	-2.663-05
8, 5	-2.670-01	8, 6	-4.222-07	8, 7	5.552-04	8, 8	-1.031-01
8, 9	-5.558-04	8, 10	-2.603-03	8, 11	-1.181-12	8, 12	2.579-07
8, 13	7.060-08	8, 14	-3.196-01	8, 15	-3.337+03	8, 16	-1.005-06
8, 17	4.768-01	8, 18	-9.095+01	8, 19	-4.708-01	8, 20	-2.266+00
9, 4	-1.688-02	9, 5	-7.943-02	9, 6	-1.252-06	9, 7	2.357-03
9, 8	-0.558-04	9, 9	-1.028-01	9, 10	-5.393-04	9, 11	6.191-09
9, 12	5.061-08	9, 13	3.378-07	9, 14	-2.026+02	9, 15	-9.929+02
9, 16	-2.981-06	9, 17	2.024+00	9, 18	-4.904-01	9, 19	-8.711+01
9, 20	-4.695-01	10, 4	2.487-04	10, 5	-2.784-01	10, 6	9.219-09
10, 7	5.453-04	10, 8	-2.603-03	10, 9	-5.393-04	10, 10	-1.031-01
10, 11	1.103-11	10, 12	2.677-07	10, 13	6.893-08	10, 14	2.984+00
10, 15	-3.480+03	10, 16	2.195-08	10, 17	4.683-01	10, 18	-2.297+00
10, 19	-4.568-01	10, 20	-8.973+01	11, 1	1.000+00	12, 2	1.000+00
13, 3	1.000+00	14, 4	1.000+00	15, 5	1.000+00	16, 6	1.000+00
17, 7	1.000+00	18, 8	1.000+00	19, 9	1.000+00	20, 10	1.000+00
21, 11	1.000+00	22, 12	1.000+00	23, 13	1.000+00	24, 24	-8.400+01
24, 26	-7.200+03	25, 25	-8.300+01	25, 27	-7.200+03	26, 24	1.000+00
27, 25	1.000+00	28, 11	-2.500+00	28, 24	2.500+00	28, 28	-2.100+00
28, 30	-2.500+00	29, 12	-2.400+00	29, 25	2.400+00	29, 29	-2.100+00
29, 31	-2.400+00	30, 28	1.000+00	31, 29	1.000+00	32, 30	1.000+00
33, 31	1.000+00						

\*\*\*\*\* SYSTEM MATRICES FOR 98 DEG ORBIT (2 OF 2) \*\*\*\*\*

\*\* G IS 33X17

1, 1	6.690-05	1, 2	4.029-09	1, 3	1.962-08	1, 15	6.690-05
1, 15	4.029-09	1, 17	1.962-08	2, 1	4.029-09	2, 2	8.219-05
2, 3	1.557-05	2, 15	4.029-09	2, 16	8.219-05	2, 17	1.557-05
3, 1	1.962-08	3, 2	1.557-05	3, 3	7.559-05	3, 15	1.962-08
3, 16	1.557-05	3, 17	7.559-05	4, 1	-6.693-05	4, 2	3.029-08
4, 3	1.475-07	5, 1	1.840-07	5, 2	-8.369-05	5, 3	-2.263-05
6, 1	1.557-06	6, 2	-1.207-05	6, 3	-5.843-05	7, 1	-1.024-05
7, 2	3.179-05	7, 3	1.543-04	8, 1	1.968-09	8, 2	-1.675-04
8, 3	-3.209-05	9, 1	-1.032-05	9, 2	-3.163-05	9, 3	-1.536-04
10, 1	-1.838-08	10, 2	-1.673-04	10, 3	-3.133-05	21, 12	-1.000+00
22, 13	-1.000+00	23, 14	-1.000+00	24, 4	8.400+01	25, 5	8.400+01
26, 4	-1.000+00	27, 5	-1.000+00	28, 12	2.500+00	29, 13	2.500+00

\*\* C IS 5X33

1, 1	-1.226+05	1, 2	-2.059-02	1, 3	3.182+01	1, 11	-3.970+05
1, 12	-6.669-02	1, 13	1.031+02	1, 21	-5.562+05	1, 22	-9.344-02
1, 23	1.444+02	2, 1	-2.059-02	2, 2	-1.038+05	2, 3	2.139+04
2, 11	-6.669-02	2, 12	-3.363+05	2, 13	6.927+04	2, 21	-9.343-02
2, 22	-4.711+05	2, 23	9.705+04	3, 1	3.182+01	3, 2	2.139+04
3, 3	-1.129+05	3, 11	1.031+02	3, 12	6.927+04	3, 13	-3.656+05
3, 21	1.444+02	3, 22	9.705+04	3, 23	-5.122+05	4, 11	1.020+00
4, 30	-2.000+01	4, 32	-2.000+01	5, 12	1.122+00	5, 31	-2.200+01
5, 33	-2.200+01						

\*\* B IS 5X12

1, 1	1.020+00	1, 4	1.226+05	1, 5	2.059-02	1, 6	-3.182+01
1, 7	3.970+05	1, 8	6.669-02	1, 9	-1.031+02	2, 2	1.020+00
2, 4	2.059-02	2, 5	1.038+05	2, 6	-2.139+04	2, 7	6.669-02
2, 8	3.363+05	2, 9	-6.927+04	3, 3	1.020+00	3, 4	-3.182+01
3, 5	-2.139+04	3, 6	1.129+05	3, 7	-1.031+02	3, 8	-6.927+04
3, 9	3.656+05	4, 7	-1.020+00	5, 8	-1.122+00		